

Abstracts of the Annual Meeting of Planetary Geologic Mappers, Flagstaff, AZ 2014

Edited by:

*James A. Skinner, Jr.
U. S. Geological Survey, Flagstaff, AZ*

*David Williams
Arizona State University, Tempe, AZ*

NOTE: Abstracts in this volume can be cited using the following format:

Graupner, M. and Hansen, V.L., 2014, Structural and Geologic Mapping of Tellus Region, Venus, *in* Skinner, J. A., Jr. and Williams, D. A., eds., Abstracts of the Annual Meeting of Planetary Geologic Mappers, Flagstaff, AZ, June 23-25, 2014.

SCHEDULE OF EVENTS

Monday, June 23– Planetary Geologic Mappers Meeting

<u>Time</u>	<u>Planet/Body</u>	<u>Topic</u>
8:30 am		Arrive/Set-up – 2255 N. Gemini Drive (USGS)
9:00		Welcome/Logistics
9:10		NASA HQ and Program Remarks (M. Kelley)
9:30		USGS Map Coordinator Remarks (J. Skinner)
9:45		GIS and Web Updates (C. Fortezzo)
10:00		RPIF Updates (J. Hagerty)
10:15		BREAK / POSTERS
10:40	Venus	<i>Irnini Mons</i> (D. Buczkowski)
11:00	Moon	<i>Lunar South Pole</i> (S. Mest)
11:20	Moon	<i>Copernicus Quad</i> (J. Hagerty)
11:40	Vesta	<i>Iterative Geologic Mapping</i> (A. Yingst)
12:00 pm		LUNCH / POSTERS
1:30	Vesta	<i>Proposed Time-Stratigraphy</i> (D. Williams)
1:50	Mars	<i>Global Geology</i> (J. Skinner)
2:10	Mars	<i>Terra Sirenum</i> (R. Anderson)
2:30	Mars	<i>Arsia/Pavonis Montes</i> (B. Garry)
2:50	Mars	<i>Valles Marineris</i> (C. Fortezzo)
3:10		BREAK / POSTERS
3:30	Mars	<i>Candor Chasma</i> (C. Okubo)
3:50	Mars	<i>Hrad Vallis</i> (P. Mougini-Mark)
4:10	Mars	<i>S. Margaritifer Terra</i> (J. Grant)
4:30	Mars	<i>Ladon basin</i> (C. Weitz)
4:50		DISCUSSION / POSTERS
~5:15		ADJOURN

Tuesday, June 24 - Planetary Geologic Mappers Meeting

<u>Time</u>	<u>Planet/Body</u>	<u>Topic</u>
8:30 am		Arrive/Set-up/Logistics
9:00	Mars	<i>Upper Dao and Niger Valles</i> (S. Mest)
9:20	Mars	<i>Tyrrhenus Mons</i> (D. Crown)
9:40	Mars	<i>Hadriacus Palus</i> (J. Skinner)
10:00	Mars	<i>MESDT Student Presentations</i>
10:20		BREAK / POSTERS
10:40	Mars	<i>Opportunity Landing Site</i> (T. Parker)
11:00	Mars	<i>MSL Landing Ellipse</i> (F. Calef)
11:20	Mars	<i>Gale Crater</i> (B. Thomson)
11:40	Mars	<i>Olympia Cavi</i> (J. Skinner)
12:00 pm		LUNCH (GEMS meeting)
2:00 pm	Mars	<i>Cerberus Plains</i> (K. Golder)
2:10	Mars	<i>Aeolis Dorsa #1</i> (D. Burr)
2:30	Mars	<i>Aeolis Dorsa #2</i> (R. Jacobsen)
2:50		GROUP DISCUSSION
~4:30		ADJOURN
~5:30		EVENING EVENT

Wednesday, June 25 – GIS and Geologic Mapping Roundtable

<u>Time</u>	<u>Topic</u>
9:00 am to 4:00 pm	GIS Potpourri (email requested topics to Trent Hare: thare@usgs.gov)

CONTENTS (sorted by body, then alphabetically by author)

Venus

- A High Resolution Tectonic Map of Irnini Mons, Venus.
D.L. Buczkowski and M.A. Matiella Novak.....1

Moon

- Compositional and Morphologic Mapping of the Copernicus Quadrangle, the Moon: Year 2 Status.
J. J. Hagerty, J. A. Skinner, L. R. Gaddis, C. M. Fortezzo, and T. D. Glotch.....3
- Update on the Geologic Mapping of the Lunar South Pole Quadrangle (LQ-30): Evaluating Mare, Cryptomare, and Impact Melt Deposits.
S. C. Mest, D. C. Berman, N. E. Petro, and R. A. Yingst.....5

Icy Satellites and Small Bodies

- A Proposed Time-Stratigraphic System for Protoplanet Vesta.
D. A. Williams, R. Jaumann, H.Y. McSween, Jr., C.A. Raymond, C.T. Russell.....7
- Iterative Geologic Mapping of Vesta During the Dawn Data Acquisition Phase: Lessons Learned.
R. A. Yingst, S. C. Mest, D. A. Williams, and W. B. Garry.....9

Mars

- Status of the Terra Sirenum Map Project: A Window into Pre-Tharsis and Tharsis Phases of Mars Evolution Robert.
C. Anderson, James M. Dohm, S. Robbins, and B. Hynek.....11
- Characterizing the History of a Diverse Inverted Fluvial Landscape: Mapping and Morphometry of the Aeolis Dorsa Region, Mars.
D. M. Burr and R. E. Jacobsen.....13
- Geologic Mapping of the Mars Science Laboratory Landing Ellipse: Update
F. J. Calef III, W. E. Dietrich, L. Edgar, J. Farmer, A. Fraeman, J. Grotzinger, M. C. Palucis, T. Parker, M. Rice, S. Rowland, K. M. Stack, D. Sumner, J. Williams, and the MSL Science Team.....15
- Geologic Mapping of the Tyrrhenus Mons Lava Flow Field, Northeast Hellas Region, Mars.
D. A. Crown and S. C. Mest.....17

Geologic Mapping of Central Valles Marineris, Mars. <i>C. M. Fortezzo, K. L. Tanaka, P. S. Kumar, and T. Platz</i>	19
Geologic Mapping of Arsia and Pavonis Montes, Mars. <i>W. B. Garry, D. A. Williams, and J. E. Bleacher</i>	21
Mapping of Flood Channels, Associated Lavas, and Fissures in the Cerberus Plains, Mars. <i>K. B. Golder and D. M. Burr</i>	24
Age-Dating and Characterizing the Fluvial Activity in Aeolis Dorsa, Western Medusa Fossae Formation, Mars. <i>R. E. Jacobsen, and D. M. Burr</i>	26
Geologic Mapping of Upper Dao and Niger Valles, Northeast Hellas, Mars. <i>S. C. Mest, D. A. Crown, J. Michalski, F. C. Chuang, K. P. Blount, and L. F. Bleamaster</i>	28
Mapping Hrad Vallis, Mars. <i>P. J. Mouginis-Mark and C. W. Hamilton</i>	30
High Resolution Geologic and Structural Mapping in West Candor Chasma, Mars: 2014 Final Status Report. <i>C. H. Okubo and T. A. Gaither</i>	32
Mapping Mars at 1-25 cm/pixel: Identification of Coastal Processes at the Opportunity Landing Site. <i>T. J. Parker and B. G. Bills, and the MER Science Team</i>	34
Geologic Mapping to Constrain the Sources and Timing of Fluvial Activity in Western Ladon Basin, Mars. <i>C.M. Weitz, S.A. Wilson, R.P. Irwin III, and J.A. Grant</i>	36
Geologic Mapping in MTM Quadrangles -20037, -25037, -30037, -30032 in Southern Margaritifer Terra, Mars. <i>S. A. Wilson and J. A. Grant</i>	38
 <u>Mars Exploration Student Data Teams</u>	
An Analysis of Spectroscopic Surface Data from CRISM to Predict a History of Borates on Mars. <i>Z. C. Chester</i>	40

Print Only

Geologic Map of the Olympus Mons Volcano, Mars. <i>J.E. Bleacher, D.A. Williams, P. Mouginis-Mark, D. Shean, R. Greeley</i>	41
The NASA Regional Planetary Image Facility Network: A Five-Year Plan. <i>J. J. Hagerty</i>	42
Progress on 1:10M Geologic Mapping of the Aphrodite Map Area, Venus. <i>V.L. Hansen, I. López, K.G. Thaisen</i>	44
Progress on the 1:10M Geologic Mapping of the Niobe Map Area, Venus: Results from the Structural Mapping of the Volcanic Plains. <i>I. López and V. L. Hansen</i>	46

Introduction: The V-20 quadrangle [1] is roughly centered on Irnini Mons, a volcano crossed by two rift systems, capped by Sappho Patera (a possible corona) and surrounded by structural complexities that include one other volcano and four coronae. Flows and other deposits from Irnini Mons are superimposed on an older, regional plains material with abundant wrinkle ridges in at least two sets: one trending generally east-west and another concentric to Irnini Mons. Radial features on top of the Irnini flows were mapped as graben or lineations [1], as resolution allowed.

We attempt to determine the stress history in the vicinity of Irnini Mons to ascertain the relationship of the volcano to the deformation of the local regional plains. The complex arrangement of cross-cutting tectonic structures surrounding Irnini Mons indicate a detailed and multi-part stress history, thus making it an ideal location to identify distinct patterns of changes in stress orientation. Determining the progression of stress directions for specific regions on Venus is the critical first step in constraining the various existing tectonic models, as most of these models predict an explicit sequence of stress orientations. To accomplish this goal we 1) mapped the structural features in the region around Irnini Mons utilizing the 75 m/pixel FMAP images and 2) used our mapping to determine the relative age relationships of sets of structural features around Irnini Mons [2, 3].

Geology of Irnini Mons: Flows and other deposits from Irnini Mons are superimposed on an older, regional plains material (Fig. 1) [1]. These superposed materials include: 1) a shield plains unit (fs) younger than the regional plains (prb), 2) flows from Irnini Mons (fl and fhI) that are also younger than the prb plains, and 3) a smooth plains unit (ps) that is younger than the fl and fhI flows. The prb plains material has abundant wrinkle ridges in at least two sets: one trending generally E-W and one concentric to Irnini Mons.

The shield plains unit (fs) is abundantly covered with small domes. Although the shield plains are crossed by wrinkle ridges, they are not necessarily oriented in the same manner as the wrinkle ridges on the regional plains (prb). Graben associated with Badb Linea cut through the shield material, which overlies a lineated plains material (pl), interpreted as being a relatively old plain of deformed volcanic rocks [1].

The Irnini flows are described as two units [1]. The first is interpreted as basaltic lava flows (fl), while the second is basaltic lava overlain by a thin pyroclastic veneer (fhI). Both units are free of wrinkle ridges, but do show fabrics of linear structures that overlie every unit save the smooth plains (ps). Radial features on top of the Irnini flows (fl and fhI) were mapped by [1] as either graben or lineations or graben, depending on whether the resolution allowed identification.

The smooth plains unit (ps) is superposed on the Irnini flows and most of the structures [1]. There are no wrinkle ridges, but small domes and some lineations are visible, though apparently covered.

Structural Features around Irnini Mons: Previous work has determined the nature of large-scale structural features proximal to Irnini Mons. The volcanic edifice is about 475 km wide and 1.75 km high [1] and the volcano is capped by Sappho Patera, a 225 km diameter depression characterized as a corona or corona-like feature [4] that is rimmed by both concentric graben and a large circumferential ridge. Irnini Mons is crossed by two rift systems, the north-south trending Badb Linea and an older rift that incorporates Guor Linea to the northwest and Virtus Linea to the southeast. Large surrounding structural complexities include four coronae and Anala Mons, a 550 km diameter, 2.25 km high volcano almost directly to the south of Irnini Mons.

High-resolution structural mapping was completed in a 1° x 1° region from 15°-16° N, 17°-18° E, northeast of Irnini Mons [2]. The difference in radar backscatter in high resolution images (75 m/pixel) indicates that some of the radial features are topographic highs [2] although they are too narrow to be resolved in altimetry data sets. These features are similar to the "horst-like lineaments" identified by [5]. Unlike the textured plains material (pt) unit of arcuate ridges mapped by [1], which is directly south, these ridges are on top of the Irnini flows and cannot be an older feature. To the north the radial features appear to be graben, also located on top of the Irnini flows. Due north, the radial graben become indistinguishable from the graben associated with the Badb Linea rift.

Structural Mapping around Irnini Mons and Timing of Events: While the V-20 quadrangle [1] included a tectonic elements map the quadrangle was mapped at a 1:5,000,000 scale, and the nature of many of the small-scale structures could not be resolved. However, at the highest FMAP resolution of 75 m/pixel many of the features that [1] had to map as "radar bright lineations" are resolvable. For example, the radial ridges found at N45E to N75E relative to Irnini [2] are not resolvable at lower resolution and were mapped as lineations by [1].

We have mapped the entire Irnini Mons region from 12°-20°N, 13°-20°E, which includes structures related to both Irnini Mons and the surrounding regional plains (Fig. 2). Structural features in this region include graben, corona structures, wrinkle ridges and fracture and ridge belts. Previous mapping in this area

provided examples of how this high-resolution structural mapping may differ from the V-20 map [2, 3].

We focus on four distinct and cross-cutting features surrounding the Sappho Patera: 1) Short Radial Grabens (dark blue); 2) Badb Linea Grabens (light blue); 3) Ridges (red); 4) Circumferential Graben (pink) (Fig. 2). The relationship of these features to Sappho Patera is also utilized to understand the stress history of the region. The assignment of relative timing of the formation of these features is based on well-known intersection relationships on Earth that have been success-

fully applied to fractures and wrinkle ridges on Venus [6]. These relationships can be used to infer the ages of different sets of wrinkle ridges relative each other and relative to fracture sets [6].

References: [1] McGill G.E. (2000) *USGS, Geo. Inv. Map I-2627*. [2] Buczkowski (2006) *JSG 28*, 2156-2168. [3] Matiella Novak & Buczkowski (2014) *LPSC 45*, abs. 2569 [4] Stofan et al. (1992) *JGR 97*, 13,347-13,378. [5] Ernst et al. (2003) *Icarus 163*, 282-316. [6] McGill (1993) *GRL 20*, 21, 2407-2410.

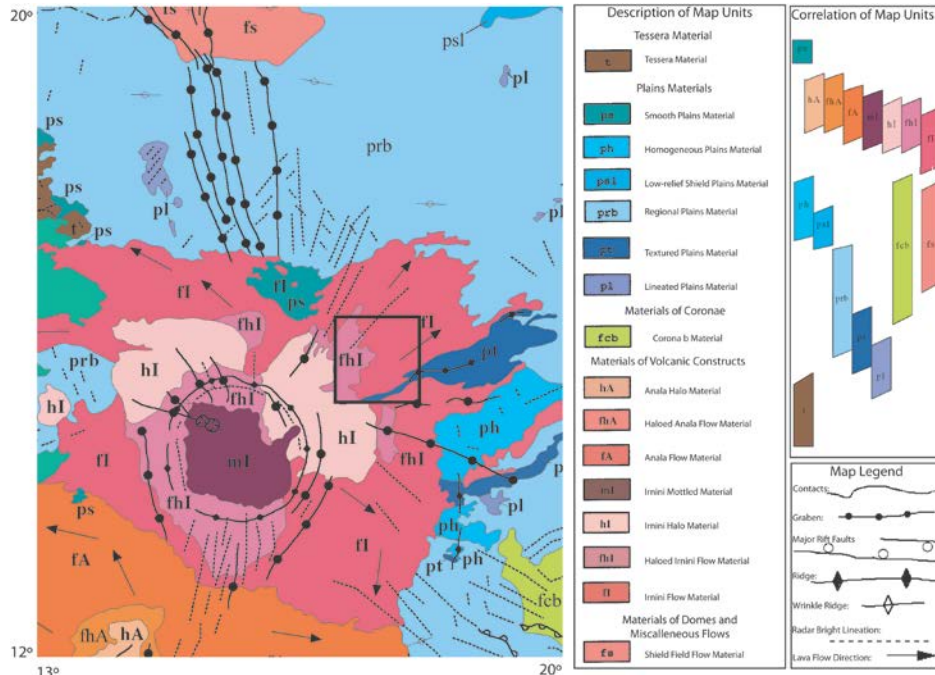


Figure 1. Geologic map of the Irnini Mons region of Venus (12° - 20°N, 13° - 20°E), adapted from the Sappho Patera Quadrangle (V-20) [1]. Inset box (roughly 100 km on each side) marks location of preliminary study by [2].

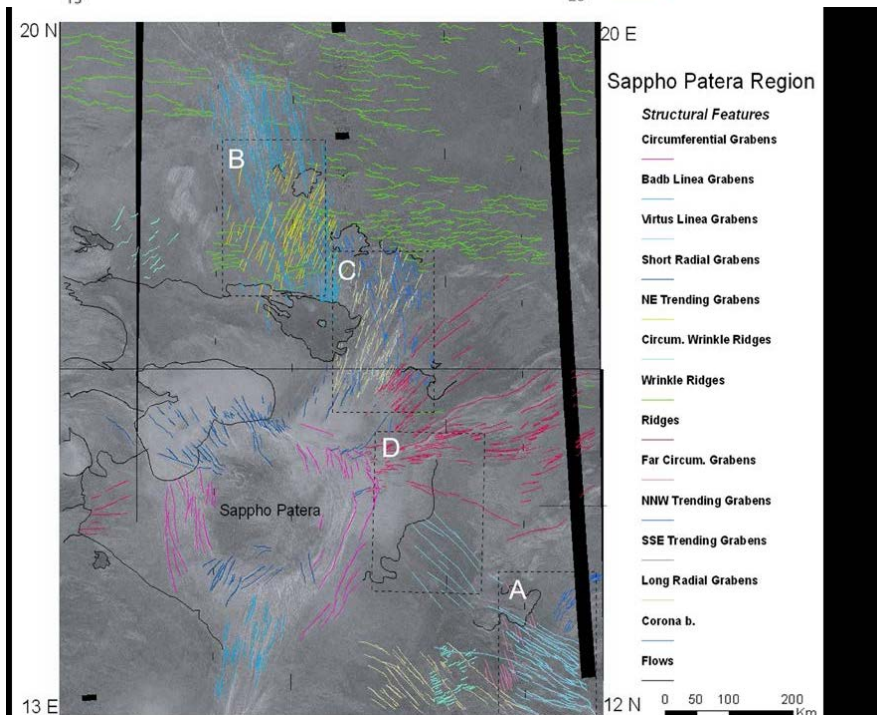


Figure 2. FMAP image of the Irnini Mons region from figure 1, with four type locations (A, B, C, D) for establishing relative timing of structural features.

COMPOSITIONAL AND MORPHOLOGIC MAPPING OF THE COPERNICUS QUADRANGLE, THE MOON: YEAR 2 STATUS. J. J. Hagerty¹, J. A. Skinner¹, L. R. Gaddis¹, C. M. Fortezzo¹, and T. D. Glotch², ¹USGS Astrogeology Science Center, 2255 N. Gemini Drive, Flagstaff, AZ 86001, ²Stony Brook University, Stony Brook, NY, email: jhagerty@usgs.gov.

Introduction: The recent flood of lunar data has provided unprecedented views of the Moon, which in turn has shown us that portions of the lunar surface, such as the Copernicus lunar quadrangle (Fig. 1), contain prime examples of numerous lithologies with several possible origins [e.g., 1 – 10]. However, the abundance and complexity of modern lunar data sets result in increasingly varied models for lunar surface processes. Interpretations of the origin of specific units or features vary depending on the data being used. In an effort to provide a comprehensive understanding of the geologic evolution of the lunar crust and surface within the Copernicus quadrangle, we are integrating multiple data sets via end-member methodologies.

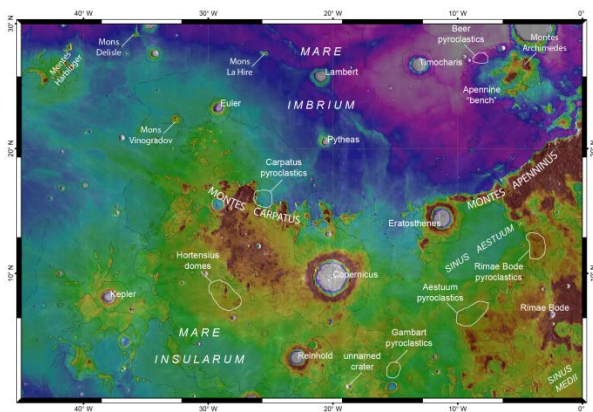


Figure 1. The base image is a color-coded version of the LRO LOLA topographic map (100 m/pixel). Also shown are features with major compositional variations that will serve as key locations to investigate.

Traditionally, two investigative strategies have been employed to determine the distribution and origin of specific geologic features and lithologies on the Moon: geologic/morphologic mapping and compositional mapping. Rarely, however, have the two methods been fused for lunar science investigations with the specific intent of producing a USGS geologic map. The abundance of high-resolution lunar data, in combination with the integration of the two end-member mapping methodologies, has the potential to provide significant new constraints on the formation and evolution of the lunar crust, to establish a comprehensive geologic and stratigraphic context wherein subsequent studies can be conducted, and to delineate refined approaches for the systematic production of geologic maps of the Moon.

This mapping project addresses several major lunar science issues including: 1) examination of the heterogeneity of lunar crustal materials and their vertical and horizontal distribution, 2) spatial and temporal variation of lunar lithologies, 3) refinements of the geologic and stratigraphic architecture of referent lunar materials, and 4) efficiency assessments of lunar mapping methods, including the role of data set type and resolution within the 1:2.5M scale quad-based mapping scheme. New constraints on the composition and structure of the lunar crust will follow which will improve estimates of the bulk composition of the Moon and allow new tests of models for its origin and evolution.

Current Mapping Efforts: In an effort to provide a comprehensive understanding of the evolution of the lunar crust within the Copernicus quad we are using compositional data sets, such as the Lunar Prospector Gamma Ray and Neutron Spectrometer elemental data, to direct our focus on two areas of interest that exhibit anomalous compositional characteristics (i.e., low iron abundances and elevated thorium abundances) compared to the surrounding terrain.

Timocharis crater. The first area of interest is dominated by Timocharis crater (Fig. 2), a 34 km diameter crater located at 26.72°N and -13.1°E, which has slumped interior walls, a central peak, and ~1 km of rim relief. Using high-resolution data from the Lunar Reconnaissance Orbiter Camera we conducted an initial morphologic study of Timocharis, which showed us that there are several unique features that could be the sources of the anomalous geochemical signatures seen in the region [11]. These unique morphologic features include an unusually shaped central peak that may have experienced an impact event, and several small (≤ 1.25 km diameter), higher-albedo, domical features at the base of the western crater wall with meter- to decimeter-sized rocky debris superposed on the finer-grained, surface materials. Using forward modeling approaches to estimate the thorium and iron abundances of individual features within the crater, we found that the exposed lithologies in the center of the crater are consistent with monzodiorites from the lunar sample suite. Monzodiorites are the intrusive equivalents of rhyodacite, indicating the presence of a compositionally evolved lithology (12-18 wt.% FeO, 1-3 wt.% TiO₂, and 10-44 ppm Th) distinctly different from the major rock types found in the mare or high-

lands. The identification of this lithology in Timocharis crater is also intriguing because the composition is consistent with lithologies found in the adjacent Apennine Bench Formation [4]. These results indicate that there is a regional distribution of monzodiorite possibly coincident with impact melt derived from the Imbrium basin.

Schröter F. The second region of interest for compositional mapping is Schröter F, a purported 29 km diameter satellite feature located at 7.4°N and -5.9°E. Preliminary characterization of the site suggests the feature is a perched basalt pond (Clementine and Kaguya spectral ratio maps confirm a mafic mineralogy). LP-GRS thorium data indicate that there is a significant thorium enhancement (i.e., > 10 ppm Th) in this region centered on this feature. The surface of the feature appears to have fewer craters compared to the surrounding terrain. We have begun crater counting on this feature in an effort to assign a relative age to the feature. Forward modeling of the thorium and iron data is in the beginning stages; these results will be presented at the meeting.

Year 2 Status: Co-Is Glotch and Gaddis are completing mosaics of Diviner and Kaguya data, respectively, for the entire quad. Collaborator Campbell has begun creating a 70-cm, earth-based, radar mosaic for the quad. Co-I Skinner has finished the initial “blind,” morphology-based geologic map of the quad, during which he established preliminary unit descriptions and flagged unusual areas for detailed compositional analysis. PI Hagerty has begun compositional mapping of specific regions of interest and will continue to do so for the remainder of the fiscal year. Skinner and Hagerty will iterate back-and-forth on unit delineation using a combination of compositional and morphologic techniques. The integration of end-member approaches, in combination with robust lunar data, will result in a powerful tool for understanding the formation and evolution of the lunar crust in the quad.

The project team has been augmented by the inclusion of a Planetary Geology and Geophysics Undergraduate Research Program (PGGURP) student from Northern Arizona University (Alex Huff). This student will conduct a detailed, systematic survey of pyroclastic and silicic volcanism within the quad.

Acknowledgements: This work is supported by NASA through the Planetary Geology and Geophysics program via grant NNH12AU82I.

References: [1] Cahill et al. (2009) *J. Geophys. Res.*, 114, E09001; [2] Chevrel et al. (2009) *Icarus*, 199, 9; [3] Glotch et al. (2010) *Science*, 329, 1510; [4] Hagerty et al. (2006) *J. Geophys. Res.*, 111, E06002; [5] Hagerty et al. (2009) *J. Geophys. Res.*, 114,

E04002; [6] Lawrence et al. (2007) *Geophys. Res. Lett.*, 34, doi: 10.1029/2006GL028530; [7] Matsunaga et al. (2008) *Geophys. Res. Lett.*, 35, L23201; [8] Spudis, P. and Taylor, G.J. (2009) *Lunar. Planet. Sci. Conf.*, 40, abstract #1039; [9] Woehler et al. (2011) *Planet. Space Sci.*, 59, 92; [10] Yamamoto et al. (2010) *Nat. Geosci.*, 384, doi:10.1038/NNGEO897; [11] Hagerty et al. (2013) *Geol. Soc. Am. Abstracts with Programs*, Vol. 45, No. 7, 405.

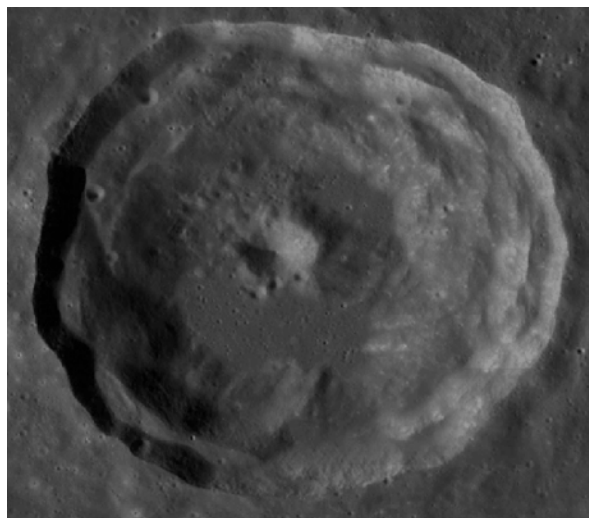


Figure 2. LRO WAC image of Timocharis crater (34 km diameter). Note the bulls-eye or peak pit crater at the center of the crater.

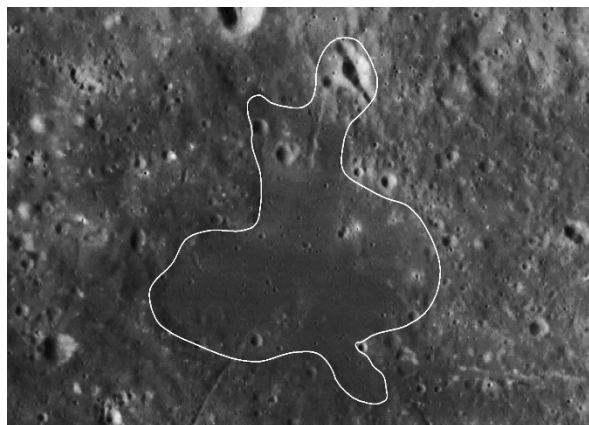


Figure 3. LRO WAC image of Schröter F (roughly 29 km diameter) outlined in white.

UPDATE ON THE GEOLOGIC MAPPING OF THE LUNAR SOUTH POLE QUADRANGLE (LQ-30): EVALUATING MARE, CRYPTOMARE AND IMPACT MELT DEPOSITS. S.C. Mest^{1,2}, D.C. Berman¹, N.E. Petro², and R. A. Yingst¹, ¹Planetary Science Institute, 1700 E. Ft. Lowell, Suite 106, Tucson, AZ 85719-2395 (mest@psi.edu); ²Planetary Geodynamics Laboratory, Code 698, NASA GSFC, Greenbelt, MD 20771.

Introduction: We are using recent image, spectral and topographic data to map the geology of the lunar South Pole quadrangle (LQ-30) at 1:2.5M scale [1-7]. The overall objective of this research is to constrain the geologic evolution of LQ-30 (60°-90°S, 0°-±180°) with specific emphasis on evaluation of a) the regional effects of impact basin formation, and b) the spatial distribution of ejecta, in particular resulting from formation of the South Pole-Aitken (SPA) basin and other large basins. Key scientific objectives include: 1) Determining the geologic history of LQ-30 and examining the spatial and temporal variability of geologic processes within the map area. 2) Evaluating the distribution of volcanic materials within the map area. And 3) constraining the distribution of impact-generated materials, and determining the timing and effects of major basin-forming impacts on crustal structure and stratigraphy in the map area.

Methodology: This project utilizes ArcGIS (v. 10.1) to compile image, topographic and spectral datasets to produce a geologic map of LQ-30. The study uses the Lunar Reconnaissance Orbiter (LRO) Wide Angle Camera (WAC) mosaic (~100 m/pixel) as its primary base to characterize geologic units from surface textures and albedo, identify contacts and structures, and map impact craters (D>1 km). Additional datasets are being used to complement the base and include mosaics (Lunar Orbiter, Clementine UVVIS and NIR), images (LROC NAC, Clementine UVVIS and HIRES, and Lunar Orbiter), Clementine color ratio data, Moon Mineralogy Mapper (M3) multispectral data, and LOLA topography.

Regional Geology: LQ-30 exhibits ~16 km of relief. The near side consists predominantly of cratered highlands, is more heavily cratered and displays higher elevations than the far side. This difference is due to the overwhelming presence of SPA, which encompasses nearly all of the far side map area (Figure 1).

SPA is the largest (D=2600 km, ~18 km deep) and oldest (pre-Nectarian) impact basin identified on the Moon [8-10]. Models suggest that SPA formed by an oblique impact that excavated material from the upper crust [11,12] to the lower crust or upper mantle [13,14]. Galileo and Clementine multispectral data show enrichment in mafic materials [15-19] and LP-GRS data show enhancements in both Fe and Th [20-23] within the basin relative to the surrounding highlands. The materials exposed within SPA, such as in central peaks or in crater walls, could be used to estimate the composition of the lower crust/upper mantle.

Mapping Progress: We are currently focusing our mapping efforts on the floors of impact basins and craters and within portions of the intercrater plains that

exhibit relatively flat surfaces in order to characterize the nature of these materials using image, spectral and topographic datasets.

LQ-30 hosts all or part of 46 impact features greater than 100 km in diameter that would have significantly affected the structure of the crust and redistributed large amounts of material across the surface [7]. Impact craters display morphologies ranging from simple to complex [7-9,24] and most contain floor deposits distinct from surrounding materials. Most of these deposits, especially for craters less than ~50 km in diameter, display moderate to bright floor materials with little to no surface expression; these materials likely consist of impact melt, possibly mantled by ejecta from nearby craters, that has been well-gardened. These higher albedo deposits also tend to contain a higher density of superposed impact craters.

Mare Deposits: Most deposits on crater and basin floors exhibit moderate to low albedos with relatively smooth surfaces. Potential mare deposits are found on the floors of several of the larger impact craters (e.g., Antoniadi, Hausen, Klaproth, Moretus, and Amundsen) and basins (e.g., Schrodinger, Bally, Poincare, Planck, and Australe) within the map area [e.g., 6-9,25-27]. Although some deposits may be mantled by ejecta from younger impact events, the lower albedo of these materials, as well as their association with other features such as floor fracturing, dome-shaped or conical features suggests a volcanic origin.

For example, volcanic materials within Schrödinger are concentrated inside the basin's peak ring, display a smooth, featureless, low albedo surface, and are more mafic relative to other Schrödinger plains materials [6]. In addition, a sinuous rille is observed in association with the mare [5-7]. Schrödinger also contains a small (D=5 km) well-preserved ovoidal cone in the eastern part of the basin, just inside the peak ring. The cone displays ~500 m of relief above the surrounding plains and is ~400 m deep from its floor to its rim [6]. The cone has been characterized as a "maar" crater [25] and a "dark-halo crater" (DHC) [26], and has been identified as the source of pyroclastic eruptions [25,26].

Antoniadi Crater: Antoniadi crater (D=150 km; 69.5°S, 172°W) is unique on the Moon in that it is the only lunar crater that contains both a peak ring and a central peak, placing it morphologically between impact craters and multi-ring basins [8,9], and it contains the lowest elevations on the Moon (-8.5 km), which may provide access to lower crustal/upper mantle materials via its central peak and peak ring. Its floor deposits consist of dark smooth material near the center of the crater, and brighter more rugged material between the peak ring and crater wall [7,28]. Recent mapping shows

that the dark material embays the rugged material, as well as the peak ring and central peak. The rugged material likely includes impact melt. Superposition relationships indicate the dark material was emplaced after the rugged material and may consist of mare [7].

Mare Australe: Mare deposits are found on the floor of Australe basin along the eastern limb near the northern edge of the map area (~62°S, 90°E). These deposits are dark and smooth in appearance, but some are brighter and more rugged suggesting they are older and have been modified since their emplacement by (1) mantling by ejecta, (2) mixing by subsequent impacts, and/or (3) gardening and regolith development [7,8].

Intercrater plains: Several areas of intercrater plains also exhibit similar morphologic characteristics as crater- and basin-filling materials, such as moderate to low albedo, relatively smooth and flay-lying. The origins of these materials are more difficult to determine due to burial by ejecta from nearby impacts, but we are in the process of analyzing the medium-resolution LROC WAC and high-resolution LROC NAC images, as well as M3 spectral data to evaluate these materials.

References: [1] Mest, S.C. (2007) LPSC XXXVIII, #1842. [2] Van Arsdall, L.E. and S.C. Mest (2008) LPSC XXXIX, #1706. [3] Mest, S.C. and L.E. Van Arsdall (2008) NLSI LSC, NASA ARC, #2089. [4] Mest, S.C. (2008) GSA Joint Annual Mtg., #324-3. [5] Mest, S.C. (2009) Ann. Mtg. of Planet. Geol. Mappers, San Antonio, TX. [6] Mest, S.C. (2010) GSA Sp. Paper 447, SPE477-04. [7] Mest, S.C. et al. (2010) LPSC XLI, #2363. [8] Wilhelms, D.E. et al. (1979) USGS MISM I-1162, 1:5M scale. [9] Wilhelms, D.E. (1987) *USGS Prof. Pap.* 1348. [10] Spudis, P.D. et al. (1994) *Science*, 266, 1848-1851. [11] Schultz, P.H. (1997) LPSC, XXVII, #1259. [12] Schultz, P.H. (2007) LPSC, XXXVIII, #1839. [13] Melosh, H.J. (1989) *Impact Cratering*, 245 pp. [14] Cintala, M.J. and R.A.F. Grieve (1998) *Met. and Planet. Sci.*, 33, 889-912. [15] Belton, M.J.S. et al. (1992) *Science*, 255, 570-576. [16] Head, J.W. et al. (1993) *JGR*, 98, 17,149-17,182. [17] Lucey, P.G. et al. (1998) *JGR*, 103, 3701-3708. [18] Pieters, C.M. et al. (1997) *GRL*, 24, 1903-1906. [19] Pieters, C.M. et al. (2001) *JGR*, 106, 28,001-28,022. [20] Lawrence, D.J. et al. (1998) *Science*, 281, 1484-1489. [21] Lawrence, D.J. et al. (2002) *New Views of the Moon, Europe*, 12-14. [22] Lawrence, D.J. et al. (2002) *JGR*, 107, doi:10.1029/2001JE001530. [23] Jolliff, B.L. et al. (2000) *JGR*, 105, 4197-4216. [24] Wood, C.A. and L. Andersson (1978) *Proc. Lunar Planet. Sci. Conf.*, 9th, 3669-3689. [25] Shoemaker, E.M. et al. (1994) *Science*, 266, 1851-1854. [26] Gaddis, L.R. et al. (2003) *Icarus*, 161, 262-280. [27] Kramer, G.Y., et al. (2013) *Icarus*, 131-148. [28] Dominov, E. and S.C. Mest (2009) LPSC, XL, #1460.

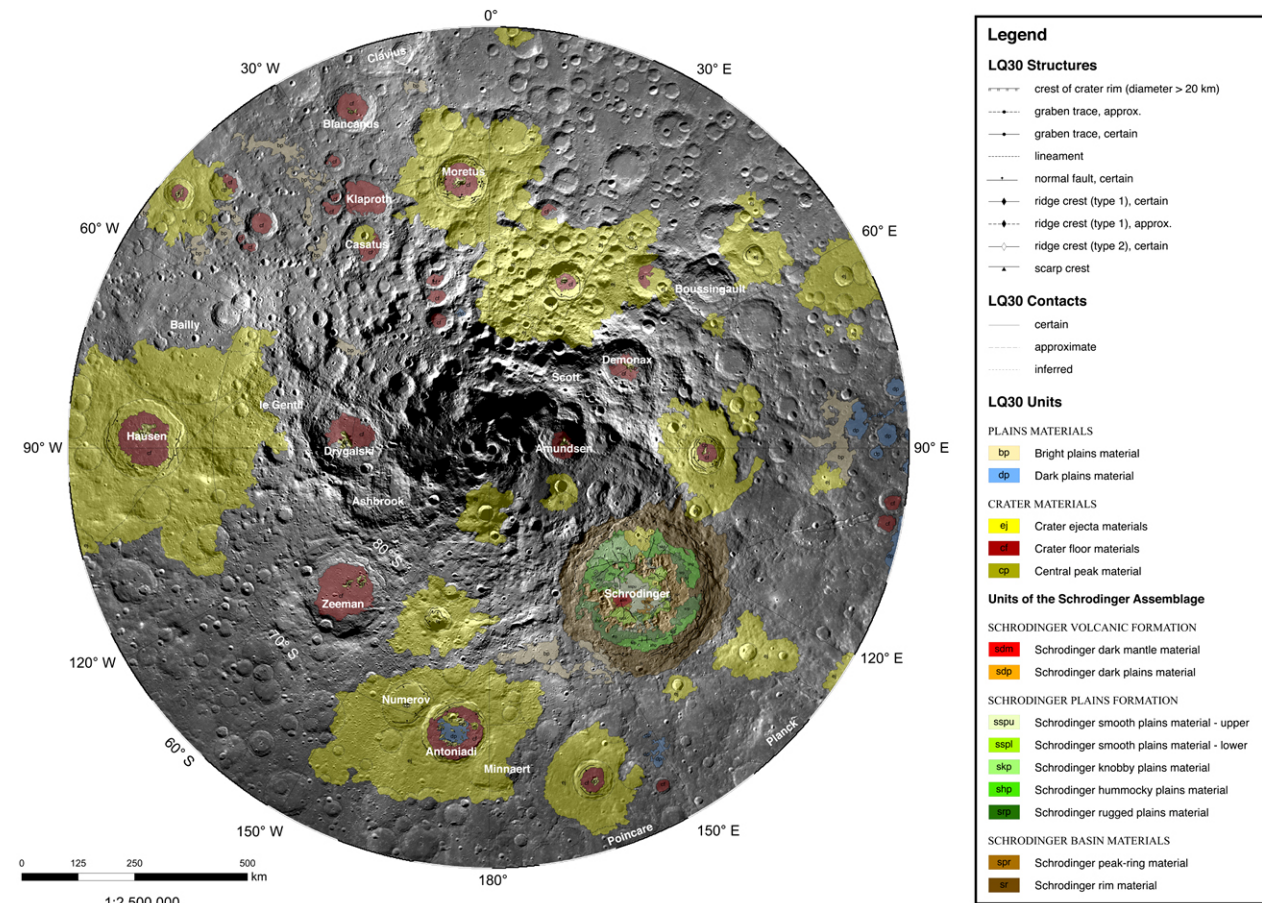


Figure 1. Geologic map of the lunar south pole quadrangle, LQ-30.

A PROPOSED TIME-STRATIGRAPHIC SYSTEM FOR PROTOPLANET VESTA. D. A. Williams¹, R. Jaumann², H.Y. McSween³, Jr., C.A. Raymond⁴, C.T. Russell⁵, ¹School of Earth and Space Exploration, Arizona State University, Tempe, AZ (David.Williams@asu.edu), ²German Aerospace Center (DLR), Berlin, Germany; ³Department of Earth and Planetary Sciences, University of Tennessee, Knoxville, TN; ⁴NASA Jet Propulsion Laboratory, California Institute of Technology, Pasadena, CA; ⁵Department of Earth and Space Sciences, UCLA, Los Angeles, CA.

Introduction: The Dawn Science Team completed a geologic mapping campaign during its nominal mission at Vesta, including production of a 1:500,000 global geologic map derived from High-Altitude Mapping Orbit (HAMO) images (70 m/pixel) [1] and 15 1:250,000 quadrangle maps derived from Low-Altitude Mapping Orbit (LAMO) images (20-25 m/pixel) [2]. In this abstract we propose a time-stratigraphic system and geologic time scale for the protoplanet Vesta, based on global geologic mapping and other analyses of NASA Dawn spacecraft data, supplemented with insights gained from laboratory studies of howardite-eucrite-diogenite (HED) meteorites and geophysical modeling.

Why a time-stratigraphic system?: A time-stratigraphic or chronostratigraphic system is a listing of all of the major time-rock units emplaced on a planet over its geologic history, in chronological order from oldest to youngest. Time-rock units are generally correlated with the major rock units defined from a global geologic map, and serve to relate the map's rock units (i.e., 3D physical units that make up a planet's crust) to the planet's time units (i.e., the subdivisions of time during which the time-rock units were emplaced). For example, on the Moon, rock units related to the Imbrium basin impact (including crater materials and Imbrium impact ejecta, called the Fra Mauro Formation) are contained in the time-rock unit called the Lower Imbrian Series, which is correlated with time unit called the Early Imbrian Epoch [3,4]. On Mercury, rock units related to the Caloris basin impact (including crater materials and Caloris impact ejecta) are contained in the time-rock unit called the Calorian System, which is correlated with a time unit called the Calorian Period [5,4]. These distinctions between rock, time-rock, and time units not only facilitate geologic mapping, but also enable better understanding of the geologic history of a planet, and comparison to the histories of the planets.

Results: We propose the following time-stratigraphic system for Vesta (**Table 1**) that relates the geologic map (rock) units identified from geologic mapping to a series of time-rock units and corresponding time units that define a geologic time scale for Vesta (**Figure 1**). During the Dawn nominal mission it became clear that the south pole of Vesta hosts two

large impact basins, the older Veneneia superposed by the younger Rheasilvia [6,7]. Two separate sets of large ridges and troughs were identified, one set encircling much of Vesta equatorial region (Divalia Fossae), and the other preserved in the heavily cratered northern terrain (Saturnalia Fossae). Structural analysis of these ridge-and-trough systems demonstrated that they are likely a tectonic response to the formation of the south polar basins: the Rheasilvia impact led to the formation of the Divalia Fossae, the Veneneia impact led to the Saturnalia Fossae [6,8]. Crater counts provide cratering model ages for the Rheasilvia impact of ~3.6 Ga and ~1 Ga, and ages for the Veneneia impact of ~3.8 Ga and >2.1 Ga using the lunar-derived and asteroid flux-derived chronologies, respectively. Despite the differences in absolute ages, it is clear that these two large impact events had global effects, and thus delineate the major periods of Vesta's geologic history.

Zones of heavily cratered terrain (HCT: [9]) in the northern hemisphere adjacent to the Saturnalia Fossae Formation [1] likely are heavily modified portions of Vesta's ancient crust. Additionally, geologic and geophysical evidence [8, 10] suggest that Vestalia Terra is probably a large surviving fragment of Vesta's original crust. Thus, these geologic units suggest that a Pre-Veneneian system and Pre-Veneneian period must be included as part of Vesta's geologic history.

We debated what the Dawn data informs us about the youngest part of Vesta's geologic history. The geologic units in and around the 68 x 58 km Marcia crater appear to delineate the most recent large impact event on Vesta. Crater counts of areas of the Marcia ejecta blanket give cratering model ages of ~120-150 Ma and ~220-390 Ma using the lunar-derived and asteroid flux-derived chronologies, respectively (Williams et al.). In contrast, a unit of smooth material on the floor of Marcia crater, interpreted to be impact melt, has a cratering model age of ~40 Ma and ~60 Ma using the lunar-derived and asteroid flux-derived chronologies, respectively. There is disagreement on the Dawn Team whether this smooth unit was formed at the time of the Marcia impact, or sometime later by a post-emplacment process, or whether the younger age of the putative floor melt is due to the effects of the different material properties of this material relative to the

ejecta blanket on the crater statistics. Regardless, the units associated with the Marcia impact event together make a set of related geologic units defined as the Marcia Formation [11], which we propose as the base of Vesta's youngest system and period. We are continuing to refine the absolute model ages of the Marcia Formation at the time of this writing.

Acknowledgements: The success of the Dawn mission is due to the efforts of a large team of engineers, scientists, and administrators in industry and government laboratories both in the United States and abroad. The Dawn mission is managed by NASA's Jet Propulsion Laboratory, a division of the California Institute of Technology in Pasadena, for NASA's Science Mission Directorate, Washington DC. UCLA is responsible for overall Dawn mission science. The Dawn framing cameras have been developed and built under the leadership of the Max Planck Institute for Solar System Research, Katlenburg-Lindau, Germany, with significant contributions by DLR German Aerospace Center; Institute of Planetary Research, Berlin; and in coordination with the Institute of Computer and Communication Network Engineering, Braunschweig. The framing camera project is funded by DLR, the Max Planck Society, and NASA/JPL. VIR has been developed under the leadership of INAF-Istituto di Astrofisica e Planetologia Spaziali, Rome, Italy and is funded by ASI, the Italian Space Agency. DAW is supported by

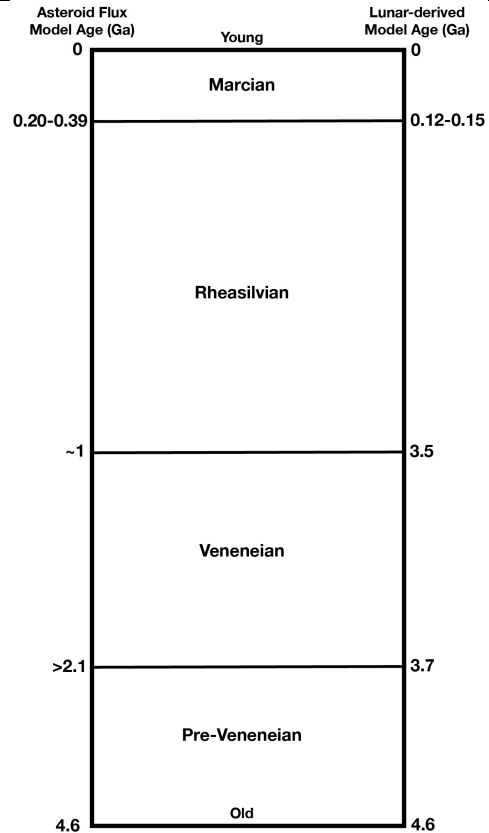
NASA's Dawn at Vesta Participating Scientist program. RJ is supported by DLR and the German Space Agency. Dawn data are archived with the NASA Planetary Data System. We thank the Dawn team for the development, cruise, Dawn orbital insertion, and operations of the Dawn spacecraft at Vesta.

References: [1] Yingst, R.A., et al. (2014) *PSS*, in press. [2] Williams, D.A., et al. (2014a) *Icarus*, in review. [3] Wilhelms, D.E. (1987) *USGS. Prof. Pap. 1348*. [4] Wilhelms, D.E. (1990), *Planetary Mapping*, Cambridge Univ. Press, New York, 208-260. [5] Spudis, P.D. (1985) *NASA TM 87563*, 595-97. [6] Jauermann, R. et al. (2012) *Science* 336, 687-690. [7] Schenk, P. et al. (2012) *Science* 336, 694-697. [8] Buczkowski, D.L. et al. (2013) *GRL* 39, L18205, doi:10.1029/2012GL052959. [9] Marchi, S. et al. (2012) *Science* 336, 690-694. [10] Raymond, C.A. et al. (2013) EGU Gen. Assem., Abs# EGU2013-12408. [11] Williams, D.A. et al. (2014) *Icarus*, published online at: <http://dx.doi.org/10.1016/j.icarus.2014.01.033>. [12] Schmedemann, N. et al. *PSS* (accepted).

Table 1. Proposed time-stratigraphic system for protoplanet Vesta. The correlation of Vesta's rock units, time-rock units, and time units is derived from geologic mapping and other Dawn data analyses [1,2,6,8].

Rock Unit	Time-Rock Unit	Time Unit
Marcia Formation	Marcian System	Marcian Period
Rheasilvia Formation, Divialia Fossae Formation	Rheasilvian System	Rheasilvian Period
Cratered highlands, Saturnalia Fossae Formation	Veneinean System	Veneinean Period
Cratered highlands, Vestalia Terra?	Pre-Veneinean System	Pre-Veneinean Period

Figure 1 (right). Proposed geologic time scale for protoplanet Vesta. The age dates at left are cratering model ages derived from the asteroid flux-derived chronology function [e.g., 7,9]. The age dates at right are cratering model ages derived from the lunar-derived chronology function [12].



ITERATIVE GEOLOGIC MAPPING OF VESTA DURING THE DAWN DATA ACQUISITION PHASE: LESSONS LEARNED. R. A. Yingst¹, S. C. Mest¹, D. A. Williams², and W. B. Garry³, ¹Planetary Science Institute (1700 E. Fort Lowell, Suite 106, Tucson, AZ 85719; yingst@psi.edu); ²Arizona State University; ³NASA Goddard Space Flight Center.

Introduction: Geologic mapping is an investigative procedure that organizes disparate datasets into geologic units, with the goal of revealing the underlying geologic processes and placing those processes into a global, contextual framework. The Dawn spacecraft mission to the asteroid Vesta provided an ideal opportunity for this approach to be utilized for an unfamiliar planetary surface. The map reported here is part of an iterative mapping effort; the geologic map was created using the first orbital images of Vesta, and then refined with each new orbit that yielded an improvement in resolution from the km to the 10s of m scale. Iterative mapping is a process that provides the geologic context for, and reveals the interrelationships of, geologic characteristics revealed by each emerging dataset within a timeframe that allows the map to inform data analysis on the mission timeline.

Geologic Setting: Vesta is an ellipsoidal asteroid of approximately 286 km long axis [1]. Earth-based and Hubble Space Telescope data suggested it had sustained large impacts, including one that produced a large crater at the south pole. Measured and inferred mineralogy results indicated that Vesta has an old, differentiated surface, with spectrally-distinct regions that can be geochemically tied to the HED meteorites [2-4]. Dawn data confirmed that Vesta has a heavily-cratered surface, with large craters evident in numerous locations. The two largest impact structures resolved are the younger, larger Rheasilvia structure, and the older, more degraded Veneneia structure, both near the south pole. Vesta's surface is also characterized by a system of deep, globe-girdling equatorial troughs and ridges, as well as an older system of troughs and ridges to the north. Arcuate troughs and ridges are also evident cutting across, and spiraling from, the Rheasilvia central mound. Notwithstanding previous spectroscopic observations, no volcanic features have been unequivocally identified [5].

Data Collection and Mapping Process: Each of Dawn's several orbital phases at Vesta provided increasingly higher spatial resolution data that were fed into the mapping process. The first map was created based on data gathered during Rotational Characterization (RC) and Optical Navigation (OpNav), including 3-9 km/pixel clear filter data from the Framing Camera (FC). The second iteration [6-7] used FC clear filter data at 200 m resolution and a Digital Terrain Model (DTM) derived from Survey orbit image data [5, 8]. The third iteration [9] was based on data from the

High-Altitude Mapping Orbit (HAMO), with an average spatial resolution of 61 m/pixel.

Preparation of all iterations followed the methods developed and described by [10-13]. Units were defined on the basis of characteristics such as morphologic features, surface textures, color, and albedo. For the initial data reduction process, "color" was defined as the color ratio scheme often used in Clementine multispectral images (ratios of 415/750 nm in red, 750/950 nm in green, and 750/415 nm in blue; the Dawn team used 440/750 nm, 750/920 nm and 750/440 nm). Unit stratigraphy was inferred by superposition and cross-cutting relationships.

The RC/OpNav orbit imaged about 40% of Vesta at 3 km/pxl. This area was mapped independently by four separate workers, who then compared and consolidated their results. This allowed all mappers to familiarize themselves with the surface, and calibrate any differences in approach. For the second iteration, each worker mapped one of four broad regions: 30–90°S, or 0–120°, 120–240° or 240–360° longitude, with each of the latter three blocks ranging from 30°S latitude to the limit of HAMO coverage in the north. Some overlap occurred where features or units straddled these longitudinal blocks; this overlap allowed the mappers to compare results and address any potential areas of disagreement. For the third iteration, each worker mapped a different one of these longitudinally-defined regions than they had previously mapped. This was done to lessen bias introduced by a single mapper.

Observations and Interpretations: Vesta can be divided very broadly into three terrains: heavily-cratered terrain; ridge-and-trough terrain (the equatorial Divalia Fossae and northern Saturnalia Fossae units); and terrain associated with the Rheasilvia crater. Local features include high-albedo and low-albedo material and ejecta (as compared to the general surface albedo); lobate deposits; and mass-wasting materials. Stratigraphically, the formation of the primary crust was followed by impact cratering, including the formation of Veneneia and the associated Saturnalia Fossae unit. Formation of Rheasilvia followed, along with associated structural deformation that shaped the Divalia Fossae ridge-and-trough unit at the equator. Subsequent impacts and mass wasting events subdued impact craters, rims, and portions of ridge-and-trough sets, and formed slumps and landslides, especially within crater floors and along crater rims and scarps. Subsequent to the formation of Rheasilvia,

discontinuous low-albedo deposits formed or were emplaced; these lie stratigraphically above the equatorial ridges that likely were formed by Rheasilvia. These discontinuous low-albedo layers were mantled by subsequent lighter-toned ejecta emplacement. The last features to be formed were craters with bright rays and other surface mantling deposits. The Marcia impact event occurred geologically recently, and marks the latest major event on Vesta. The last features to be formed were craters with bright rays and other surface mantling deposits. The global map was utilized to develop a vestan time-stratigraphic system and proposed geologic time scale (from oldest to youngest: Pre-Veneneian, Veneneian, Rheasilvian, and Marcian Systems), which is being correlated with crater chronologies for absolute model ages developed by the Dawn Science Team.

Lessons Learned — Data Acquisition: Executed progressively throughout data acquisition, the iterative mapping process provided the team with geologic proto-units in a timely manner. One aspect of the methodology that contributed to that success was the use of a small crew of experienced mappers to conduct the iterative mapping activities. The original plan to utilize two mappers was dropped early on, in favor of using four mappers, as it was clear within a few days of data acquisition that two people could not meet the compressed science team-imposed timeline given the rate of data flow. This team of four had significant collective experience in geologic mapping of a wide range of small rocky bodies, and this experience was critical to successfully meeting the goal of producing a reasonable map of geologic proto-units within a few-week timeframe. This short time between data acquisition and product generation meant that overthinking was minimized among the mappers.

On the other hand, the pressure upon the global mapping team was enormous to produce precise unit boundaries that fed into the investigations of the science team (crater counting statistics, for example, or other mapping projects), as rapidly as possible. This pressure drove the mapping team to retain shortcuts longer than they might have been ideally used. For example, we retained much of the standardized nomenclature and symbology originally adopted as a preliminary step, rather than allowing unit definitions and nomenclature to evolve more organically with each iteration. We believe that interpretation of the resulting map was hampered by the necessity to provide the team with a standard nomenclature and symbology early in the process, and we might have learned

more about the unique features of Vesta if we had been less driven by the mission timeline to formalize features and symbology quickly. We thus recommend retaining generic descriptors and symbology for as long as possible into the global mapping process.

Lessons Learned — Mapping and Interpretation: Units, and thus the potential processes from which they stem, were difficult to identify or interpret based solely on differences in morphology or albedo. This was especially true for the cratered terrain units. When only coarse resolution was available, features with a larger topographic range, such as craters, and ridges and troughs, were easier to identify than other features and terrains. We believe that for small, irregular bodies, topography is a more discriminating characteristic than morphology for identifying and characterizing features and units, especially when the available resolution is very coarse.

The fact that fully calibrated VIR multispectral data was not available, and only limited GRaND data on H abundance was available, was a hindrance to the mapping process and subsequent interpretation. On a body like Vesta, where few clues exist to distinguish one cratered terrain from another besides crater density, this was especially true. Additionally, without a way to estimate the mineralogy of crater ejecta we could not utilize craters as probes into the composition of the subsurface. Ultimately we were never able to use VIR multispectral to define or refine units, only to more specifically describe units. Future iterative mapping efforts should be aware of this difficulty.

References: [1] Russell, C.T. et al. (2012) *Science*, 684–686, <http://dx.doi.org/10.1126/science.1219122>. [2] Binzel, R.P. et al. (1997) *Icarus*, 128, 95-103. [3] Gaffey, M.J. (1997) *Icarus*, 127, 130-157. [4] Li, L. et al. (2010) *Icarus*, 208, 238-251. [5] Jaumann, R., et al. (2012) *Science*, 336, 687-690. [6] Yingst, R.A. et al. (2011) *Proc. AGU*, abs. P43B-0248. [7] Yingst, R.A., et al. (2012) *LPSC*, abs. 1359. [8] Preusker, F. et al. (2012) *LPSC*, abs. 2012. [9] Yingst, R.A., et al. (2014) *Planet. Space Sci.*, <http://dx.doi.org/10.1016/j.pss.2013.12.014i>. [10] Shoemaker, E.M. and Hackman, R.J. (1962) *The Moon*, Kopal, Z., Mikhailov, Z.K. (Eds.), *Internat. Astronomical Union Symposium 14*, Academic Press, London, UK, pp. 289–300. [11] Wilhelms, D.E. (1990) *Planetary Mapping*, Greeley, R. and Batson, R.M. (Eds.), Cambridge Univ. Press, pp. 208–260. [12] Tanaka, K.L. et al. (2010) *The Planetary Geologic Mapping Handbook*, USGS Open File Report, 21 pp. [13] Greeley, R. and Batson, R.M. (1990) *Planetary Mapping*, Cambridge Univ. Press, p. 296.

Status of the Terra Sirenum Map Project: A Window into Pre-Tharsis and Tharsis Phases of Mars Evolution

Robert. C. Anderson^a, James M. Dohm^b, S. Robbins^c, B. Hynek^c, ^aJet Propulsion Laboratory, California Institute of Technology, Pasadena, CA 91109, ^bThe Museum, The University of Tokyo, Hongo 7-3-1, Bunkyo-ku, Tokyo 113-0033, Japan, ^cLaboratory for Atmospheric and Space Physics, University of Colorado, Boulder, Colorado USA.

Introduction: The Terra Sirenum region, which is located to the southwest of Tharsis, records not only the development of the Tharsis magmatic complex, at least since the Middle Noachian [1-3] up to present-day, but just as importantly, contains some of the oldest stratigraphic units of the western hemisphere region of Mars. Detailed examination of the structures and units within this region provided an excellent window into identifying the tectonic processes that influenced the geologic evolution of the ancient (pre-Tharsis) phase of the evolution of Mars. Here, we present an overview from our mapping effort detailing the status of our mapping project as well as detailing the earliest geologic history for this region.

Mapping Status: We have completed a detailed 1:5,000,000-scale geologic map for the Terra Sirenum region, which includes mapping all stratigraphic units and identifying all tectonic, erosional, depositional, and impact structures (**Fig. 1**). We followed the procedure for mapping surface units defined by *Tanaka et al.*, [2005]. Stratigraphic units were differentiated on both stratigraphic (crosscutting, overlap, and embayment) and contact relations and morphologic characteristics. High resolution MOC, NA, CTX, HiRise, and HRSC data was utilized to produce the base map and provided detailed spatial and temporal paleotectonic information.

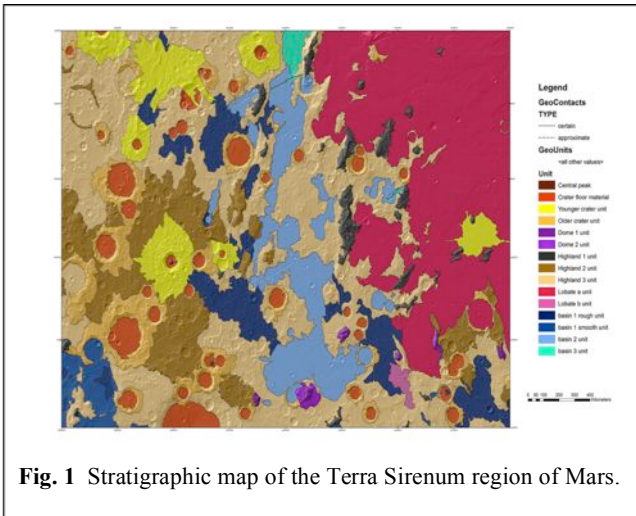


Fig. 1 Stratigraphic map of the Terra Sirenum region of Mars.

Crater statistics have been completed for our stratigraphic map of the Terra Sirenum region using a new global impact crater database [6-7]. In addition, all impact craters with diameters ≥ 3 km were manually examined to identify only those superposed on the most recent resurfaced terrains: those impact craters that display pristine rims and ejecta blankets and well-defined, bowl-shaped basins with little to no infill that have no visible evidence of volcanic, fluvial, and tectonic resurfacing. The superposed impact craters were verified through ConTeXt camera images where there was coverage [8]. The impact crater retention ages are shown in **Fig. 2** based on the modeling schemes of [9] and [10].

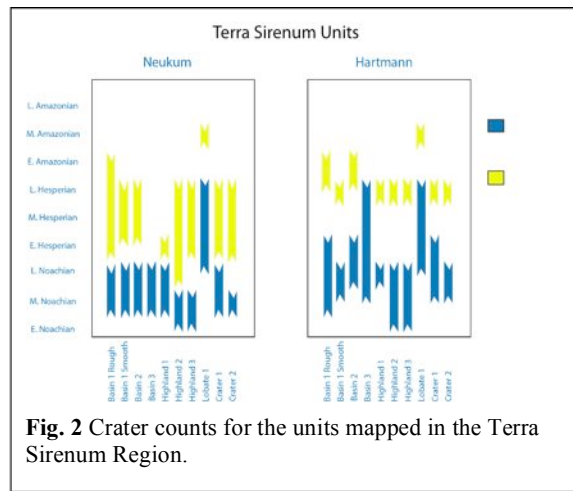


Fig. 2 Crater counts for the units mapped in the Terra Sirenum Region.

Results of the Mapping- Tharsis Terrains: Tharsis-Influenced Terrains: Susequent to such an early dynamic ancient stage of Mars evolution, the growth of Tharsis intermingled with the pre-existing Tharsis structures. Some of the structures attributed to the formation of Tharsis in this region include reactivation of ancient basement structures and the formation of the South Tharsis Ridge Belt, additional basin formation, and the formation of large faults systems (e.g., Sirenum Fossae) and dike emplacement centered about Tharsis [2-5]. There is strong evidence suggesting interplay between the macrostructures, the water-enriched structural basins, and the Tharsis-centered faults and dikes. Examples of this interplay include Mangala Valles that sources from a Tharsis-centered fault in one of the large north-trending basins and collapse structures along

some of the Tharsis-centered faults, some of which display fluvial activity.

Results of the Mapping- Ancient Pre-Tharsis Terrains: Early tectonism in the Terra Sirenum region is expressed by 1) large, north-trending prominent faults (defined as macrostructures [4] due to their enormous geometric proportions including lengths reaching thousands of kilometers), 2) structurally-controlled basins (widths vary from kilometers to hundreds of kilometers) displaying water enrichment in the substrate, and 3) stratigraphic units displaying magnetic signatures. **Fig. 3** displays the ancient, large macrostructures mapped in this region. The white arrows illustrate the bounding normal faults surrounding the large basins. Mangala Valles (M.V.), which is located at the top of the figure, represents one of the large fluvial basins identified in this region.

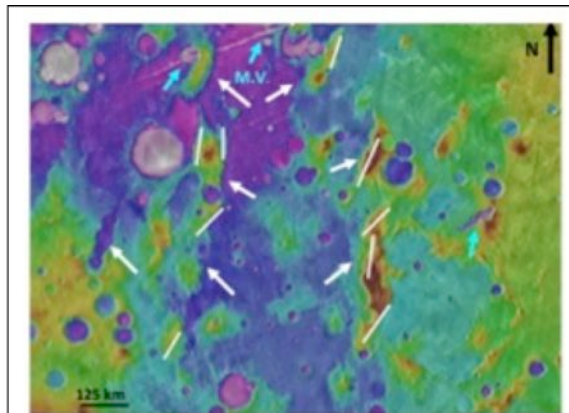


Fig. 3 MOLA topography map showing ancient structures trending north-south and bounded by large normal faults representing the margins of large basins. M.V. equals Mangala Valles.

From **Fig. 1**, the structures identified in **Fig. 3** represent the oldest unit identified and mapped in this region and belongs to the Highland 1 unit (dark grey). As previously mentioned, this unit is found predominately in the central region of the map region and consists of north-south trending massifs. Figure 4 is an overlaid of the MGS magnatic field map onto the mapped stratigraphic units shown in Figure 1. From **Fig. 3**, the magnetic data shows predominate, north-south trending underlying ancient basement sturtures. The distribution of these sources is consistent within this region and because of they contained reversed signatures (e.g. red and blue region in **Fig. 3**), therefore, they were formed when reversing dynamo was still active before it halted early in Mars evolution (e.g. Noachian). Although Mangala Valles occupies one of the ancient basins, it is much younger and originates from one of the younger fault system associated with the formation of the Tharsis Rise.

Summary: The following is observed through crater counting in conjunction with the geologic mapping for the Terra Sirenum region: (1) ancient cratered highlands basements (**Fig. 4**), including macrostructures identified in **Fig. 3**, are Early Noachian-Middle Noachian; (2) basin formation was established by the Middle Noachian with possible subsequent growth; (3) lavas on the western flank of Tharsis were emplaced during the Late Noachian to Late Hesperian (Stages 2-4; see [1-3]) and even as late as Middle Amazonian based on the superposed crater counts and are the result of the formation of the Tharsis Rise; (4) Late Noachian-Early Amazonian resurfacing of cratered highlands material, tectonic structures, and basins based on the superposed crater counts, correlative with the significant stages of Tharsis development (Stages 1-4), and (5) the source region of Mangala Valles has no superposed impact craters, indicating an Amazonian resurfacing event.

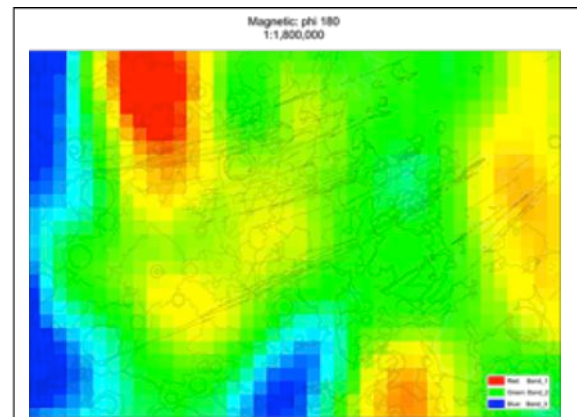


Fig. 4 The Mars Global Surveyor spacecraft obtained a globally-distributed vector magnetic field measurements that were acquired approximately 400 km above the surface of Mars.

References. [1] Dohm, J.M., et al., 2001. *J. Geophys. Res.* 106, 32 943-32 958. [2] Anderson, R.C., et al., 2001. *J. Geophys. Res.* 106, 20,563-20,585. [3] Dohm, J.M., et al., 2007. In *Superplumes: beyond plate tectonics*. D.A Yuen, S. Maruyama, S-I Karato, and B.F. Windley (eds.). Springer, London, 523-537. [4] Dohm, J.M. et al. (2002) *Lunar Planet. Sci.* XXXIII, 1639 (abstract). [5] Scott, D.H., and Tanaka, K.L. (1986) *USGS Misc. Inv. Ser. Map I-1802-A (1:15,000,000)*, [6] Robbins, S.J., 2011. Ph.D. Thesis, CU, Boulder. Robbins, S., and Hynek, B., [7] Robbins, S.J.; and Hynek, B.M., 2011. Submitted to *JGR-Planets*. doi: 10.1029/2011JE003966. [8] Malin, M.C., et al., 2007. *J. Geophys. Res.* 112, doi: 10.1029/2006JE002808. [9] Hartmann, W.K., 2005. *Icarus* 174, 294-320. [10] Neukum, G., et al., 2001. In *Chronology and Evolution of Mars* (R. Kallenbach, J. Geiss, and W. K. Hartmann, eds.), Kluwer Academic Publishers, 55-8.

CHARACTERIZING THE HISTORY OF A DIVERSE INVERTED FLUVIAL LANDSCAPE: MAPPING AND MORPHOMETRY OF THE AEOLIS DORSA REGION, MARS. D. M. Burr and R. E. Jacobsen, Earth & Planetary Sciences Dept., Univ. of Tennessee, Knoxville, TN (dburr1@utk.edu and RJacobsen@utk.edu).

Introduction: This abstract describes a mapping project recently selected for funding. The pre-proposal observations for this project are presented in a companion abstract [1], which provides detail on the proposed scientific and morphometric analyses.

Objectives and Expected Significance: The Aeolis Dorsa (AD) region (see Figure 1 in [1]), located just north of Mars' highland-lowland boundary (HLB) and ~800 kilometers east of Gale Crater, contains a rich and layered history of fluvial activity, interspersed with aeolian, sedimentological, tectonic, and collapse events. The fluvial history is recorded in an areally extensive, morphologically varied, and stratigraphically stacked population of fluvial features, most of which are inverted. Previous MDAP-funded research in the region has documented evidence for substantial climate change and landscape evolution. Outstanding questions involve the timing and conditions of fluvial feature formation, their subsequent modification by other landscape processes, and how these fluvial features fit into the larger history of water on Mars.

The *objectives* of this mapping project are: 1) to define and characterize the fluvial, aeolian, sedimentological, tectonic, and collapse events that formed AD, and 2) to compare the AD fluvial features to fluvial networks elsewhere on Mars. These objectives will be accomplished through mapping and morphometric analysis of geologic units and fluvial features, synthesis of that information into a description of AD fluvial history, and comparison of that history with published information on fluvial networks elsewhere on Mars. The mapping will result in a 1:500k geologic map with one 1:100k inset map for publication by the U.S. Geological Survey (USGS). An upcoming USGS 1:2M map [2] distinguished and crater-counted three Medusae Fossae Formation (MFF) members in this region. That time-stratigraphic framework for the western MFF, within which the AD are found, will provide the chronological context for our more detailed mapping.

Background: Multiple inverted fluvial landscapes exist within Mars' tropics [e.g., 3-8]. Inverted fluvial landscapes form through fluvial runoff, resultant fluvial sediment transport and deposition, and induration. The final exhumation of mappable morphologic and lithostratigraphic units with inverted fluvial features enables this history of fluvial activity, sedimentation, and erosion to be examined.

Of these multiple inverted fluvial landscapes, the AD show the largest documented population of inverted fluvial deposits (~1,400 individual links comprise

(O)10² networks that extend over 6x10⁴ km² and through an elevational range of ~1 km) [9,10]. The large spatial coverage of the fluvial features and their individual and branching network morphologies imply formation by runoff sourced from precipitation, likely in the form of snowmelt [7,8,11]. Aeolian modification and mobilization of the landscape is also apparent, along with the repeated embayment of the formation by Cerberus lavas [12]. Tectonism and/or basal sapping may also have modified the landscape [e.g., 13].

The AD fluvial deposits have various morphologies that may be grouped into 3 categories: flat sinuous ridges, thin sinuous ridges, and fan-shaped deposits. These three morphologies are hypothesized to be deposits from meandering rivers, sinuous rivers, and alluvial fans, respectively [7,9]. In 4 localized regions (see Figure 1 in [1]), these morphologies have a consistent stratigraphic stacking, with fans located stratigraphically above thins or flats (Figure 1).

Hypothesis and questions: This stacking leads us to hypothesize the following (simplest possible) progression of events in the AD region. (a) Long-duration, broad or broadly meandering rivers deposited sediments within valleys at least a few kilometers wide. (b) Volcaniclastic and/or aeolian sedimentation infilled these river valleys to a depth comparable to at least the relief of the thin paleochannels. (c) Sinuous but more narrow and/or less vigorously meandering rivers exploited some of the same river valleys, depositing sediment within their channels. (d) The fluvial sediments from both (a) and (c) underwent induration. (e) The host MFF, including the river valley walls, was eroded, resulting in paleochannel inversion. (f) Relief developed along the interior margins of Aeolis and Zephyria Plana. (g) At some locations along these margins, alluvial fans formed. (h) At least some fans became indurated. (i) Volcaniclastic and/or aeolian sedimentation covered the region, including the fans. (j) Exhumation and erosion inverted the (indurated) fans and revealed the (previously inverted) paleochannels. (k) Local to sub-regional deformation (e.g., by collapse or tectonism) occurred. Our hypothesized scenario leaves some salient questions, including: i) how robust and regionally applicable is this scenario? ii) what kind of climates and climate changes do these features imply? iii) what non-fluvial modification occurred and when? iv) How does the AD fluvial activity fit within Mars' history?

Testing our hypothesis and addressing the questions: We will test our hypothesis and address these

questions through both regional and local geologic mapping (see Figure 1 in [1]), to document the spatial distribution of fluvial features, their absolute elevations, their superpositional relationships, and their host units. This documentation will let us determine whether the stratigraphic relationships observed in detailed mapping to date (e.g., Figure 1) are indeed consistent regionally or, if not, their prevalence and location(s) of occurrence versus those of other stratal relationships. We will also document nonfluvial strata along with any tectonic and collapse features that may have caused fluvial feature modification. Lastly, through mapping, we will assess whether the topographically low surfaces with lava-like textures constitute a Hesperian-age lava basement beneath the MFF [see 1].

In addition to mapping, we will conduct morphometric analysis, including paleodischarge calculations [cf., 14, see also 1] and drainage density estimates [cf., 15]. Synthesis of these quantitative results with our stratigraphic analysis will allow us to assess the change in paleohydrology with time and to compare AD paleohydrology to that of other regions [e.g., 15].

Outcome: The comparison of flow magnitudes

and drainage densities over time within AD will document regional climate changes. Comparison with paleohydrologic parameter for networks elsewhere on Mars will both augment, and set the AD fluvial activity into, the history of fluvial activity on Mars.

References: [1] Jacobsen and Burr (2014), Planetary Geology Mappers Workshop. [2] Zimbleman and Scheidt, in revision, Geologic Map of the Western and Central Regions of the Medusae Fossae Formation (MC-23 NW and MC-16 NW) on Mars. [3] Mangold et al., (2008) JGR 113, E08009. [4] Weitz et al., (2010) Icarus 205, 73-102. [5] Edgett (2005) Mars Journal, 1, 5-58. [6] Anderson and Bell (2010) Mars Journal, 5, 76-128. [7] Burr et al. (2009) Icarus, 200, 52-76. [8] Zimbleman and Griffin (2010) Icarus, 205, 198-210. [9] Jacobsen & Burr (2012) LPSC Abstract 2398. [10] Jacobsen & Burr (2013) LPSC Abstract 2165. [11] Kite, (2012) LPSC Abstract 2778. [12] Kerber and Head (201) Icarus, 206,669-684. [13] Tanaka et al. (2005) Geologic map of the northern plains of Mars. [14] Burr et al. (2010) JGR 115, E07011. [15] Hynes et al. (2010) JGR 115, E09008. [16] Zimbleman and Scheidt (2012) Science 336, 1683.

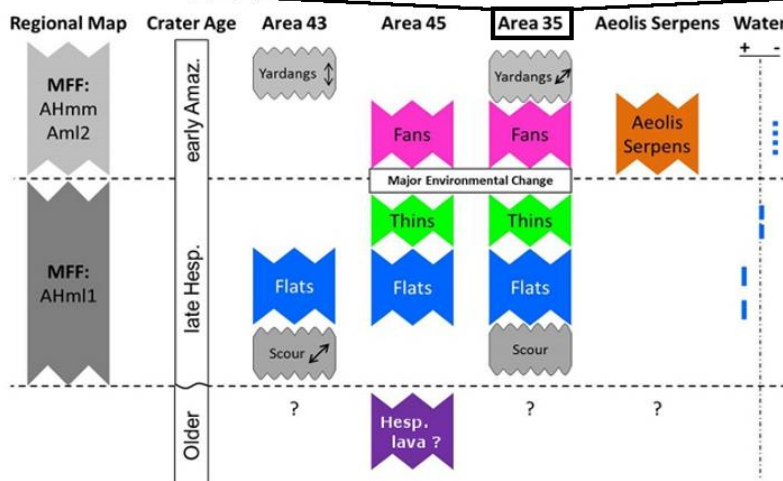
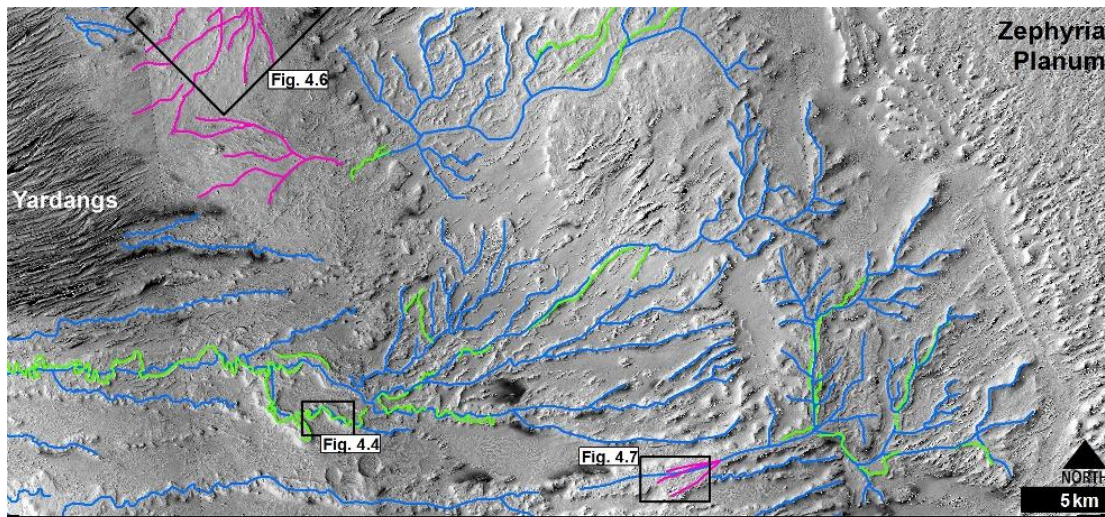


Figure 1: (top) CTX mosaic of Area 35 [7] within AD, showing superposed fluvial features of different morphologies. (left) Local stratigraphies from this and 3 other areas (locations in Figure 1 in [1,10]), along with MFF map units [2] and inferred time-stratigraphic epochs [16]. Double-headed arrows indicate feature orientations. “Water” column indicates relative amounts of water suggested by feature morphologies.

GEOLOGIC MAPPING OF THE MARS SCIENCE LABORATORY LANDING ELLIPSE: UPDATE

F. J. Calef III¹, W. E. Dietrich², L. Edgar³, J. Farmer⁴, A. Fraeman⁵, J. Grotzinger³, M. C. Palucis², T. Parker¹, M. Rice³, S. Rowland⁶, K. M. Stack³, D. Sumner⁷, J. Williams⁷, and the MSL Science Team, ¹Jet Propulsion Laboratory, Pasadena, CA, ²University of Calif., Berkeley, CA., ³Calif. Institute of Technology, Pasadena, CA, ⁴Arizona State Univ., AZ, ⁵Washington Univ. St. Louis, MO, ⁶Univ. of Hawaii, HI, ⁷Univ. of Calif., Davis, CA., ⁷Univ. of New Mexico, NM.

Introduction: The MSL project “crowd sourced” a geologic mapping effort of the nominal landing ellipse in preparation for tactical and strategic mission operations [1]. Six major geologic/geomorphic terrains are defined within the landing ellipse [2]: alluvial fan, smooth hummocky plains, bright-toned “rugged” terrains, flat-lying cratered plains/surfaces, “striated” light-toned outcrops, and light-toned bedded-fractured surfaces. Initial stratigraphic models of these units have been proposed based on our traverse from Bradbury Landing to Glenelg [3]. We’re now in the process of preparing the map for submission with the U.S. Geological Survey.

Geologic Unit Extent: We’ve filled in a few gaps in the geologic map to make mapping complete within the landing ellipse. No units are being introduced in or past the basaltic Baghbold Dunes which run southwest-northeast across the bottom of the ellipse. Peave Vallis fan is being included in the map despite being predominantly outside the landing ellipse. It is considered a major contributor to the landing site geologic unit material.

Map Parameters: The final map will be published at 1:24000 at 40 x 40 inches. Minimal mapping area is set at 400² m (20 x 20 m) which is the approximate size of individual outcrops MSL has visited while remaining visible at the map scale. The projection will be Equidistant Cylindrical with center longitude = 0. A HiRISE visible basemap as well as digital elevation model (DEM) will be distributed with the release including a digital copy of the geologic units and contacts.

Geology: MSL has done contact science on all the major geologic units, except the Peace Vallis alluvial fan material, including drilling on the ‘bedded-fractured’ units in Yellowknife Bay and recently a sandstone unit overlying the complexly layered, fine-grained ‘striated’ unit. A description from in-situ measurements will be provided for every major geologic unit, though some generalization will be necessary to fit the map scale.

The geologic map presented here (Figure 1) contains 6 major units: a texturally smooth unit that makes up the Peace Vallis alluvial fan unit (AF) with many inverted channels that are several meters vertical, the bedded fracture unit (BF) with light-tone and sub-

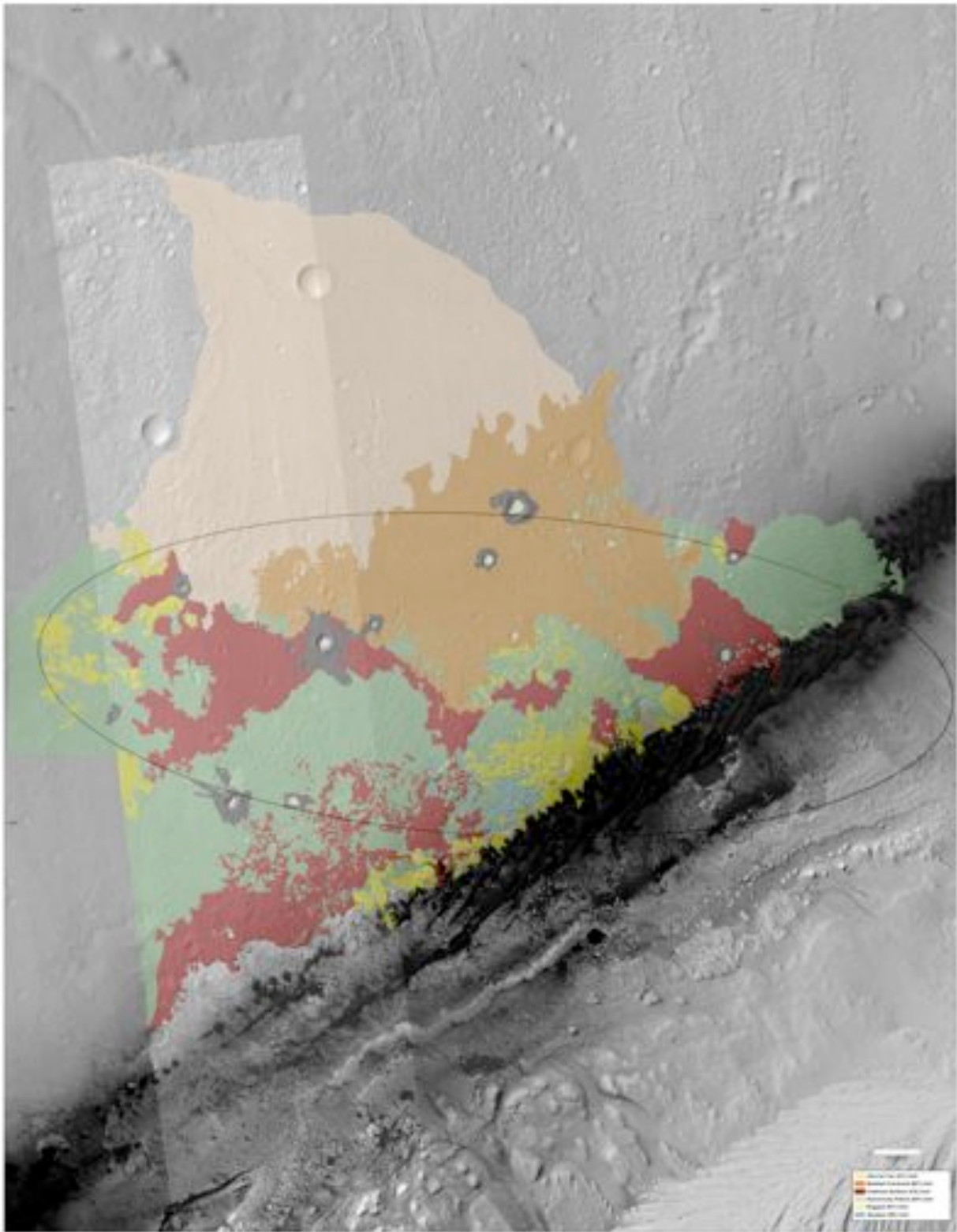
meter width fractures of variable length and spacing, several flat-lying more heavily cratered surfaces (CS), tonally-smooth though topographically hummocky plains unit (HP), bright-toned topographically variable ‘rugged’ unit (RT) composed of material that is not fractured, and a light-toned ‘striated’ unit (ST) made up of crossbedded sandstones. Units for eolian fill/bedforms and obvious continuous ejecta blankets that occasionally covered the major units were also designated, though they are minor components. HP terrain was distinguished as unique and separate from terrain that exists between the northern crater rim and the fan which can contain bright smooth fill in low-lying depressions, although the distinction between these terrains may be minor. RT terrain appears as outcrops on or up through the hummocky plains terrain as ridge or mesa outcrops. The majority of the HP terrain appears as a gravelly lag mixed with other centimeter-sized angular breccia fragments of unknown origin, though some visually look basaltic. Initial stratigraphic relationships have been proposed based on this mapping [3] and the terrains are in approximate stratigraphic order on the map legend, though some relationships are still being debated. For example, there are several spatially and topographically distinct occurrences of cratered surfaces that may be broken out into separate designations based on stratigraphic relationships gleaned from observations along the traverse.

Future work: With our initial mapping complete, the MSL mapping group continues to refine mapped terrains along the rover traverse to Murray Buttes at the lower reaches of Mt. Sharp. Our goal is to have a completed map ready for submission this summer.

References: [1] Calef et al. (2013) LPSC2014, [2] Grotzinger et al. (2014) *Science* [3] Stack et al. (2013).

Acknowledgements: Gale Quad Mapping team: R. Arvidson, J. Berger, J. Blank, J. Bridges, N. Bridges, T. Bristow, F. Calef, P. Conrad, B. Dietrich, G. Dromart, L. Edgar, K. Edgett, J. Eigenbrode, J. Farmer, M. Fisk, J. Grant, S. Gupta, V. Hamilton, A. Hayes, C. Hardgrove, K. Herkenhoff, J. Johnson, L. Kah, R. Leveille, K. Lewis, N. Mangold, R. Milliken, D. Oehler, M. Palucis, T. Parker, M. Rice, S. Rowland, D. Rubin, M. Schmidt, K. Stack, D. Sumner, D. Vaniman, R. Williams, J. Wray, A. Yingst.
JPL/Caltech Copyright 2014. All rights reserved.

Figure 1 (below): Geology map of the MSL landing ellipse.



GEOLOGIC MAPPING OF THE TYRRHENUS MONS LAVA FLOW FIELD, NORTHEAST HELLAS REGION, MARS. David A. Crown and Scott C. Mest, Planetary Science Institute, 1700 E. Ft. Lowell Rd., Suite 106, Tucson, AZ 85719, crown@psi.edu.

Introduction: The ancient, eroded Martian volcano Tyrrhenus Mons is one of the areally extensive, low relief highland paterae found in the circum-Hellas highlands [1-4]. The main edifice of Tyrrhenus Mons is 215 x 350 km; its summit rises only 1.5 km above the surrounding plains resulting in flank slopes of $\sim 1^\circ$ [5]. The volcano displays a central caldera complex (41 x 55 km), and relatively flat-lying, layered deposits heavily dissected by radial valleys characterize its flanks [5-8]. Recent images confirm earlier suggestions that the flanks of Tyrrhenus Mons are composed of friable deposits dissected by fluvial processes. Formation of Tyrrhenus Mons has been attributed to large explosive eruptions in the Late Noachian Epoch that emplaced thick sequences of pyroclastic flow deposits around the volcano's summit for hundreds of kilometers [6, 9-10]. Subsequent effusive activity occurred in the summit region and also formed a large field of lava flows that extends to the southwest toward Hellas basin [6, 11].

Geologic Mapping Study: As part of a new geologic mapping study across the upper reaches of Dao and Niger Valles, we are examining the volcanic landforms and geologic evolution of the Tyrrhenus Mons flow field. New digital geologic mapping using ArcGIS incorporates THEMIS IR (100 m/pixel) and CTX (5 m/pixel) images as well as constraints from MOLA topography. This effort will result in a detailed map of the flow field showing its spatial extent and the distribution of volcanic and erosional features, as well as provide new age constraints on associated volcanic and erosional activity.

Tyrrhenus Mons Lava Flow Field - Previous Studies: Lava flow lobes were recognized southwest of Tyrrhenus Mons, although this region was initially considered to be part of Hesperia Planum, with no direct connection to eruptive vents associated with Tyrrhenus Mons [12]. Systematic mapping studies using Viking Orbiter images defined the boundaries of the flow field and analyzed its surface morphology [6, 11, 13]. Viking-based mapping indicated that the flow field extended for 1000+ km southwest from the volcano's summit, was connected to the central caldera complex via a prominent sinuous rille, and exhibited a series of lava flow lobes (with typical lengths > 50 km) and volcanic channels. Age estimates for various parts of the flow field from superposed craters ranged from middle Hesperian to Early Amazonian [13-14]; a recent analysis using craters ≥ 5 km in diameter suggests a Hesperian age for the entire flow field [15].

Geologic Mapping Results: Mapping progress to-date has included delineation of the boundaries of the flow field, identification and mapping of volcanic and erosional channels within the flow field, and mapping and analysis of lava flow lobes [16]. The high spatial resolution of CTX images, in particular, reveals a variety of previously unrecognized geologic features and allows investigation of the spatial and temporal relationships between volcanic and erosional events.

Lava Flow Lobes: THEMIS IR and CTX images allow improved discrimination of the numerous flow lobes that are observed in the flow field, including refinement of the margins of previously known flows [11] and identification of additional and smaller lobes. Flow lobes have elongate, broad, and digitate forms. Lobes may have central channels and display lateral levees. Lobe widths are relatively uniform in medial and distal zones but flow widening is also observed [17]. Lobe margins range from subtle to well-defined and variations are observed both within an individual flow and between different flows. Some steep-sided margins are evident, similar to those attributed to flow inflation in other regions [e.g., 18]. Several lobes appear to be segmented, suggesting stagnation of the front followed by renewed advance.

Volcanic Channels: A prominent sinuous rille extending from Tyrrhenus Mons' summit caldera defines the flow field's northern margin. The rille changes to a leveed channel at the base of the volcano and discontinuous segments can be observed at distances of up to 650 km from the summit, suggesting it served as a major distributary feature [11]. Flows both emanate from and bury channel segments. Smaller volcanic channels are common throughout the flow field; some occur in segments along crests of local topographic highs and may delineate lava tubes.

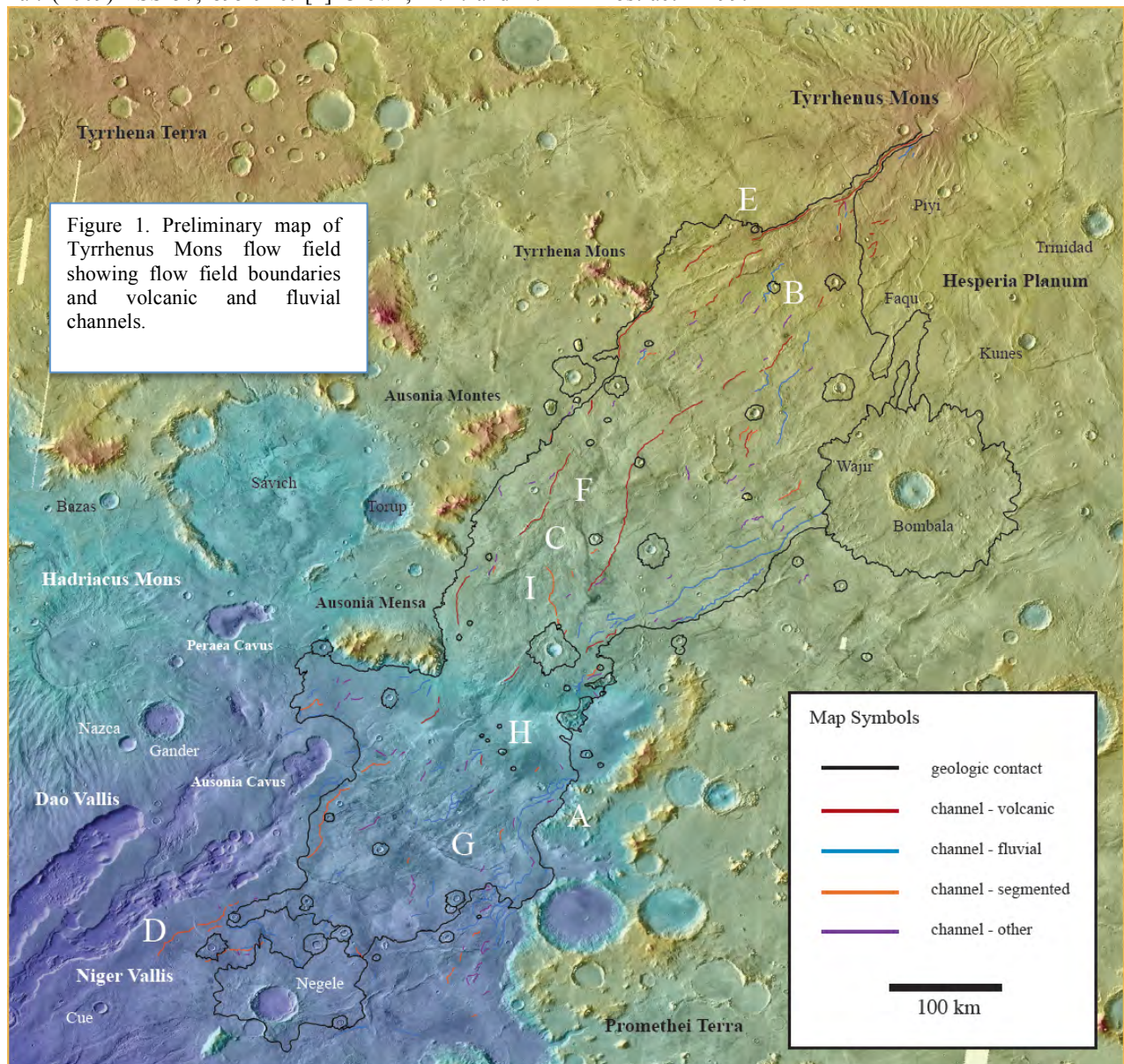
Erosional Channels: Numerous channels are found throughout the flow field, with concentrations noted SW of Bombala crater and in the plains between Dao Vallis and the eroded highland of Promethei Terra. Scour marks, lateral benches or terraces, variations in channel width and depth, braided morphologies, and sinuous planforms are attributed to fluvial processes with contributions from local mass-wasting. In addition, segmented channels consisting of sometimes discontinuous chains of elongate troughs and pits define curvilinear pathways that may delineate sapping channels. These are distinct from features interpreted to be lava tubes because there is no apparent association with flow lobes and because they appear to

cross-cut flow lobes and wrinkle ridges within the flow field and extend beyond flow field margins.

Future Work: THEMIS and CTX images provide important insights into the distribution, nature, and diversity of volcanic and erosional features that characterize the Tyrrhenus Mons flow field and surrounding regions. Further geologic mapping studies, including analyses of individual flow lobes and derivation of flow age estimates, will provide constraints on the volcanic and geologic evolution of Tyrrhenus Mons and the timing and nature of fluvial activity in eastern Hellas.

References: [1] Peterson, J.E. (1978) Proc. LPSC 9th, 3411-3432. [2] Greeley, R. and P.D. Spudis (1981) Rev. Geophys. 19, 13-41. [3] Williams, D.A. et al. (2009) PSS 57, 895-916. [4] Crown, D.A. and R.

Greeley (2007) USGS SIM 2936. [5] Plescia, J.B. (2004) JGR 109, E03003. [6] Greeley, R. and D.A. Crown (1990) JGR 95, 7133-7149. [7] Gregg, T.K.P. et al. (1998) USGS I-2556. [8] Crown, D.A. et al. (2005) JGR 110, E12S22. [9] Crown, D.A. and R. Greeley (1993) JGR 98, 3431-3451. [10] Williams, D.A. et al. (2008) JGR 113, E11005. [11] Crown, D.A. et al. (1991) LPS XXII, 261-262. [12] Greeley, R. and J.E. Guest (1987) USGS I-1802B. [13] Crown, D.A. et al. (1992) Icarus 100, 1-25. [14] Mest, S.C. and D.A. Crown (2001) Icarus 153, 89-110. [15] Crown, D.A. et al. (2007) LPS XXXVIII, Abstract #1169. [16] Crown, D.A. and S.C. Mest (2014) LPS XLV, Abstract #2471. [17] Peitersen, M.N. and D.A. Crown (1999) JGR 104, 8473-8488. [18] Crown, D.A. et al. (2013) LPS XLIV, Abstract #2499.



GEOLOGIC MAPPING OF CENTRAL VALLES MARINERIS, MARS. C. M. Fortezzo¹, K. L. Tanaka¹, P. S. Kumar², and T. Platz^{3,4}, ¹U.S. Geologic Survey, Astrogeology Science Center, 2255 N. Gemini Dr., Flagstaff, Arizona 86001 (cfortezzo@usgs.gov); ²National Geophysical Research Institute, Hyderabad, India; ³Planetary and Remote Sensing, Freie Universität, Berlin, Germany; ⁴Planetary Science Institute, Tucson, AZ.

Introduction: Valles Marineris (VM) constitutes the largest canyon system in the Solar System and has a correspondingly complex history. It consists of interconnected and enclosed troughs that extend from the Tharsis volcanic complex to the southern circum-Chryse outflow channels [1]. The central portion of VM (CVM, Fig. 1) includes the deepest of these troughs.

Within these troughs occur the thickest exposed sections of (a) layered wall rocks on the planet, thought to be mostly lavas and other early crustal rocks [2-3], and (b) light-toned interior layered deposits (ILD), generally thought to be sedimentary or volcanic rocks [4]. The trough floors are extensively covered by landslides, alluvial/delta fans and eolian deposits. In addition, they appear locally dissected by channel networks and include patches of fractured terrain development.

The plateau surfaces that surround these troughs are extensively cratered and modified by contractional (wrinkle) ridges and extensional faults and grabens, some of which are aligned with pit chains. The plateau surfaces are also covered by various types of flow deposits including some of possible volcanic and sedimentary origin. Other surface deposits include patches of light-toned layered deposits (LTLD) and eolian mantles.

Despite numerous studies over the four decades since VM's discovery by the Mariner 9 spacecraft [e.g., 1, 4-6], VM stratigraphy and spatial and temporal evolution remain largely based on lower resolution Viking Orbiter image data and interpolated MOLA topography. Newer image, topographic, and spectral data justify revisiting previous work including (1) mapping of stratigraphic, tectonic, volcanic, mass-wasting, and other geologic landforms and features that document trough development; (2) documentation and interpretation of ILD stratigraphic and compositional variability and timing of formation; and (3) potential far-field influences (e.g., climate, regional geophysics) on CVM development. Given the higher resolution (0.25-100 m/pixel) of the newer data, we limit our study to the CVM region (Fig. 1), where the largest troughs and majority of the ILD occur. This focus still includes most of the typical features of VM.

In this study, we apply stratigraphic and structural mapping and analysis, crater statistics, and hyper-

spectral analyses. In this, our first year of a four year study, we detail the eastern half of the map area.

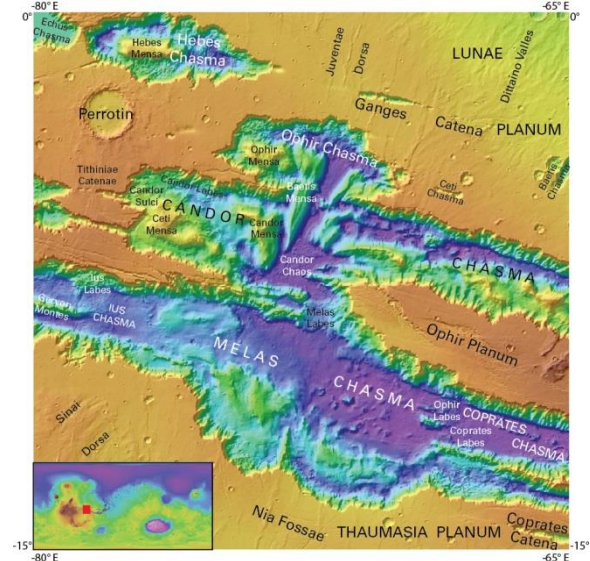


Figure 1: MOLA shaded relief (463 m/pix) overlying THEMIS daytime infrared mosaic (100 m/pix) of the mapping region (0° to 15°S, -80° to -65°E) with nomenclature.

Methodology: Using geographic information system (GIS) software, we are characterizing and mapping the distribution of materials and features exposed within the canyons and on the plateaus surrounding CVM at 1:1,000,000-scale, with drafting at 1:250,000-scale using a linear vertex spacing of 500 m. We are examining the timing relationships among unit outcrops and features through mapping relations (i.e., unit contacts, marker beds, unconformities) and crater densities. For the latter, we are using CraterTools [7], a GIS add-on, to count craters on discrete geologic materials, and CraterStats [8] to plot and determine ages [e.g., 9]. For stratigraphic analysis, we are using the GIS add-on LayerTools [10] to measure orientations of layered materials to help interpret depositional environment and document changes in stratigraphy. Tectonic analyses include (1) characterization of various deformational features (wrinkle ridges, fractures, faults (dip-slip and strike-slip), grabens and folds), (2) their spatial distribution, and relative age relationships, (3) kinematic and dynamic analyses to understand the nature of crustal motion and the stress regimes that were involved in the generation of the deformational features, and (4)

modeling of oblique extension (a right-lateral strike-slip motion followed by rifting).

Datasets: The Mars Reconnaissance Orbiter (MRO) Context Camera (CTX) mosaic provides ~95% coverage over the map area, with 99% coverage within the troughs, at 6 m/pix. This mosaic provides fine details of unit relationships and bulk layering. The CTX mosaic will allow tracing of layered packages throughout the wall rock and within the ILD. The Mars Express High-Resolution Stereo Camera (HRSC) provides both visible-range at 12.5 - 25 m/pix and topography at 50 m/pix. The topography is unprecedented for CVM and provides topographically derived products (e.g., hillshade and slope), and allows detailed 3D visualization. Mars Odyssey THEMIS daytime and nighttime infrared mosaics provide details at 100 m/pix and will aid in determining material variation based on thermal differences. OMEGA and CRISM hyperspectral data will be used to look at the composition of discrete units and examine variance within outcrops at select locations. In addition, we also utilize Mars Global Surveyor MOLA for topographic context outside the map area (460 m/pix), and MRO HiRISE images (≥ 25 cm/pix), where supportive.

Initial CVM mapping results: We have thus far identified eight categories of material units, based on their typical geographical settings, geomorphic expressions, and geologic origins. Categories are made up of multiple map units, subdivided by additional morphology criteria, and by relative age. In addition, we are documenting further temporal relationships within units, including terraces within wall rocks and individual landslide lobes within overlapping sequences. Temporal inferences can be made based on (a) cross-cutting relationships among outcrops of the same unit separated by internal contacts and structures and on (b) dating of temporally related features such as landslide alcove development.

The unit groups consist of: (1) *Surficial materials* including low-albedo mantles, sand sheets, and transverse aeolian ridge fields; (2) *crater and ejecta materials*; (3) *mass wasting* typically proximal to canyon walls with lineated, blocky, stratified blocks, and flow-dominated landslides; (4) *catena materials*, including a floor and a wall unit; (5) *chasma floor materials* consisting of ridged, smooth, rugged materials, and terrace-forming blocks; (6) *interior layered deposits* within VM troughs that include cap rock, and massive or poorly lineated underlying units; (7) *wall deposits* consisting of a gullied unit and smooth, granular unit; and (8) *plateau materials* made up of three widespread plateau units, three fluvial terrace units, flow materials, and a highland massif unit.

In addition, we are mapping linear features where useful in reconstructing the geologic history. These features include unit *contacts* with certain, approximate, buried, and internal younger/older relationship types. *Tectonic features* include inferred grabens, normal faults, and contractional wrinkle ridges. Some *ridges* are differentiated as sinuous (possible inverted fluvial features), curvilinear on landslides, and erosional geomorphologies (yardangs and massifs). *Scarps* are mapped at collapse margins, landslide heads and toes, and flow margins.

The tectonic feature mapping has revealed 5 generations of graben development preserved on the plateau and within the canyon walls: (1) oriented roughly NNE-SSW, mostly confined to Sinai Dorsa, surrounding an ancient caldera; (2) circumferential to the alcoves in southern Melas Chasma, possibly key in the expansion of these alcoves; (3) oriented roughly NNE-SSW, paralleling most of the wrinkle ridges, located in Thaumasia and Lunae Plana, and in the the Tithonian Catenae region; (4) oriented WNW-ESE and paralleling and bounding the chasmata throughout the region, these graben are prevalent on Ophir Planum, may be responsible for canyon widening; (5) isolated to Ophir planum, these are curvilinear faults expressions that may be reactivations of older structures.

Channels and *rilles* are also differentiated to show the influence of volcanic and fluvial processes in the development of CVM. Finally, we map *crater rim crests* and *buried crater* features larger than 5 km.

Future work: In this first year, we are investigating the eastern half of the CVM study area. During the second year we will focus on the western half of the map area, develop a description and correlation of map units, continue crater statistics, bedding orientations in the interior layered deposits, and begin testing formational hypotheses using the mapped structures.

References: [1] Lucchitta B.K. et al. (1992) in Kieffer H.H. et al. (eds.) *Mars*, U. Arizona Press, p. 453-492. [2] McEwen A.S. et al., (1999) *Nature*, 397. [3] Murchie S.L. et al. (2010) *J. Geophys. Res.*, 114. [4] Lucchitta B.K. et al. (1994) *J. Geophys. Res.*, 99. [5] Witbeck N.E. et al. (1991) *USGS Map I-2010*. [6] Dohm J.M. et al. (2009) *J. Volcan. Geotherm. Res.*, 185. [7] Kneissl T. et al. (2010), *Planet. Space Sci.*, 59 (11-12). [8] Michael G.G. and Neukum G. (2010) *Earth Planet. Sci. Lett.*, 294. [9] Platz T., et al. (2013), *Icarus*, 225. [10] Kneissl T. et al. (2010) *LPSC XVI*, Abs. #1640. [11] Tanaka, K.L. et al. (2011) *Euro. Planet. Sci. Conf.*, Abs. #EPSC-DPS2011-269.

GEOLOGIC MAPPING OF ARSIA AND PAVONIS MONTES, MARS. W.B. Garry¹, D.A. Williams², and J.E. Bleacher¹ ¹Planetary Geodynamics Laboratory, Code 698, NASA Goddard Space Flight Center, Greenbelt, MD 20771, brent.garry@nasa.gov, ²School of Earth and Space Exploration, Arizona State University, PO Box 871404, Tempe, AZ 85287.

Introduction: Arsia and Pavonis Montes are two of the three large shield volcanoes that comprise the Tharsis Montes on Mars. Detailed mapping of a limited area of these volcanoes using HRSC images (13-25 m/pixel) revealed a diverse distribution of volcanic landforms within the calderas, and along the flanks, rift aprons, and surrounding plains [1]. We are funded by NASA's Mars Data Analysis Program to complete digital geologic maps of both Arsia and Pavonis Montes based on the mapping style defined by [1,2]. Here, we report on the progress from year 4 of the project [3].

Data and Methods: We are mapping the two volcanoes in ArcMap 10.2 at 1:1,000,000 scale to produce two geologic maps for the USGS. A CTX mosaic serves as the primary basemap, supplemented by HRSC, THEMIS daytime IR, HiRISE, and MOLA data. Our primary objective is to show the areal extent, distribution, and stratigraphic relations of the different lava flow morphologies across each volcano to better understand their evolution and geologic history.

Mapping Progress: Our main objective this year was to map the contacts between different volcanic provinces on each volcano (e.g., main shield, rift aprons, and lava plains) then define the morphologic units on the main shield and rift aprons (Fig. 1). Recent efforts have focused on the northern flank of Pavonis Mons because the rift apron is confined by the main shield, the surficial fan deposit, and the plains lava flows, providing a control area to create a detailed preliminary map at the proposed map scale (Fig. 2). We have also mapped the surficial fan deposits on Pavonis Mons using a sketch map from [5] as a guide and mapping similar units (e.g., smooth, ridged, knobby).

Geologic Units: The current mapping units have evolved from the original proposed mapping units to correspond with units used for the recent geologic map of Olympus Mons [6]. Detailed imagery from CTX has allowed us to diversify the units based on various eruption styles. The units are distinguished primarily by morphology and are grouped for each edifice (main shield, rift apron, fan deposit, lava plains).

Discussion: Our current progress has provided several insights into the eruption processes and evolution of these volcanoes.

Main Shield. The northern region on the main shield of Pavonis Mons (the area west of the northeast rift apron) is comprised of a field of lava fans that begin ~20 km from the edge of the caldera and extend to the base of the shield. The morphology of the lava

fans are characterized by a topographic high at an upslope apex that transitions to a series of flows that spread out downslope. Lava fans embay adjacent fans and appear to serve as the source for fans downslope. The fans are more prominent in the THEMIS daytime IR basemap. Distinct flow features on the lava fans are difficult to determine because they are mantled by dust. No sinuous channels or collapse features are associated with or present along any topographic crests within this particular group of lava fans. These lava fans are morphologically similar to ones identified on Olympus Mons that were not associated with a lava-tube origin [5]. Several lava fans are cross-cut by circumferential graben in that region, indicating these fans were part of the main shield building phase of Pavonis Mons.

Rift Aprons. The NE rift apron on Pavonis Mons is confined on either side by the main shield and surficial fan deposit [4,7,8], plus it is truncated downslope by lava flows that extend from the SW rift apron (Fig. 2). The collapse terrain in this area is not as complex as the other rift aprons. Collapse features have coalesced to form an approximately 25 km-wide, horseshoe-shaped, amphitheater surrounded by additional collapse pits and sinuous channels on the main shield. The majority of the flows present on the apron are muted by dust cover. The younger flow fields (e.g., less dust cover, well-defined flow features) create a channel-fed flow field with individual channels ≤ 150 m wide. These flows extend from partially buried linear vents and sinuous, rille-like channels at the apex of the collapse terrain. The young flows appear to cascade into some of the collapse features to the east, but these flows are cross-cut by prominent, circumferential graben at the base of the apron, which are partially buried by the surficial fan deposit [4,7,8]. Additional mapping will reveal the spatial relationship and relative timing of eruptions to the surrounding plains lava flows and with the other rift aprons.

Recent Volcanism within Surficial Fan Deposits. There are two features, one on each volcano, that appear to be evidence for young, post-glacial volcanism. On Pavonis, a dome (1.5 km diameter) and a lobate feature (5 km) are mapped in the fan deposit. The dome cross-cuts a 5 km long ridge that contains preserved cracks that appear to disturb the surrounding unit. The morphologies are consistent with a volcanic dome & lava flow. The lack of apparent burial by fan-deposit units and well-defined ridge cracks suggest it is a post-glacial eruption feature (<100 Ma) [4,7,8].

On Arsia, flows emanate from a narrow, linear chain of cones in the northern extent of the deposit. The flows appear to embay the ridged unit indicating they were emplaced after the interpreted periods of glaciation in the region. The fan-shaped deposits at Arsia Mons have a cratering model age of <100Ma [7]. This suggests that volcanism associated with the linear cones occurred within the last several 10s of Ma.

General Formation Sequence: Mapping reveals a similar sequence of events for the evolution of both volcanoes that agrees with [1,2,9]: 1) main shield forms, 2) eruptions from the NE/SW rifts emplace long lava flows that surround the main flank, 3) eruptions wane and build up the rift aprons and shield fields, 4) glaciers deposit surficial fan deposit material [4,7,8], and 5) localized recent eruptions along the main flanks, in the calderas, and within the fan-shaped glacial deposits. One of our ongoing questions is whether or not there were eruptions along the flanks of the main shield that coincide with eruptions at the rift aprons. Initial mapping results reveal eruptions that originate along circumferential graben at the base of Pavonis Mons that appear to merge with the plains lava flows. Further mapping will reveal the relative geologic timing of eruptive units on the main shield and provide a more complete analysis of the spatial distribution of tube-fed versus channel-fed flows as originally discussed by [1].

References: [1] Bleacher J. E. et al. (2007) *JGR*, 112, E04003, doi:10.1029/2006JE002826. [2] Bleacher J. E. et al. (2007) *JGR*, 112, E09005, doi:10.1029/2006JE002873. [3] William D. A. et al. (2012) *LPSC 43*, Abstract 1528. [4] Shean D.E. et al. (2005) *JGR*, 110, E05001, doi:10.1029/2004JE002360. [5] Bleacher J.E. et al., (2013) *LPSC 44*, Abstract 2074. [6] Rich-

ardson P.W. et al., (2009) *LPSC 40*, Abstract 1527. [7] Shean D.E. et al. (2007) *JGR*, 112, E03004, doi:10.1029/2006JE002761. [8] Head J.W. and Marchant D. R. (2003) *Geology*, 31, 641-644. [9] Crumpler L.S. and Aubele J.C. (1978) *Icarus*, 34, 496-511.

Acknowledgements: This research is funded by NASA's Mars Data Analysis Program (MDAP) grant NNX10AO15G awarded to D.A. Williams (Arizona State University).

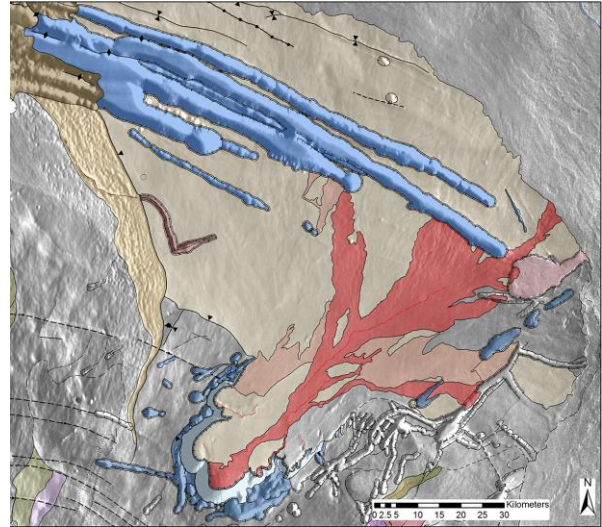


Figure 2. Preliminary geologic map of the NE rift apron on Pavonis Mons overlain on the CTX basemap. The apparent youngest lava flows are in dark red and light red. Relatively older lava flows on the apron are in light yellow. Collapse terrain is in darker blue.

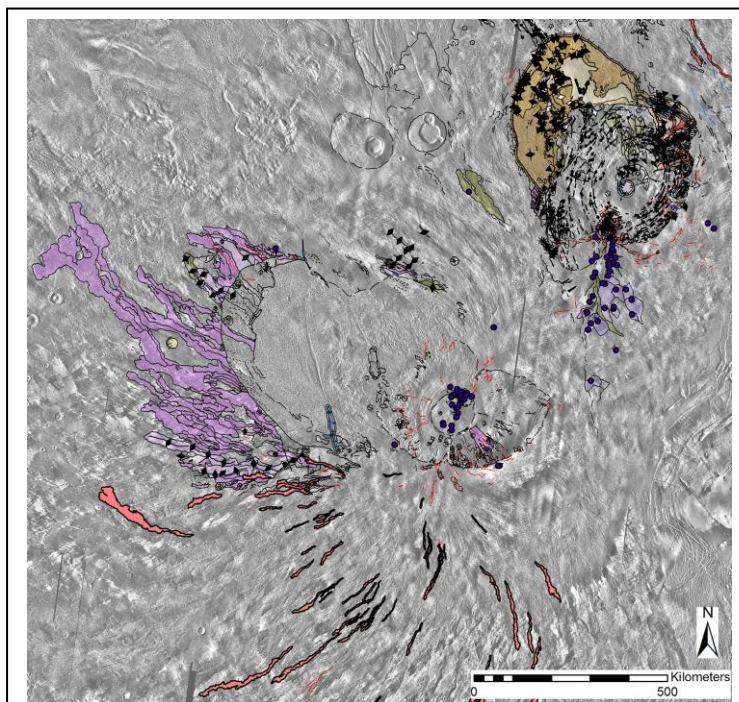


Figure 1. Current progress on the Arsia & Pavonis Montes map.

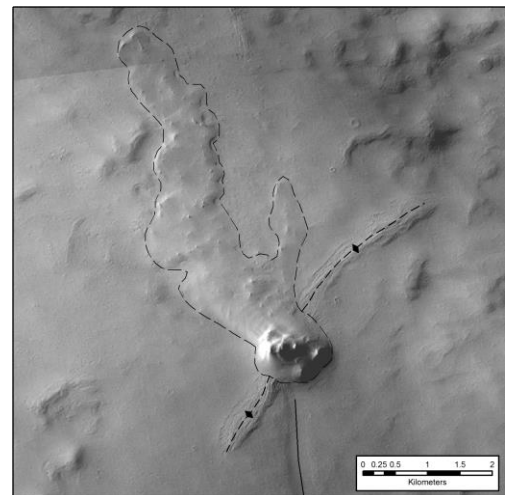


Figure 3. Dome and lava flow (2.9° N, 244.6° E) in surficial fan deposit on Pavonis Mons represents potential post-glacial vol-

canism (<100 Ma). CTX image [NASA/MRO/MSSS].

MAPPING OF FLOOD CHANNELS, ASSOCIATED LAVAS, AND FISSURES IN THE CERBERUS PLAINS, MARS. K. B. Golder and D. M. Burr, Department of Earth & Planetary Sciences, University of Tennessee, 1412 Circle Drive, Knoxville, TN 37996 (kgolder@utk.edu and dburr1@utk.edu)

Introduction: Three large, late Amazonian-aged flood channels are located within the Cerberus plains region of Mars (Fig. 1), each originating from Cerberus Fossae [e.g. 1-4]. Athabasca, Grjotá, and Marte Valles show geomorphological evidence of multiple aqueous flooding events, along with extensive infilling of the channels by lava flows [e.g. 2,4-6]. Previous work documented the flood history within the channels and identified both large- and small-scale flow features originating from the fossae network [2,4,7]. Recently funded work is focused on the implications of the tectonic and lava features, but we have determined that in order to understand the interaction of fissuring events, lava emplacement, and water floods, regional geologic mapping is necessary. An unofficial geologic map with contemporary high-resolution images is newly in development, in order to: (1) investigate the fossae to identify and/or confirm origination site(s) of water and/or lava, including any new flood channels, and (2) study the temporal and spatial relationships among the channels, the fissure system, and volcanic features.

Methods: Our project will build upon previous global [1,8,9] and regional [10-12] geological maps with the aims of refining unit descriptions and spatial distributions, determining contacts between units, and constraining the timing of unit emplacements. Our map will use gridded topography of Mars Orbiter Laser Altimeter data overlain by individual Context Camera images, supplemented with images from the High Resolution Stereo Camera, High Resolution Imaging Science Experiment, and Thermal Emission Imaging System (infrared day- and nighttime images).

Crater counts will be performed in the region in an attempt to bound the timing of the water floods. Late-Amazonian age-dates of lavas within the channels will provide the timing of the latest lavas and of the last geomorphically effective aqueous flooding [2,6,13,14]. Crater counts on the streamlined structures would provide constraints on the timing of earlier in-channel events, and crater counts on the surrounding lava into which the channels are incised will provide age-dates of the pre-flood terrain [6,13,14]. In addition, crater counts will be used to age-date the multiple episodes of lava emplacement (and potentially the associated fissuring) on the Cerberus plains.

Map Units: The following initial map units and brief unit descriptions were developed from previous maps [1,8-12] and new observations in the higher resolution data sets listed above: *Mountainous Terrain:* Closely spaced rugged and degraded plateaus and conical hills, forming highstanding sequences which pro-

trude from embaying low-lying plains materials. *Knobby Terrain:* Conical hills or knobs in irregular concentrations contained within both smooth terrain and embaying plains, with an apparent gradational relationship to Mountainous Terrain. *Cratered Terrain:* Generally highly cratered, uneven surfaces with local high relief that are comprised of significantly modified surfaces. Younger, less modified craters exhibit distinct ejecta blankets. *Ridged Terrain:* Broad planar surfaces with occasional lobate margins, located in intercrater plains. Often contain long, mare-type wrinkle ridges. *Etched Terrain:* Widespread etched materials, varying in texture from relatively smooth and sparsely cratered to rough and eroded, with multiple members and/or units. *Smooth Terrain:* Flat featureless plains, with extremely light cratering. Few distinguishing characteristics observed. *Embaying Terrain:* Low-lying plains that embay highland margins, such as Mountainous and Knobby terrains. Contains apparent flows with lobate margins and small-scale mare-type wrinkle ridges. *Flood Channels:* Outflow channels and margins with erosional features, such as terraces and streamlined mesas. Sinuous and intertwining, with younger channels overprinting larger, older channels. Thermal variance within channels may be indicative of compositional differences in materials [15].

Flood Channels: *Athabasca Valles:* This channel is located along a southwestern extension of the fossae network, and has a flow direction to the southwest [2,4]. The source area is apparently concentrated along one fossa segment with possible initial outflow surge or fountaining to the north and south of the fossa, before being funneled downslope to the south (Fig. 2). The main channel includes numerous streamlined mesas and secondary overprinting channels. Terraces along the streamlined features and islands may be indicative of multiple flows within the main channel body [4]. *Grjotá Valles:* This channel system originates along a northwestern extension of the fossae network with multiple closely-spaced fossa segments [2,4]. Flow direction was initially to the east-northeast, and then (to the east of Tartarus Montes) shifted to the south. *Marte Valles:* This system, the largest of the three channel networks, is located in the eastern portion of the Cerberus plains. Flow direction was initially to the east and then shifted to a north-northeast direction [4]. No source area has previously been identified on the surface, and is likely a now-buried segment of the SE Cerberus Fossae [2,16].

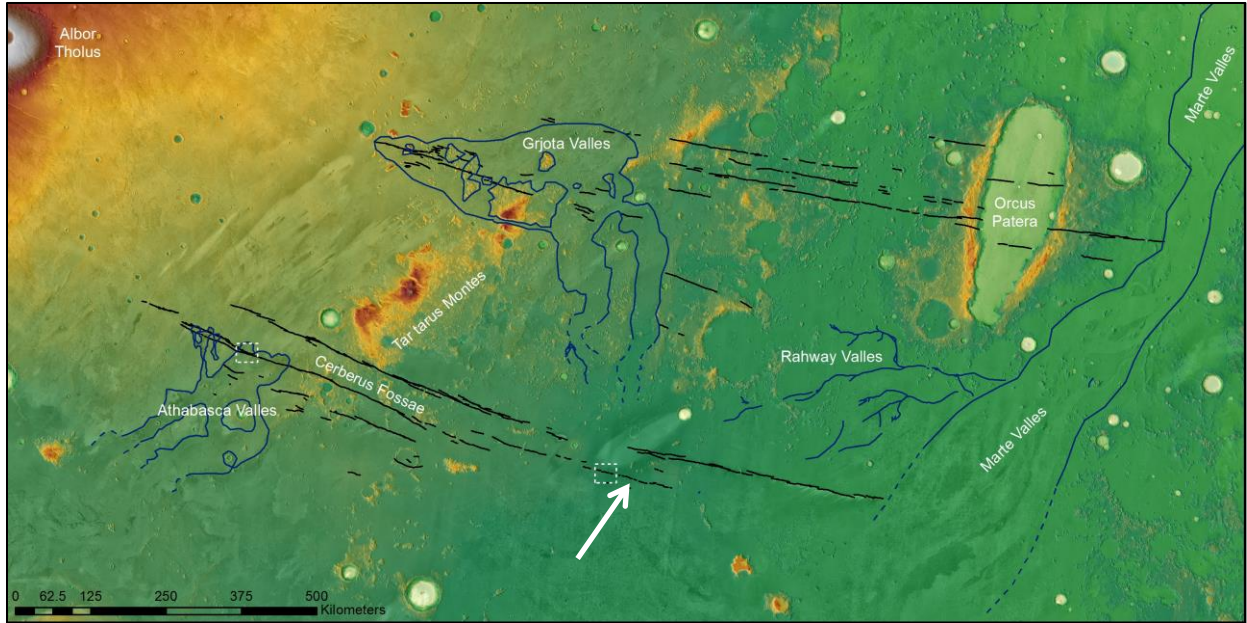


Figure 1: Context image with locations of major flood channels, fossae, and structural elements. Left dashed box denotes location of Figure 2, right dashed box denotes location of Figure 3. Arrow indicates one area of newly mapped fossae segments.

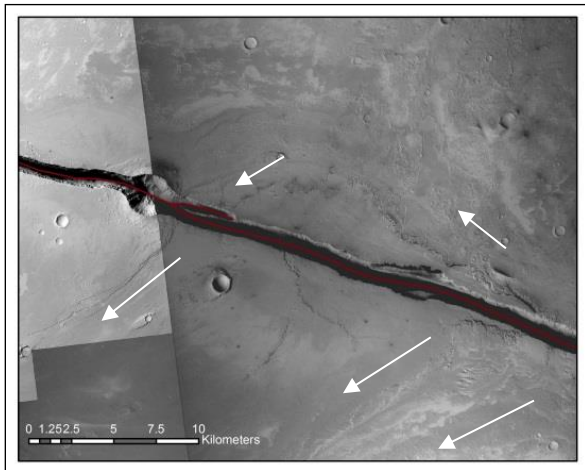


Figure 2: Source of Athabasca Valles. Arrows indicate general flow direction on either side of the fossae segment (red line).

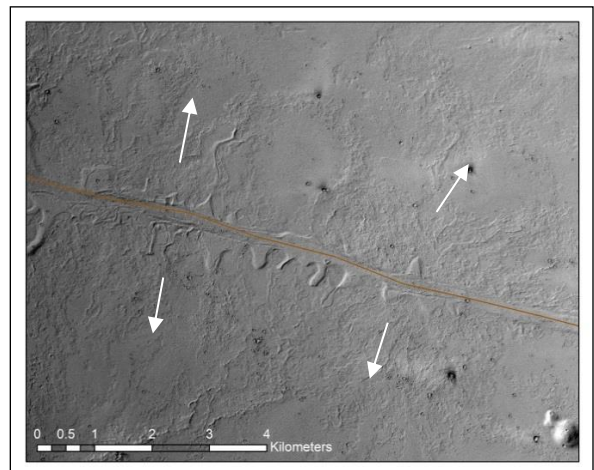


Figure 3: Possible source of Marte Valles. Positive relief lobate features may indicate a radial flow (arrows) from either side of the fossae segment (orange line).

Additional Flows: Rahway Valles is found to the west of Marte Valles, though it is comprised of a branching network of thinner valleys rather than an apparent catastrophic flow channel [3]. Smaller flows of either water or lava emanating from or near the fossae east of Athabasca have previously been identified [e.g. 6,7]. Additional, previously unidentified, large- and small-scale flows may also be present. For example, newly mapped segments of the fossae (Fig. 1, white arrow) exhibit small-scale, positive-relief, lobate margins that may be flow features (Fig. 3).

Future Work: We will continue to explore the interrelationships among these and other features, at both large- and small-scales, in this incipient mapping.

References: [1] Tanaka, K.L. et al. (1992). *USGS Misc. Inv. Ser. Map I-2147*. [2] Burr, D.M. et al. (2002) *Icarus*, 159, 53-73. [3] Plescia (2003). *Icarus*, 164, 79-95. [4] Burr, D.M. et al. (2009). *Cambridge Univ. Press*, 194-208 [5] Plescia, J.B. (1990) *Icarus*, 88, 465-490. [6] Vaucher, J. et al. (2009). *Icarus*, 204, 418-442. [7] Thomas, R.J. (2013) *JGR*, 118, 789-802. [8] Scott, D.H. and Tanaka, K.L. (1986). *USGS Misc. Inv. Ser. Map I-1802-A*. [9] Greeley, R. and Guest, J.E. (1987). *USGS Misc. Inv. Ser. Map I-1802-B*. [10] Scott, D.H. and Allingham, J.W. (1976). *USGS Misc. Inv. Ser. Map I-935*. [11] Scott, D.H. and Chapman, M.G. (1995). *USGS Misc. Inv. Ser. Map I-2397*. [12] Tanaka, K.L. et al. (2005). *USGS Sci. Inv. Map*, SIM2888. [13] Hartmann, W.K. and Berman, D.C. (2002). *JGR*, 105, 15011-15026. [14] McEwen et al. (2005). *Icarus*, 176, 351-381. [15] Keszthelyi, L. et al. (2000). *JGR*, 105, E6. [16] Morgan et al. (2013). *Science*, 340, 607-610.

AGE-DATING AND CHARACTERIZING THE FLUVIAL ACTIVITY IN AEOLIS DORSA, WESTERN MEDUSAE FOSSAE FORMATION, MARS

R. E. Jacobsen, and D. M. Burr, Earth & Planetary Sciences Dept., Univ. of Tennessee, Knoxville, TN (RJacobsen@utk.edu and dburr1@utk.edu).

Introduction: The Aeolis Dorsa (AD) are located in the western Medusae Fossae Formation (MFF), ~800 km northeast of Gale Crater. They comprise a stratified population of ~1,500 sinuous ridges, interpreted to be inverted fluvial deposits [1-4] (Figure 1). These deposits extend from the eroded margins of the westernmost MFF lobes, and into the topographic low between the lobes. The hypothesis of formation for the AD involves orographic precipitation, fluvial run-off, subsequent period(s) of geochemical cementation and burial, and finally, exhumation by aeolian erosion [1-5 and refs. therein]. The AD appear most often in the lowest member of the MFF [1,5,6], which has a minimum age of Late Hesperian [6,7]. A Late Noachian-Early Hesperian age for their fluvial activity has also been posited [8]. Thus, observations of geomorphology and mapping suggest the AD preserve a geospatially extensive record of precipitation and fluvial run-off, but the timing of this activity is not well-constrained.

Whereas our previous work derived local-scale stratigraphy to document relative fluvial history [4,5], we will in future work identify stratigraphic relationships between AD and surrounding geologic units [9,10] to test the maximum age for the fluvial activity. We will also use morphometric analyses to quantify the paleohydrology of AD for comparison with the paleohydrology of the widespread valley networks [11]. These combined efforts will provide a formation-al history of this dense population of fluvial features.

Regional Geologic Setting: North of AD are well-studied lavas plains [12] of Hesperian to Amazonian ages [9 and refs. therein] (Figure 1). Late-Hesperian lava previously embayed the western MFF, indicating a minimum age of Late Hesperian for the deposit [6,7]. Topographic lows in northwestern AD (dashed yellow outlines in Figure 1) expose smooth surfaces with interesting ejecta morphologies [7] and wrinkle ridges. Are these smooth surfaces exposures of a basement unit beneath the AD? Do these surfaces correlate with any surrounding (crater-age-dated) units?

The Aeolis Mensae, located west of AD, are a massive deposit, eroded into troughs, mesas, buttes, and knobs (Figure 1). The Aeolis Mensae overlie a heavily cratered and fluvial eroded, Noachian slope of the southern highlands [10]. Although Aeolis Mensae and the MFF differ in form and possibly age, both preserve complex histories of widespread deposition and erosion [10]. Are the stratigraphies of Aeolis Mensae and the western MFF complementary in the overall regional geologic history? What do their stratigraphic rela-

tionships suggest about the maximum age of the AD?

Hypotheses: Our null hypothesis is that the AD have a maximum age-date of Late Noachian to Early Hesperian [8], coincident with the climatic optimum and the age of most fluvial activity on Mars. Our alternative hypothesis is that the AD are no older than Late Hesperian.

Methods for hypotheses testing: To test the hypotheses, we will look for and date a basement unit beneath AD, e.g., smooth surfaces in northwestern AD. The age of a basement unit would provide a maximum age for AD, by reason of superposition. Correlation of these surfaces and MFF units with the plains lavas [9,12] and Aeolis Mensae [10] may provide additional indicators of age. Structural attitudes will be measured and projected to infer stratigraphic relationships.

Methods for paleohydrology characterization: Measurements of drainage density and estimates of paleodischarge will describe the paleohydrology in AD and provide opportunity to compare fluvial conditions between AD and the fluvial valley networks. Total length of inverted fluvial features for each stratigraphically coeval drainage network will be divided by the convex-hull area around each network (Figure 2). This method overestimates drainage density, but is synonymous with the technique used to calculate drainage density for the valley networks [11, and refs. therein], and so will yield technically comparable results.

Hydrologic techniques for estimating paleodischarge couple measurements of paleochannel width, wavelength, and radius of curvature with empirical relationships between channel morphology and discharge. Relationships are derived from measurements of meandering channels over a wide range of terrestrial environments (Table 1) [e.g., 14]. Paleodischarge estimates from width are considered minimums due to degradation of the paleochannel feature, which may be substantial for some paleochannels in AD [3].

Project Implications: If the maximum age of the AD is during the Noachian-Hesperian transition, the fluvial deposits in AD may be coeval with the majority of valley networks and globally extensive precipitation. This older maximum age would suggest AD preserves an extensive record of fluvial activity that may coincide with the fluvial record in Gale Crater. Alternatively, a maximum age for the AD of Late Hesperian would suggest a period of regional precipitation and channelized run-off, relatively late in Martian history. Such results would expand the geologic context of fluvial activity during the Late Hesperian to beyond the slopes of volcanic edifices [11].

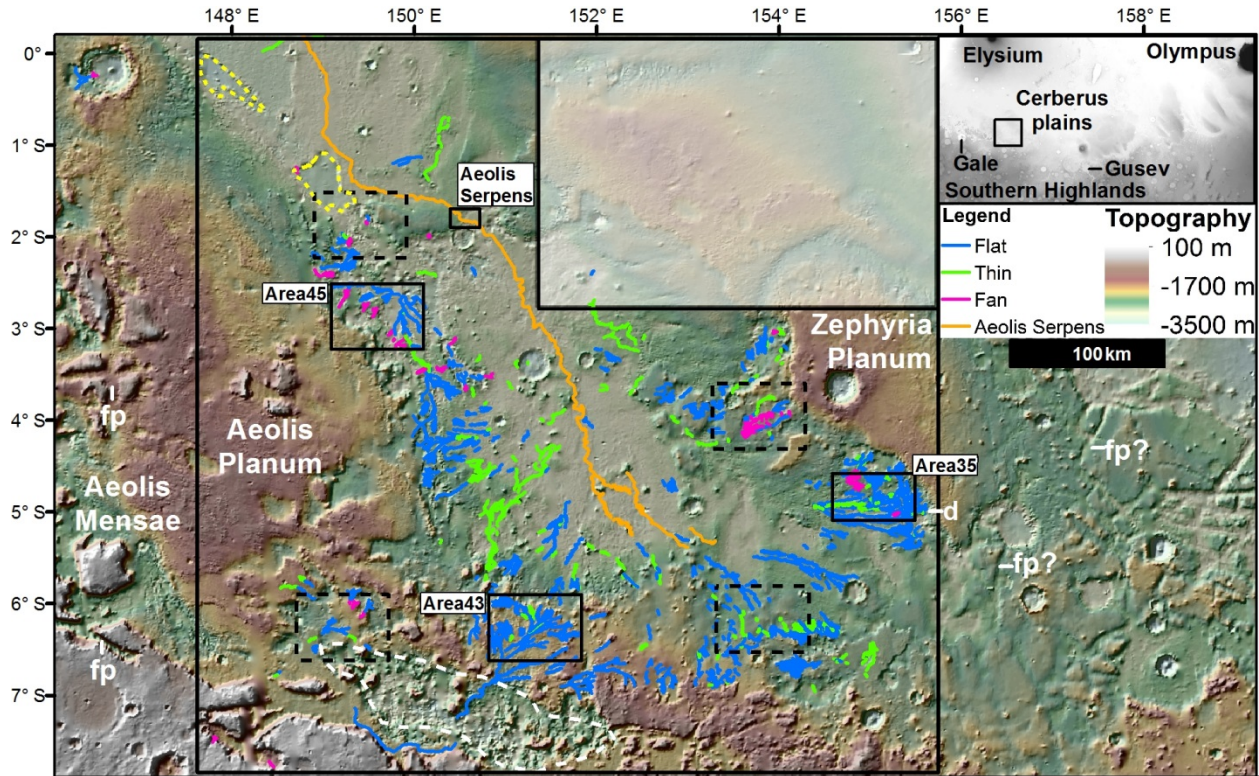


Figure 1: Topographic maps of the AD study area and regional setting (upper right). Large black box shows boundaries of the selected mapping project and position for high-resolution inset map (shaded box, upper center). Delineations shows fluvial features by type [4]. Four small, solid black boxes show locations of previous local-scale stratigraphies [5]. Four small, dashed black boxes show possible locations of additional local-scale geologic mapping and stratigraphy. Yellow dashed outlines show low-elevation surfaces with lava-like textures. White dashed outline shows collapse feature, suggesting regional tectonic deformation across Aeolis Mensae and AD. “fp” denotes the fretted plateau of Aeolis Mensae [10] and “d” shows a hypothesized delta [13].

Table 1: Empirical relationships for estimating discharge (Q) from paleochannel morphology. Measurements include bankfull flow width (W_b), meander wavelength (L_m), and radii of curvature (R_c), which will be measured to estimate W_b . Q_{ave} = average discharge; Q_2 = 2-year-flood discharge; $Q_{1.5}$ = 1.5-year-flood discharge. Empirical relationships from [14 and refs. therein].

$W_b = 0.17R_c^{0.89}$	$Q_{ave} = 0.027W_b^{1.71}$	$Q_2 = 1.9W_b^{1.22}$	$Q_{ave} = 0.000017L_m^{2.15}$	$Q_{1.5} = 0.011L_m^{1.54}$
------------------------	-----------------------------	-----------------------	--------------------------------	-----------------------------

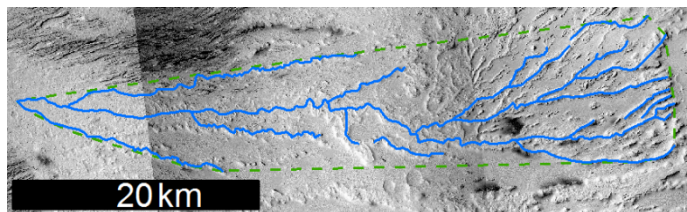


Figure 2: Example of delineated, paleochannel network in eastern AD. Network is identified by interconnected paleochannels of the same morphology. Drainage area (dashed green outline) is taken as the convex hull of the network polylines. Drainage density is calculated from the total length of paleochannels, divided by the area of the drainage network [11].

References: [1] Burr et al. (2009) *Icarus* 200, 52-76. [2] Zimbelman & Griffin (2010) *Icarus* 205, 198-210. [3] Burr et al. (2010) *JGR* 115. [4] Jacobsen & Burr (2012) *LPSC* Abstract 2398. [5] Jacobsen & Burr (2013) *LPSC* Abstract 2165. [6] Zimbelman & Scheidt (2012) *Science* 336, 1683. [7] Kerber & Head (2010) *Icarus* 206, 669-684. [8] Kite et al. (2013) *Icarus* 225, 850-855. [9] Tanaka et al. (2005) *USGS Map*, SI-2888. [10] Irwin et al. (2009) *JGR: Planets* 109. [11] Hynek (2010) *JGR: Planets* 115. [12] Keszthelyi et al. (2000) *JGR: Planets* 105. [13] DiBiase et al. (2013) *JGR: Planets* 118. [14] Williams (1988) in *Flood Geomorphology*, Baker, ed.

GEOLOGIC MAPPING OF UPPER DAO AND NIGER VALLES, NORTHEAST HELLAS, MARS. Scott C. Mest^{1,2}, David A. Crown¹, Joseph Michalski¹, Frank C. Chuang¹, Katherine Price Blount³, and Les F. Bleamaster^{1,4}, ¹Planetary Science Institute, 1700 E. Ft. Lowell Rd., Suite 106, Tucson, AZ 85719; ²Planetary Geodynamics Laboratory, Code 698, NASA GSFC, Greenbelt, MD 20771; ³Texas A&M University-Commerce, Commerce, TX 75428; ⁴Trinity University, San Antonio, TX, 78212; mest@psi.edu.

Introduction: The Hellas basin (~2000 km across, ~8.2 km deep) is the largest well-preserved impact structure on Mars [1,2]. The basin played a significant role in development of the surrounding region, from emplacing its ejecta across the southern highlands, to influencing the locations and orientations of structural, volcanic, and fluvial features, to acting as Mars' largest depositional sink and the origin for seasonal dust storms [e.g., 2-11]. The rim of Hellas and the surrounding highlands have been modified by a diversity of processes and preserve landforms and materials that span the Martian time-scale, including ancient Noachian highlands, Hesperian volcanic and fluvial deposits, and Amazonian eolian deposits and ice-rich flow features.

This abstract highlights the research being conducted in the first year of a four-year project funded through the Planetary Geology and Geophysics Program. This investigation is evaluating the geologic and hydrologic histories of an area along the eastern rim of the Hellas basin where important spatial and temporal relationships between volcanic and volatile-driven processes are preserved (Figure 1). Our study area displays a unique confluence of ancient highland, volcanic (effusive and explosive), fluvial (channels and valles) and mass wasting features and deposits that span much of Mars' history. This location is well suited to evaluate the distribution, relative roles, potential interactions and histories of volcanism and volatiles in one area on Mars using currently available image, spectral, and topographic data. The features of interest for this investigation include the canyons of Dao and Niger Valles, the Tyrrhenus Mons lava flow field, the flanks of Hadriacus Mons, remnants of rugged highlands, extensive channelized plains, and geologically young volatile-rich mass wasting and mantling deposits.

Methodology: This project uses ArcGIS to compile image, topographic and spectral datasets in order to produce a 1:1M-scale geologic map of MTM quadrangles -35262, -35267 and -35272 (Figure 2). This study uses the MO THEMIS daytime thermal infrared (dTIR) brightness temperature global mosaic (~100 m/pixel) as the primary base for mapping geologic contacts, structures, valleys and impact craters (D>1 km). We use CTX images (~5 m/pixel) and THEMIS VIS (~18 m/pixel) multi-band images to provide complementary spatial coverage and to serve as context for high-resolution HiRISE images (<1 m/pixel) and MOC-NA images (~1.5-12 m/pixel), which allow us to provide detailed descriptions of units and features. We

are using THEMIS dTIR images to map compositional variations among surface materials and to distinguish between units with different thermophysical properties, and CRISM multispectral mapping (~100-200 m/pixel) and hyperspectral targeted (~18-36 m/pixel) data to identify the occurrence and distribution of primary minerals, their alteration products within geologic materials at the surface, and outcrops exposed along the walls of the valles, craters and HM flank channels. Relative ages for units and features mapped in MTM Quads -35262, -35267 and -35272 are being determined by compiling crater size-frequency distribution statistics (CSFDs) and evaluating stratigraphic relationships (superposition, cross-cutting, and embayment).

This map area shares its boundaries with five adjacent quadrangles along the northeast/east Hellas rim that have been mapped and published, including MTM Quadrangles -30262 and -30267 [12] and -40262, -40267 and -40272 [10,13]. This effort will complete mapping of most of Hadriacus Mons and all of Dao and Niger Valles at this scale, providing a critical link to these previously mapped quadrangles.

Year 1 Mapping Progress: We are mapping structures, fluvial features, and contacts related to the Tyrrhenus Mons flow field (TMff), and we are beginning to identify and measure impact craters with diameters greater than 1 km to be used for relative age determinations.

Structures within the map area include wrinkle ridges, impact crater rims, and lineations. Wrinkle ridges are observed within the TMff, the widespread plains materials, and on the flank of Hadriacus Mons (HM).

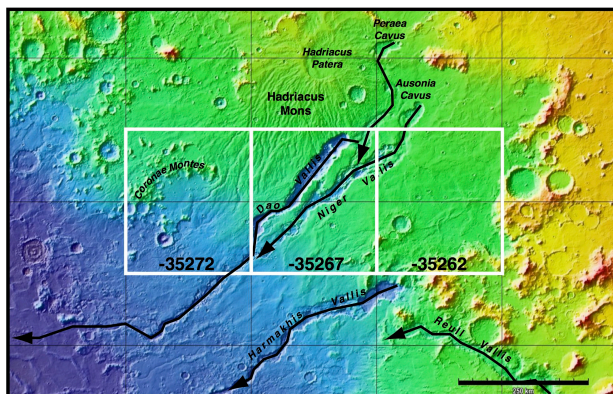


Figure 1. Regional map showing the 3-quad map area (white boxes; Figure 2), locations of valles and montes, and inferred direction of flow through the valles (arrows).

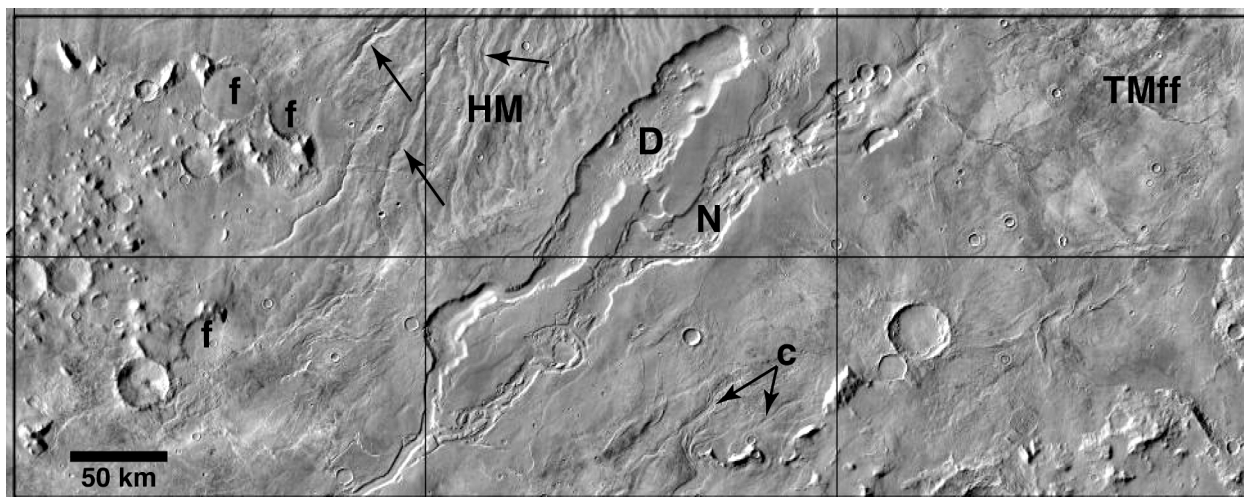


Figure 2. THEMIS daytime TIR mosaic (100 m/pixel) of the 3-quadrant map area includes sections of Dao (D) and Niger (N) Valles, the channelled flanks of Hadriacus Mons (HM; arrows), channeled plains (c), the terminus of the Tyrrenus Mons flow field (TMff), and remnants of highlands and impact craters filled (f) by plains.

The rims of impact craters larger than 3 km in diameter are being mapped along the rim crests; at this scale, 3 km is an adequate size to display the structure and any associated ejecta deposit. Craters of different preservation state – fresh, degraded, and buried – are being mapped with the appropriate symbology. Numerous lineations are being mapped throughout the map area. Lineations are found primarily in the plains and on the TMff, and generally include linear sets of elongated depressions. These features may indicate locations of collapsed volatile-rich plains or collapsed lava tubes [14,15].

Channels and valley features of various types are found on all terrains within the map area. Narrow sinuous channels and broad, flat-floored braided channels are found throughout the plains and TMff. Some of the narrow channels in TMff display leveed margins and are associated with flow lobes, and are likely volcanic in nature; however, some channels in TMff and all narrow channels in the plains lack these features and appear to be erosional [14,15]. The broader flat-floored channels display morphologies produced by fluvial erosion with subsequent modification and widening by mass wasting. Valleys also dissect the flanks of HM, radiating from the volcano's summit [4]. These valleys cut into layered strata interpreted to be pyroclastic deposits [4,16-20].

THEMIS IR and CTX images are being used to provide an improved view of the lobes that compose the TMff [14,15]. This includes refinement of previously known flow margins and identification of additional and smaller lobes. Most lobes have sinuous planform shapes and are oriented in a NE-SW direction, appearing to have flowed to the southwest along the shallow regional slope toward Hellas. Lobes have elongate, broad, and digitate margins that are consistent with lava flows. Lobes may

have central channels and display lateral levees. Lobe margins range from subtle to well defined, and variations are observed both within an individual flow and between different flows [14,15].

Future Work: Plans for our second year of this project include continuing to map contacts, especially within the flow field, plains and HM flanks, and evaluating the origins of valley features and their relationships to the units in which they formed. We will also continue to evaluate the nature of materials in the map area using CRISM.

References: [1] Wilhelms, D.E. (1973) *JGR*, **78**, 4084-4096. [2] Schultz, R.A., and H.V. Frey (1990) *JGR*, **95**, 14,175–14,189. [3] Greeley, R., and J.E. Guest (1987) U.S.G.S. Misc. Inv. Ser. Map, I-1802-B, 1:15M. [4] Crown, D.A., et al. (1992) *Icarus*, **100**, 1-25. [5] Crown, D.A., et al. (2005) *JGR*, **110**, E12S22, doi:10.1029/2005JE002496. [6] Tanaka, K.L., and G.J. Leonard (1995) *JGR*, **100**, 5407-5432. [7] Leonard, G.J., and K.L. Tanaka (2001) U.S.G.S. Geol. Inv. Ser. Map I-2694, 1:5M. [8] Mest, S.C., and D.A. Crown (2001) *Icarus*, **153**, 89-110. [9] Schultz, P.H. (1984) *Proc. Lunar Planet. Sci. Conf.*, 15th, 728–729. [10] Bleamaster, L.F., and D.A. Crown (2010) U.S.G.S. Sci. Inv. Ser. Map 3096, 1:1M. [11] Moore, J.M., and K.S. Edgett (1993) *Geophys. Res. Lett.*, **20**, 1599-1602. [12] Crown, D.A., and R. Greeley (2007) U.S.G.S. Sci. Inv. Ser. Map 2936, 1:1M. [13] Price, K.H. (1998) U.S.G.S. Misc. Inv. Ser. Map I-2557, 1:1M. [14] Crown, D.A., and S.C. Mest [2014] *Lunar and Planet. Sci. Conf. 45th*, Abstract **2471**. [15] Crown, D.A., and S.C. Mest (2014) abstract submitted to Annual Planetary Geologic Mappers Meeting, Flagstaff, AZ. [16] Greeley, R., and P.D. Spudis (1981) *Rev. in Geophys.*, **19**, 13-41. [17] Crown, D.A., et al. (1988) *LPSC XIX*, 229–230. [18] Crown, D.A., and R. Greeley (1993) *JGR*, **98**, 3431–3451. [19] Crown, D.A., and R. Greeley (2007) U.S.G.S. Sci. Inv. Ser. Map 2936, 1:1M. [20] Williams, D.A., et al. (2007) *JGR*, **112**, E10004, doi:10.1029/2007JE002924.

Mapping Hrad Vallis, Mars. P. J. Mouginis-Mark¹ and C. W. Hamilton²; 1. Hawaii Institute Geophysics Planetology, University of Hawaii, Honolulu, HI 96822 (pmm@higp.hawaii.edu); 2. Lunar Planetary Laboratory, University of Arizona, Tucson, AZ, 85721.

Introduction: The flows that originated from Hrad Vallis have been studied for almost 30 years [1–3], and yet numerous aspects of their formation remain unresolved. Possible modes of formation include being lahar deposits [4, 5] or flows generated by the intrusion of a sill into a water-rich substrate [6]. As part of a new 1:175K-scale mapping project, a reappraisal of the properties of these flows and the enigmatic superposed craters is under way, aided by the significantly improved spatial coverage from Context Camera (CTX) images over earlier data. The new map area (Fig. 1a) extends from 33.3°N to 35.7°N, and 140.7°E to 142.6°E.

Two discrete flows within the lobate deposits from Hrad Vallis have been identified [3, 6, 7], with a lower flow unit originating from the eastern section of fractures and an upper flow from the western segment of the Hrad Vallis fracture. Superposition relationships show that the upper flow formed second, and emerged from the same (western) fissure segment from which water originated but that the detailed stratigraphy remains unresolved and hence the exact timing (perhaps on an hour-by-hour basis) of material flow is not known so the mechanism of flow formation is currently unresolved.

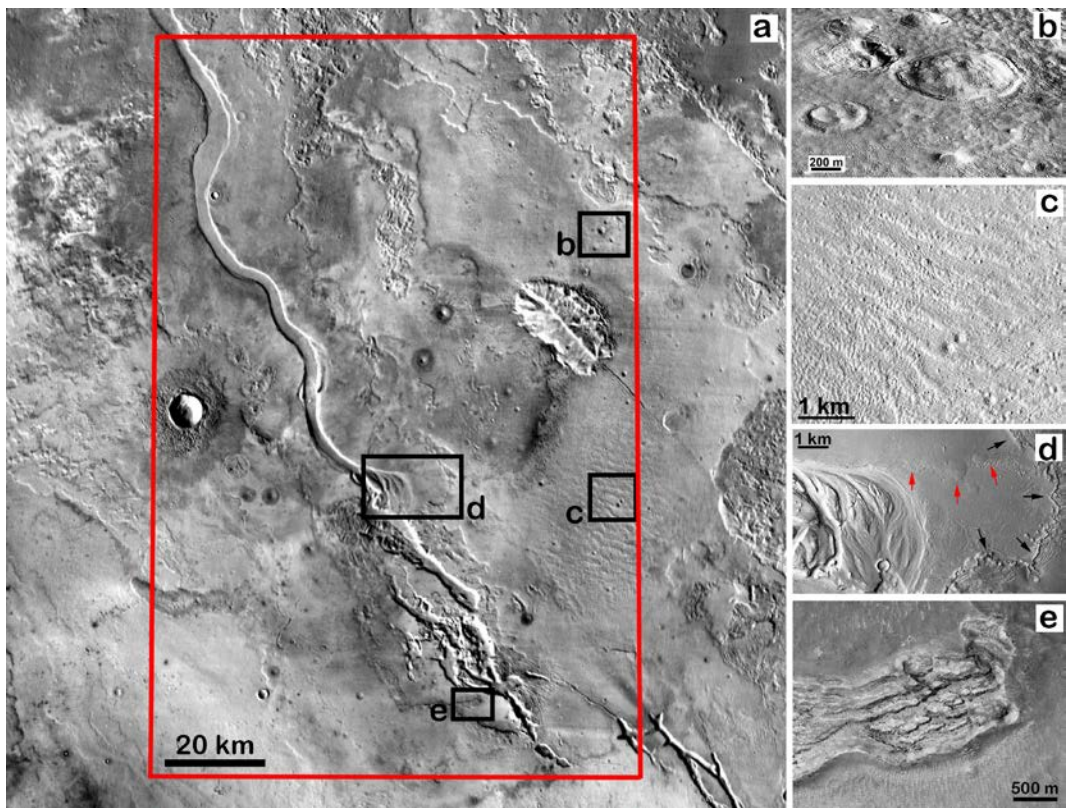


Fig. 1: (a) The map area (red box). Base is a mosaic of THEMIS daytime IR images. Boxes at right show just some of the attributes of this area that will be studied in detail, including: (b) domes ~20–25 m high [7], (c) ridges on the flow unit that may better define the flow regime during emplacement; (d) over-spill areas associated with the discharge of more fluid material (perhaps aqueous) late in the formation of Hrad Vallis. Black arrows point to a depositional ridge, and red arrows mark the edge of a flow that moved back towards the fracture; and (e) a late-stage flow lobe that moved towards the main fissure.

Objective	Goal	Significance
2.1: Generate geologic maps and to establish the chronology of units near Hrad Vallis.	Determine the spatial and temporal relationship between unusual geologic units near the Hrad Vallis source region to better constrain their origins and significance.	Hrad Vallis and related lobate units may represent the products of aqueous floods or lava flows, but these origins imply very different paleo-environmental conditions.
2.2: Evaluate the prevailing hypothesis for the origin of Hrad Vallis.	Assess if Hrad Vallis formed in association with phreatomagmatic explosive activity and mud flows generated by shallow igneous intrusions into ice-rich rock.	If this integration is correct, Hrad Vallis represents an archetypical end-member for aqueous flooding events on Mars during the Amazonian Era.
2.3: Test alternative hypotheses for the origin of Hrad Vallis.	An alternative hypothesis for the origin of lobate units in near Hrad Vallis is that they are inflated lava flow features that may have interacted with near-surface ground-ice.	Careful geologic mapping and spatial analysis of lobate units and features within them will help to discriminate between proposed aqueous and volcanic origins.
2.4: Examine five critical localities near the Hrad Vallis source region.	Examine (a) flow around pre-existing obstacles; (d) delta deposits; (c) late-stage remobilized flows; (d) morphology of the Hrad Vallis rim; and (e) structural controls.	Characterizing facies relationships in these regions will complement general geologic maps and spatial analysis to better understand unit emplacement processes.

Table 1: Objectives, goals and significance for the production of this new map.

Key questions addressed with the new map:

Table 1 lists the objectives, goals and perceived significance of the new mapping effort. The new 1:175K map will be supplemented with higher resolution mapping (at scales of 1:50K to 1:100K) of selected areas using CTX and High Resolution Imaging Science Experiment (HiRISE) images and digital elevation models derived from these data. This will enable us to focus on the identification of features that might support or refute the idea that the landscape formed as a consequence of a dike intrusion into permafrost [6], and to deduce details of the timing of the geologic processes. In addition, the origin of >625 craters [7] on the lobate deposits will be investigated. The larger (>1 km diameter) examples of these craters have already been shown to possess thermal anomalies [8]. These craters may have formed by explosive activity associated with hot material flowing over ice-rich ground. Alternatively, they could be analogous to lava pits [9], wherein they represent depressions on the flow lobe surface due to inflation of material around this location. A spatial analysis of the distribution of these craters will be conducted to infer if there is any preferential

pattern to their distribution. Details of the flow lobes movement will also be investigated. Mapping of ridges that exist on the surface of the flow will provide information on motion of the flows as they encountered topographic highs. The largest of these pre-existing obstacles is Galaxius Mons (34.8°N, 142.3°E), which will be studied in detail in order to determine if either of the lobate flows over-rode the crest of the ~130 meter-high obstacle.

References: [1] Mouginis-Mark, P. J. (1985). *Icarus* 64, 265–284. [2] De Hon, R. A. (1992). *Proc. Lunar Planet. Sci. Conf.* 22, 45–51. [3] De Hon, R. *et al.* (1999). *U.S.G.S. Misc. Map I-2579*. [4] Christiansen, E. H. (1989). *Geology* 17, 203–206. [5] Pedersen, G. B. M. and J. W. Head (2013). 44th *LPSC*, abstract #1514. [6] Wilson, L. and P. J. Mouginis-Mark (2003). *J. Geophys. Res.* 108, doi: 10.1029/2002JE001927. [7] Mouginis-Mark, P. J. (2014). 45th *LPSC*, abstract #1139. [8] Morris, A. R. and P. J. Mouginis-Mark (2006). *Icarus* 180, 335–347. [9] Walker, G. P. L. (1991). *Bull. Volcanol.* 53, 546–558.

HIGH RESOLUTION GEOLOGIC AND STRUCTURAL MAPPING IN WEST CANDOR CHASMA, MARS: 2014 FINAL STATUS REPORT. C. H. Okubo¹ and T. A. Gaither², ¹US Geological Survey, 1541 E. University Blvd., Tucson, AZ 85721, cokubo@usgs.gov, ²US Geological Survey, 2255 N. Gemini Dr., Flagstaff, AZ, 86001.

Introduction: Our current PGG-funded project to construct high resolution (1:18,000 scale) geologic and structural maps of four areas in west Candor Chasma is nearing completion. The first of these maps [1], which covers the western Candor Colles region is currently in press. The remaining three maps are complete and have been submitted for review. These maps focus on the southwest Ceti Mensa, west Ceti Mensa and east Candor Sulci regions (Fig 1). This abstract provides a brief overview of these latter three maps.

The objectives of this project are to gather high-resolution structural measurements in order to 1) refine the geologic unit boundaries in this area that were previously established by [2], 2) revise the local stratigraphy where necessary, 3) characterize bedforms to help constrain depositional processes, and 4) determine the styles and extent of deformation to better inform reconstructions of the local post-depositional geologic history. These observations in key areas of west Candor Chasma will form the basis for refining current understanding of the present-day geology and past history of this part of Valles Marineris.

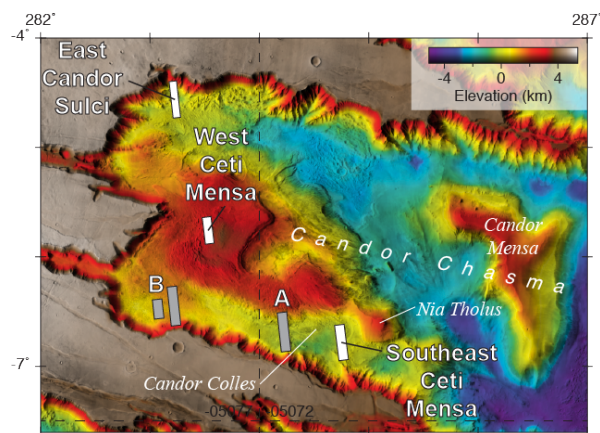


Fig 1. Locations of the southeast Ceti Mensa, west Ceti Mensa and east Candor Sulci map areas in west Candor Chasma. Also shown are the locations of previous high-resolution mapping (A) [1] and (B) [3, 4]. Basemap is colorized MOLA elevation overlaid on THEMIS daytime IR.

Data: Stereo observations from the High Resolution Imaging Science Experiment (HiRISE) camera were used as the primary data set for these maps. DEMs with 1-m post spacings were extracted from the

red bandpasses of the respective HiRISE stereo observations following [5]. In turn, each HiRISE image was orthorectified to the DEM and output at 1 m/pixel and 0.25 m/pixel. The 1 m/pixel versions of the orthorectified HiRISE images served as the mapping base. Mapping was conducted exclusively within the areal extent of each DEM, thus the region of stereo overlap in the HiRISE data defines the extent of each map area. All data used in the construction of these maps were obtained from the NASA Planetary Data System.

Methodology: All mapping was conducted using the ArcMap® 10.1 and 10.2 geographic information system software package. A separate ArcMap® project was set up for each map area, and the corresponding HiRISE DEMs and orthorectified images were imported into each project. Features were point digitized at 1:4,000 to 1:6,000 scale. Linear features with a length of less than 50 m and area features less than 20 m in maximum extent were not mapped. All structural orientation measurements (strike and dip) were made using the Layer Tools plug-in for ArcMap® [6].

In these maps, all units are allostratigraphic; that is, they are defined by unconformities at their upper and lower contacts. Allostratigraphy was selected because at HiRISE scale, bounding unconformities can be directly observed, are the most prominent stratigraphic divisions, and are mappable in a systematic way.

Map symbology is taken from the Federal Geographic Data Committee's (FGDC) digital geologic map standard in compliance with U.S. Geological Survey cartographic standards. The FGDC standards developed for terrestrial mapping applications are used here instead of the traditional planetary map standards. The planetary map standards do not sufficiently capture the level of classification and certainty that is obtained at the scale of mapping done here.

Age Determinations: Previous geologic maps of west Candor Chasma assigned chronostratigraphic designations (Noachian, Hesperian, Amazonian) to the various mapped units (e.g., [2, 7, 8]). These ages were not adopted here because the significant increase in mapping scale enabled by HiRISE and CTX data calls for a reassessment of these classic Viking-based units and relative ages. New crater counts of the units mapped here were not acquired because these sedimentary rocks likely consist of sulfate-rich sands similar to those found in Meridiani Planum [9], and the standard techniques for relative age dating based on impact

crater retention cannot be relied upon in these highly friable deposits. Thus the relative ages of the mapped units are determined on the sole basis of superposition.

Southeast Ceti Mensa: This map area contains six units of layered sedimentary material, plus one unit of colluvium derived from the volcanic wall rock of west Candor Chasma (unit cf). The four oldest units in this map area comprise the adjacent Nia Tholus and are named the Nia Tholus lower 1 through 4 units. The lowest of these, NiT₁₁ buries unit cf and the volcanic wall rock of west Candor Chasma. This unit was subsequently buried by units NiT₁₂, NiT₁₃, and NiT₁₄. Layers within these four units are sub-horizontal, with some northerly-dipping bedding prevalent in units NiT₁₁ and NiT₁₂ near the south wall of west Candor Chasma. Deposition of each Nia Tholus lower unit was followed by a period of regional deflation.

Unit NiT₁₄ is buried by the Candor Colles unit (CaC), which was first described in the adjacent map of [1]. Following the deposition and subsequent regional deflation of unit CaC, several (~3 to 5) other layered sedimentary units were deposited, each bounded by a regional unconformity. These units are not present in this map area, but can be observed in adjacent HiRISE and CTX data.

This stack of sediments was then subjected to an episode of deep deflation, which cut down through unit CaC, its subsequent units and all of the Nia Tholus lower units. This deflation event produced a paleo-moat between the wall of west Candor Chasma and Ceti Mensa, similar to the region's present-day moat.

During formation of the paleo-moat, the sedimentary units above unit CaC became unstable, and a portion of Ceti Mensa failed, forming a large landslide. This landslide was composed of materials from an undetermined number of sedimentary units that post-date unit CaC, and the landslide came to rest within the nascent paleo-moat. This landslide deposit is delineated as the Ceti Mensa southeast blocky unit (CeM_{SEb}). Unit CeM_{SEb} contains a breccia facies that is interpreted to consist of comminuted fragments of the failed sedimentary rocks. The morphology of this landslide resembles an earth flow, suggesting that the affected sediments were poorly consolidated and water saturated at the time of failure (c.f., [10]). The triggering mechanism for this landslide has not been determined, but may have involved conditions such as oversteepening of the slopes of Ceti Mensa due to erosion (deflation), a rise in the groundwater table, or seismic shaking from a nearby marsquake or impact event.

West Ceti Mensa: This map area contains three units of layered sedimentary material and is near the summit of Ceti Mensa. The oldest unit is the Ceti Mensa west hummocky unit (CeM_{Wh}), which was deposited

on top of older layered sedimentary units that comprise Ceti Mensa. Following deposition, unit CeM_{Wh} experienced slope failure and landsliding, resulting in the formation of its characteristic elongated knobs and ridges. Each knob is a block within the landslide, and the ridges are interpreted as pressure ridges within the toe region of the slide. The morphology of this landslide is consistent with an earth spread, indicating that unit CeM_{Wh} was poorly consolidated and water saturated at the time of failure (c.f., [10]).

Following the landsliding of unit CeM_{Wh}, the Ceti Mensa west mottled unit (CeM_{Wm}) was deposited. Deposition of unit CeM_{Wm} eventually ceased and the region experienced a period of deflation. This deflation event eroded through unit CeM_{Wm} and exposed the underlying landslide blocks of unit CeM_{Wh}. The Ceti Mensa west upper unit (CeM_{Wu}) was then deposited on top of this deflation surface. Meter-scale cross bedding and dune-forms within unit CeM_{Wu} indicate that these sediments were subjected to unidirectional lateral transport during deposition.

East Candor Sulci: This map area contains exposures of the volcanic rock in the north wall of west Candor Chasma (cwr), unit cf, portions of the Candor Labes landslide (CaL), and one unit of layered sedimentary material, the Candor Sulci (CaS) unit.

The oldest unit in the map area is unit cwr. Units cf and CaL were then derived from unit cwr through slope degradation and failure. Unit CaS was subsequently deposited. This deposition appears to have occurred in a low energy environment, since the accumulations of unit cf and the primary landslide textures of unit CaL were preserved.

Unit CaS then experienced a large slope failure. Unit CaS contains a breccia facies that is interpreted to be comminuted CaS material along the basal shear zone of this landslide. The landslide moved in a northerly direction, which is downslope from portions of unit CaS located at higher elevations to the south (on the lower slopes of Ceti Mensa). The morphology of this landslide is consistent with a translational slide, suggesting unit CaS was water saturated at the time of failure and that sliding occurred along subhorizontal bedding planes (c.f., [10]).

References: [1] Okubo, C.H. (2015) *USGS SIM in press*. [2] Witbeck N.E. et al. (1991) *USGS Map I-2010*. [3] Okubo C.H. et al. (2008) *JGR*, 113, E12002. [4] Okubo C.H. (2010) *Icarus*, 207, 210-225. [5] Kirk R.L. (2008) *JGR*, 113, E00A24. [6] Kneissl T.A. et al. (2010) *LPSC XLI*, Abstract #1640. [7] Scott D.H. and Tanaka K.L. (1986) *USGS Map I-1802-A*. [8] Lucchitta B.K. (1999) *USGS Map I-2568*. [9] Murchie S.L. et al. (2009) *JGR*, 114, E00D05. [10] Varnes D.J. (1978) *Transportation Research Board Spec. Pub. 176*, 12-33.

MAPPING MARS AT 1-25 CM/PIXEL: IDENTIFICATION OF COASTAL PROCESSES AT THE OPPORTUNITY LANDING SITE. T. J. Parker¹ and B. G. Bills¹, and the MER Science Team, ¹Jet Propulsion Laboratory, California Institute of Technology, (timothy.j.parker@jpl.nasa.gov, bruce.bills@jpl.nasa.gov).

Introduction: Ground access to geologic units identifiable from orbit has enabled unequivocal determination of their origins. Or has it?

Observations: Opportunity is currently working its way south along the west rim of the 22-km Endeavour Crater at Cape Tribulation. The rim and interior of the crater is partly obscured by the familiar sulfate sandstones and mudstones of Meridiani Planum. The contact between the plains and the rim inselbergs is defined by an apron, typically about 15-20 meters in width and elevated slightly above the surrounding plains. In monoscopic orbiter images, this bench suggests a horizontal surface at the base of the inselbergs. However, digital elevation models made from CTX and HiRISE stereo images show these aprons define approximate planar surfaces sloping downward into the crater interior by several degrees (Fig 1).

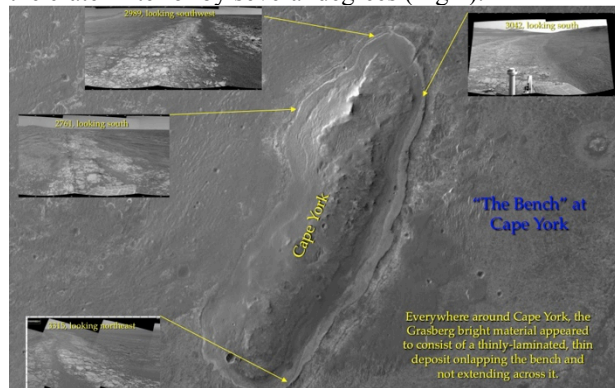


Figure 1: Cape York, with examples of bench morphology observed by the Opportunity rover. Scene width ~1400m.

The bench is best exposed along the west and east rim mountains. From orbit, it exhibits four principal elements. From the plains, upslope, they are: 1, a basal scarp up to a few tens of centimeters high; 2, a margin of bright outcrop that appears to either onlap or protrude from beneath 3, a smooth darker slope ex-

tending from the bright outcrop up to 4, a low escarpment or “berm” at the base of the rougher-looking surface of the Endeavour rim and a few meters upslope from the basal scarp.

Cape York (Figs 1, 2) was the first of the west rim mountains visited by Opportunity, followed by Sutherland Pt./Nobbys Head (Fig 3), Solander Pt, and finally Cape Tribulation (at time of this writing). Opportunity has imaged the bench at several locations around these inselbergs with the navigation and panorama cameras (navcam and pancam). From the ground, the basal scarp does appear to be an erosional feature, as does the berm separating the bench or apron from the Endeavour rim surfaces. The bright outcrop margin (the “Grasberg unit”) is the most prominent of several successive onlaps of thinly-laminated sulfate sediments onto the crater rim inselbergs.

Coastal Interpretation: Morphologically and stratigraphically, these onlaps are strikingly similar to terrestrial beachrock, but are sulfate rather than carbonate. If the bench, berms and onlaps once defined horizontal erosional and depositional surfaces, then the tilt of both the plains margin and the inselbergs inward toward the crater interior must indicate a subsidence of these surfaces within and near the crater that is opposite the isostatic rebound one finds with paleolakes on Earth. The crater seems to be too small a feature for a tectonism to be the cause of the tilt. Perhaps sediment dewatering and compaction over time is responsible. This might also suggest that the sediment is thicker or was deposited more rapidly inside the crater interior than outside, which might be expected in partially-buried cratered highland topography.

References: [1] Benson L. (2004) *USGS Circ* 1267. [2] Alsharhan A. S. and Kendall, C. G. St. C. (2003) *Earth-Sci. Rev.* 61, 191-243

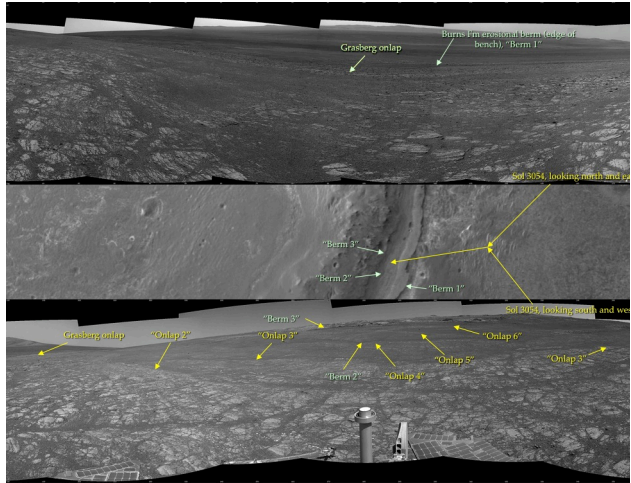


Figure 2: Navcam 360° panorama taken from apron on east side of Cape York by the Opportunity rover on Sol 3054. Burns Fm. is beyond “Berm 1” in top scene (viewing east). The rover is located on one of the Grasberg units, which appear to onlap Cape York in a series of as many as 6 flaps (indicated in yellow) – similar to shingles installed backwards on a roof. The sulfates are thinly-laminated, with the laminations dipping downslope away from Cape York. In green, 3 berms are interpreted as erosional features of the apron. The surface of the apron is smoother than that of the Shoemaker Fm rim materials comprising the Cape York rim inselberg. Thus both erosional reworking and sediment deposition is implied.

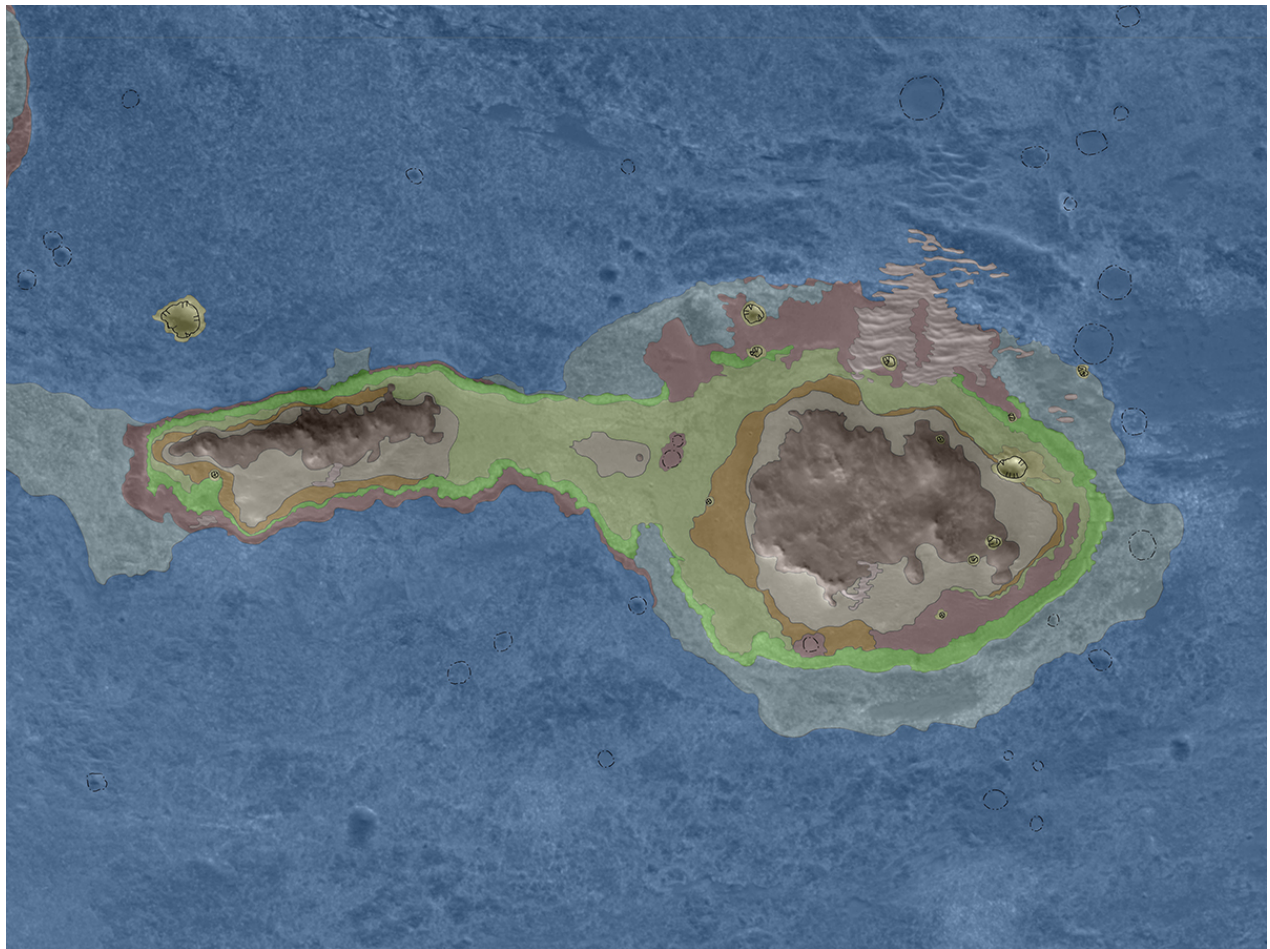


Figure 3: Preliminary geologic map of Sutherland Pt and Nobbys Head, west Endeavour crater rim (North toward left, scene width 675 meters, crater interior toward top). Units are inferred to represent a series of successively less-extensive onlaps onto the crater rim inselbergs (dark brown). Youngest to oldest: Blue = undifferentiated Burns Fm (“onlap 2”). Light blue = Burns Fm “onlap 1”. Bright green = Grasberg member of Burns Fm. Olive = Lower Grasberg member, Burns Fm. Sepia = Apron “onlap 2”. Tan = Apron “onlap 1”. Brown = Shoemaker Fm, undifferentiated.

GEOLOGIC MAPPING TO CONSTRAIN THE SOURCES AND TIMING OF FLUVIAL ACTIVITY IN WESTERN LADON BASIN, MARS. C.M. Weitz¹, S.A. Wilson², R.P. Irwin III², and J.A. Grant², ¹Planetary Science Institute, 1700 E Fort Lowell, Suite 106, Tucson, AZ 85719 (weitz@psi.edu); ²Smithsonian Institution, National Air and Space Museum, Center for Earth and Planetary Studies, MRC 315, Independence Ave. at 6th St. SW, Washington DC 20013.

Introduction: The western section of Ladon basin and its bounding basin ring structures to the west hold numerous clues to understanding the long history of drainage across the Margaritifer Terra region of Mars. Recent and ongoing studies have placed important constraints on water-driven degradation of Ladon basin, Ladon and Uzboi Valles to the south, Holden crater, Eberswalde crater, and numerous intracrater alluvial fans in the region (1-7). In addition, preliminary analysis suggests that the intervening region and the west side of Ladon basin hold important new clues to understanding the regional to perhaps global conditions when water was flowing on the surface.

We are currently mapping two quadrangles in Margaritifer Terra (–15032 and –20032, Figure 1) to define the evolution of the western Ladon basin region as it relates to fluvial/alluvial events occurring on surrounding surfaces (e.g., 8,9). As part of this mapping, we are also evaluating the morphology, mineralogy, and distribution of newly identified sedimentary deposits in small inter-ring basins in the highlands west of Ladon basin. We hope to determine how they may relate to either a past discharge out of Argyre basin along the Uzboi-Ladon-Morava mesoscale outflow system (10,11), a possible lake in Ladon basin (12), deposition in Holden crater and(or) Ladon and Uzboi Valles to the south (13), or alluvial-fan-forming events recognized in the region (6,7).

Results: Light-toned layered deposits are one of the geologic units that we have analyzed in detail utilizing HiRISE and CRISM images. Figure 1 shows the locations of these deposits that we have identified thus far. All of the deposits along the western Ladon uplands are associated with lower lying topography along crater floors or within valleys. Light-toned deposits along the Ladon basin floor appear to represent small preserved deposits that have not yet been removed by erosion. These deposits are covered by darker capping material which means we can only identify the deposits where this capping material has been removed or along steep edges where a vertical exposure is observable. The largest exposures of light-toned layered deposits are observed at the distal end of Ladon Valles. These deposits could have resulted from discharge associated with flooding that created Ladon Valles or, alternatively, from lacustrine sediment that accumulated in Ladon basin.

Our preliminary CRISM analyses indicate that variations are present in the type of Fe/Mg-phyllosilicate unit. Smectite appears to be dominant for the unit having bands near 1.9 and 2.3 μm ; however, the spectral character is more consistent with nontronite (2.29 μm) in some regions and saponite (2.31 μm) in other regions. The figure 2 red spectrum is consistent with nontronite while the blue spectrum could be saponite. Both spectra were extracted from light-toned sediments along a valley floor in the uplands to the west of Ladon basin. By examining the relative stratigraphy for these two types of clays, we may be able to understand how the phyllosilicate chemistry changed through time.

Emerging similarities or differences in inferred processes responsible for forming the deposits will be important for determining whether environmental effects were regional and similar across all of Margaritifer Terra or if they were localized, and also how conditions may have changed through time. For example, an analysis of the Eberswalde region by *McKeown et al.* [14] indicates the source rocks for the delta contained Fe/Mg-smectites, high-calcium pyroxene, and olivine. They further suggested the Eberswalde delta contains materials (clays) derived from Holden and Eberswalde ejecta that sampled a regional phyllosilicate layer. By examining numerous smaller upland deposits to the northeast of Eberswalde and tracing valley networks from these deposits to potential upland sources, we, too, may be able to support a detrital origin for these deposits that would indicate a widespread period of fluvial activity across this region, perhaps related to synoptic precipitation [6,7].

References: [1] Grant J. A. et al., 2008, *Geology*, 36, 195-198, doi: 10.1130/G24340A; [2] Grant J.A. et al., 2010, in *Lakes on Mars*, edited by N. A. Cabrol and E. A. Grin; [3] Irwin R. P., III, and J. A. Grant, 2009, in *Megafloods on Earth and Mars*, edited by D. M. Burr et al., 209-224; [4] Pondrelli M. et al., 2005, *J. Geophys. Res.*, 110, 2004JE002335; [5] Pondrelli M.A. et al., 2008, *Icarus*, 197, 429-451, doi:10.1016/j.icarus.2008.05.018; [6] Grant J. A. and S.A. Wilson, 2011, *Geophys. Res. Letts.*, 38, L08201, doi:10.1029/2011GL046844; [7] Grant J. A. and S.A. Wilson, 2012, *Planet. Space Sci.*, 10.1016/j.pss.2012.05.020; [8] Grant J.A. et al., 2009, *U.S.G.S. Scientific Investigations Map 3041*, scale 1:500,000. [9] Irwin and Grant, 2013, *U.S. Geological Survey Scientific Investigations*. [10] Parker, 1985, *Master's Thesis*, California State Univ., Los Angeles;

[11] Jones A.P. et al., 2011, *Icarus*, 211, 259-272. [12] Grant J.A. and T.J. Parker, 2002, *J. Geophys. Res.*, 107, 10.1029/2001JE001678. [13] Grant J.A. et al., 2010, *Lunar*

Planet. Sci., XLI, Abstract 1834. [14] McKeown N.K. et al. , 2011, *LPSC 42*, Abstract 2450.

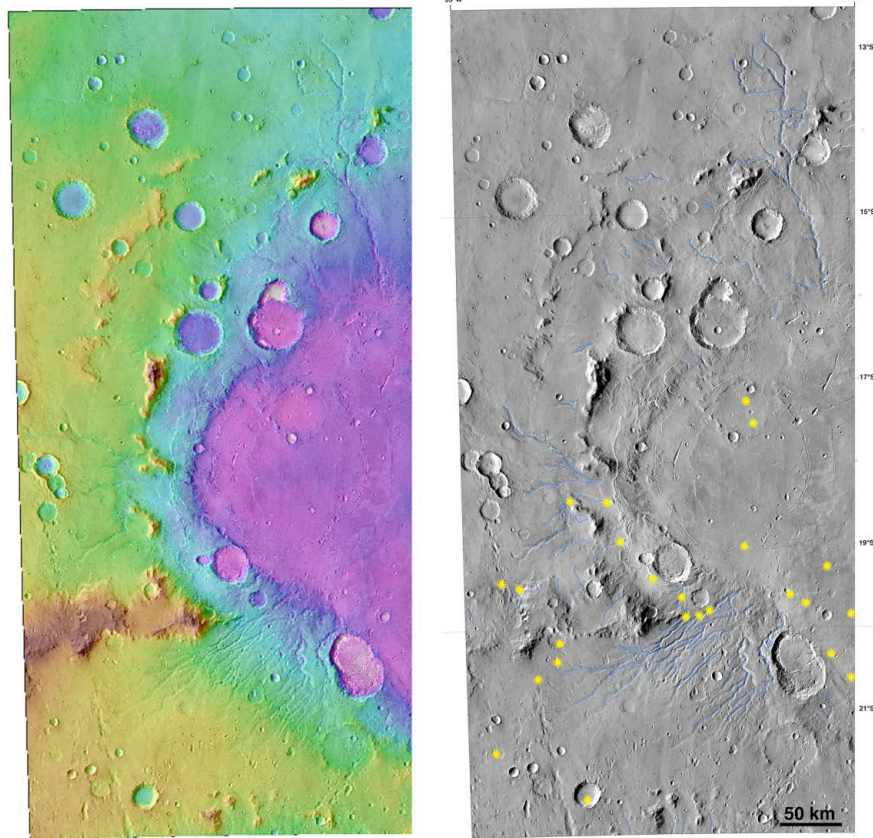


Figure 1. (left) MOLA topography overlain on THEMIS daytime IR mosaic of the two quadrangles in western Ladon basin. (right) THEMIS daytime IR mosaic showing where we have mapped valleys (blue lines). Yellow asterisks indicate where we have identified light-toned deposits, many of which contain hydrated minerals seen in CRISM images. Most of these deposits are too small to map at the 1:1M scale but we have analyzed them in order to understand the aqueous history of this region.

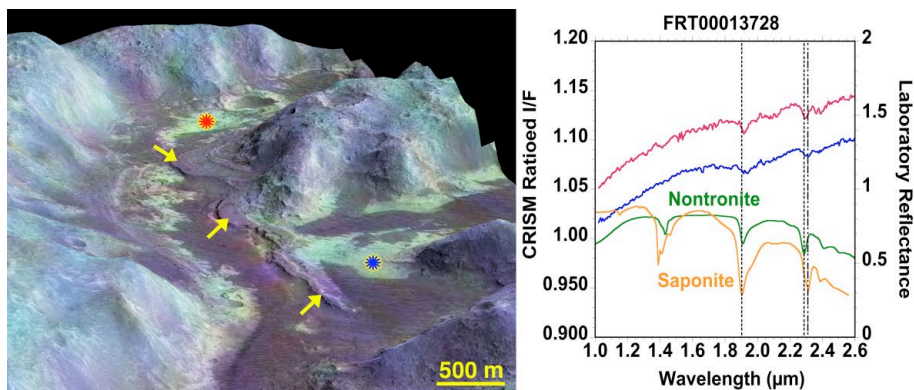


Figure 2. HiRISE DTM at 5X vertical exaggeration merged with CRISM spectral parameters in color (red is Olivine Index, green is band depth at 1.9 μm , blue is band depth at 2.5 μm). Red and blue asterisks correspond to the locations where CRISM spectra were extracted and are plotted to the right. The red spectrum exhibits an absorption at 2.29 μm that is consistent with nontronite while the blue spectrum has an absorption at 2.31 μm that matches saponite. Yellow arrows identify a 15-m high inverted channel within a 120 m deep valley at Arda Valles.

GEOLOGIC MAPPING IN MTM QUADRANGLES -20037, -25037, -30037, -30032 IN SOUTHERN MARGARITIFER TERRA, MARS S. A. Wilson¹ (purdys@si.edu) and J. A. Grant¹ (grantj@si.edu), ¹Center for Earth and Planetary Studies, National Air and Space Museum, Smithsonian Institution, 6th at Independence SW, Washington, DC, 20560.

Introduction: Geologic mapping in Mars Transverse Mercator (MTM) quadrangles -20037, -25037, -30037 and -30032 delineates the gradational history of southern Margaritifer Terra (17.5°S-32.5°S, 320°E-325°E and 27.5°S-32.5°S, 325°E-330°E, **Fig. 1**). This region on Mars preserves a long history of aqueous activity and the deposits in the map area constrain the timing, duration and regional importance of fluvial, alluvial, lacustrine and impact processes.

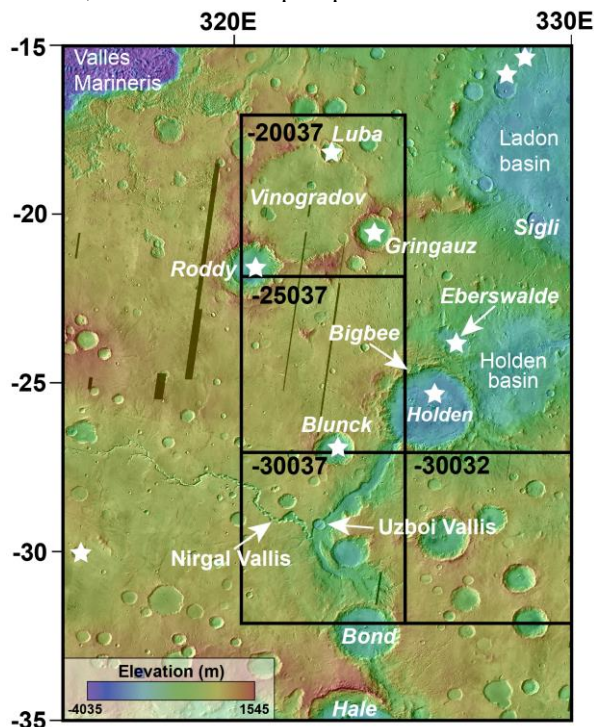


Figure 1. Southern Margaritifer Terra with location of MTM map quadrangles (black boxes) and major place names. Craters hosting alluvial fans (stars) [14, 20] are ~500+ km from Hale. MOLA over THEMIS day IR.

Geologic History, Stratigraphy and Preliminary Map Units (Fig. 2): The oldest material in the map area are remnant high-standing bedrock promontories from the Ladon and Holden basin ring structures, mapped as Early to mid Noachian Mountainous unit (*Nm*) [1]. The underlying structure of these ancient basins controls the regional drainage in southern Margaritifer Terra.

MTM quadrangle -20037 is dominated by Vinogradov, a large (224 km-diameter), highly degraded and infilled crater. Preliminary mapped as a Noachian crater [2], Vinogradov is centered at 20°S, 322.3°E and impacted into a relatively high-standing region, straddling

the western edge of the Ladon impact basin ring just northwest of the Holden impact basin ring. Remnant knobs of unit *Nm* from the Ladon and Holden ring structures limited backwasting of Vinogradov along its south/southeastern rim. Vinogradov lacks large contributing valleys and contains light-toned, Fe/Mg phyllosilicates [3].

The Late Noachian to Early Hesperian Terra unit (*HNt*), characterized by widespread, smooth to rolling, cratered and variably dissected surfaces between degraded impact craters [4], occurs throughout the map area. In MTM -25037, unit *HNt* occurs beneath the continuous Holden ejecta (unit *Hc₂*) and was modified by secondary craters related to the impact. To the south in MTM -30037, unit *HNt* is dissected by Uzboi Vallis and Niral Vallis. Unit *HNt* west of Uzboi Vallis consists of a ~10 meter-thick, laterally continuous Fe/Mg-smectite phyllosilicate-bearing layer located a few meters below the surface cap material and stratigraphically above Al-phyllosilicates [5-6]. Spectral evidence of the Fe/Mg-smectite layer is particularly evident in CRISM data along the walls of Niral Vallis and the interior rims of craters to the west of Uzboi Vallis [6]. The three available CRISM FRTs east of Uzboi do not show evidence of the phyllosilicate layer, thereby suggesting a different unit may be present. Due to the paucity of CRISM data and complications from Holden and Hale impact processes, our understanding of the geologic history east of Uzboi is ongoing.

Craters Gringauz and Roddy formed along the rim of Vinogradov in the mid to late Noachian, respectively [7].

Uzboi Vallis is the southernmost segment of the northward-draining Uzboi-Ladon-Morava (ULM) meso-scale outflow system that dominates drainage in southwest Margaritifer Terra [8-11]. Initial incision of Uzboi likely occurred during the late Noachian to Hesperian [9], but the floor of Uzboi Vallis is mapped as Early to Late Hesperian Etched unit (*He*), characterized by erosionally resistant material exposed where aeolian deflation has selectively removed light-toned layered material. The fluvially dissected surfaces adjacent to Uzboi Vallis are mapped as Early Hesperian to Late Noachian Channel unit (*HNch*) [4], characterized by streamlined outcrops of unit *HNt*.

Holden crater formed in the late Hesperian and the widespread field of associated secondaries from the impact event to the north/northwest provides a useful regional stratigraphic maker. The southern rim of

Holden dammed the previously through-flowing Uzboi Vallis in the late Hesperian [4]. As a result, a large paleolake formed in Uzboi between the rims of Holden and Bond craters [12]. Morphologic evidence suggests the Uzboi lake reached to ~ -350 m relative to the MOLA datum and may have modified older NHch units. The lake exceeded 4000 km^3 [12] before overflowing Holden's rim and draining into the crater [13]. Nirgal is the largest Uzboi tributary valley and may have been a source of water for the Uzboi lake [12].

Crater Luba is mid to Late Hesperian in age and deposited fluidized, lobate ejecta on Vinogradov's northern crater floor [3].

Large alluvial fan deposits within craters Luba, Gringauz, Roddy and Holden [14-15] are mapped as a Late Hesperian to Early Amazonian Fan unit (*AHf*) [3, 15]. The relatively young age of the alluvial fans in the map area correlates with the last period of activity and does not preclude earlier (older) contributions to the fans. The young age of late activity, however, is consistent with a gap in time between the formation of Holden and the latest period of fluvial activity. This gap would have allowed time for several craters to accumulate on Holden's rim before they were fluvially modified (e.g., Bigbee crater) during the proposed late-stage activity responsible for the final fan development. Several observations suggest the fans are likely not related to a local source of water such as impacts including Holden or Hale [16]. Late activity independent of triggers related to Holden or other impacts is supported by the observation that the alluvial fans in craters Roddy and Luba do not contain secondaries from Holden. There is a possible secondary from Holden crater on the floor of Gringauz that appears to excavate light-toned (playa?) layers, though it is uncertain at CTX-scale if the elongated depression is filled with younger Amazonian aeolian material or fluvially-derived sediment related to the fan activity originating from the northern rim of Gringauz.

Hale crater, located to the south of the map area (35.8°S , 323.5°E , 149 km in diameter) formed near the Amazonian-Hesperian boundary [17] or perhaps during the early-to-middle Amazonian [18]. Deposits sourced near the rim of Hale flow into pre-existing valleys, topographic depressions, and craters [17]. The material is often darker-toned than bounding surfaces, smoother (at scales of 10s to 100s of meters), and embay secondary craters from Hale, thereby constraining the timing of their emplacement [19]. West of Bond crater, the deposits locally form lobes with distinct margins after passing through topographic constrictions [19]. Although the deposit appears to thin considerably with distance from Hale, the margins of this dark-toned

Amazonian to Hesperian Smooth Unit (*Ahs*) can be mapped into Uzboi Vallis and the surrounding plains.

Concentrations of dark-toned dunes are mapped as the Amazonian Dune unit (*Ad*).

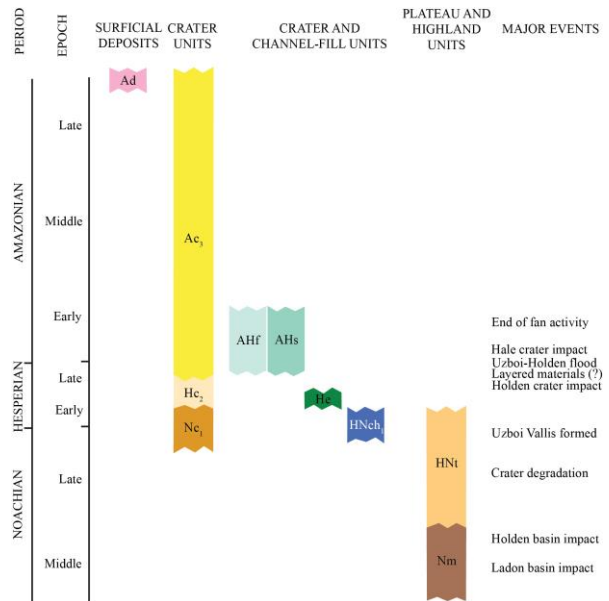


Figure 2: Preliminary correlation of map units (COMU) in MTM quadrangles -20037, -25037, -30037 and -30032 in Southern Margaritifer Terra.

References: [1] Shultz et al. (1982), *JGR*, 87, 9803-9820. [2] Scott, DH and MH Carr (1978), *USGS Map I-1083*. [3] Wilson et al. (2014), *LPSC* Abst. 2382 [4] Irwin, RP III and JA Grant (2013), *USGS Map 3209* [5] Buczkowski, DL et al. (2010), *LPSC*, Abst. 1458 [6] Buczkowski, DL et al. (2013), *LPSC*, Abst. 2331 [7] Scott, DH and KL Tanaka (1986), *USGS Map I-1802-A*. [8] Grant, JA (1987), *Advances in Planet. Geol.*, NASA Memo. 89871, 1-268 [9] Grant, JA and TJ Parker (2002), *JGR*, 107, doi:10.1029/2001JE001678 [10] Parker, TJ. (1985), M.S. Thesis, California State Univ. [11] Saunders, SR (1979), *USGS Map I-1144* [12] Grant et al. (2011), *Icarus*, doi:10.1016/j.icarus.2010.11.024 [13] Grant, JA et al. (2008), *Geology*, 195-198, doi:10.1130/G24340 [14] Moore, JM and AD Moore (2005), *JGR*, 110, doi:10.1029/2005JE002352. [15] Grant, JA and SA Wilson (2011), *GRL*, 38, L08201, doi:10.1029/2011GL046844 [16] Grant, JA and SA Wilson (2012), *PSS*, 72, 44-52. [17] Cabrol, N. A., et al. (2001), *Icarus*, 154, 98-112, doi:10.1006/icar.2001.6661 [18] Jones et al. (2011), *Icarus*, doi:10.1016/j.icarus.2010.10.014. [19] Wilson SA et al., (2013), *Abs. Ann. Mtg. Planet. Geol. Mappers*, Washington, DC. [20] Wilson et al. (2013), *LPSC* Abst. 2710.

An Analysis of Spectroscopic Surface Data from CRISM to Predict a History of Borates on Mars. Z. C. Chester¹, ¹1129 Turkey Point Road, Edgewater, Maryland zacharychester@gmail.

Introduction: A Martian meteorite found in the Miller Range region of Antarctica, called MIL 090030, during the 2009/10 ANSMET field test was found to have high levels of borates on both its exterior and interior [1]. Borates are oxygenated boron compounds [2], and this discovery prompted research which found that borates can enhance the formation of RNA when they react with minerals like molybdate. However, at the time that RNA was thought to have been formed; Earth was theoretically an inhospitable place for borates to form. Mars, on the other hand was ideal for the formation of borates [3]. This research project uses CRISM, the Compact Reconnaissance Imaging Spectrometer for Mars, to analyze data from the surface of Mars to find where borates are located to help predict where future research should be focused.

Once CRISM has compiled the data, it is sent to and stored in the PDS Geoscience Node. This data can be analyzed using JCAT, the JAVA CRISM Analysis Tool and compared with reflectance data from different borates such as tinalconite, ulexite, and colemanite [4]. Currently there are competing theories that suggest that it would be easier for RNA to form in cooler climates [5], but other theories suggest that it was more likely to have formed in a warmer region [6]. This means many areas; such as Olympus Mons, Nia Fossae, Elysium Planitia, and the Polar Caps, must be analyzed to ensure that these theories are both represented.

After the data is analyzed in JCAT, its spectral angle is calculated with respect to each of the different borates. The spectral angle is used to determine how similar the measured surface data is to referenced data. If it is very similar, it will return a low angle. If the data are very different from each other, then they will return values that are very large. The results will be compiled and stored in a spreadsheet so that data from various points can be analyzed [7]. Once the reflectance data from these different locations has been analyzed, the areas with the highest concentrations of borates will be considered the area's most likely for RNA to have formed, potentially suggesting where further research should be focused.

References: [1] Stephenson, J. D., Hallis, L. J., Nagashima, K., & Freeland, S. J. (June 6, 2013). Boron Enrichment in Martian Clay. *PLoS ONE* 8(6): e64624. doi:10.1371/journal.pone.0064624. [2] Lyday, P. A. (2004). Boron. *Chemistry: Foundations and Applications, Volume 1*, 142. [3] Zimmer, C. (September 12, 2013). A Far-Flung Possibility for the Origin of Life. *The New York Times*, pp. D5. [4] Slavney, S. (September 9, 2013). MRO: CRISM. *Geosciences Node Data*. [5] Price, P. B. (August 2010). Microbial Life in Martian Ice: A Biotic Origin of Methane on Mars? *Planetary and Space Science, Volume 10*, 1199-1206. [6] Benner, S. A., Kim, H., & Yang, Z. (2011). Setting the Stage: The History, Chemistry, and Geobiology behind RNA. *RNA Worlds: From Life's Origin to Diversity in Gene Regulation, Volume 1*, 1-14. [7] BAE SYSTEMS Advanced Technologies. (2002). Topic 4: Introduction to Hyperspectral Classification Methods. *BLM Hyperspectral & Lidar Training Course*.

Additional Information: The author gratefully acknowledges the help and support that he received from several sources throughout the course of the project. First of all, the entire MESDT team who provided help and guidance through the course of the project, without their help none of this would have been possible. Acknowledgements also go to Mr. Mathew Schrader, who was always willing to take time out of his schedule to provide assistance, and Dr. David Chester whose software and guidance made the final product what it is.

GEOLOGIC MAP OF THE OLYMPUS MONS VOLCANO, MARS. J.E. Bleacher¹, D.A. Williams², P. Mougini-Mark³, D. Shean⁴, R. Greeley², ¹Planetary Geodynamics Laboratory, Code 698, NASA GSFC, Greenbelt, MD, 20771, Jacob.E.Bleacher@nasa.gov, ²School of Earth & Space Exploration, Arizona State University, Tempe, AZ, 85282, ³Hawaii Institute of Geophysics and Planetology, University of Hawaii. ⁴Malin Polar Science Center, Applied Physics Lab, University of Washington, Seattle, WA, 98105

Introduction/Background: We have completed a first draft of a Mars Data Analysis Program-funded project to map the morphology of the Olympus Mons (OM) volcano, Mars, using ArcGIS by ESRI (Figure 1). The final product of this project is to be a 1:1,000,000-scale geologic map. The scientific questions upon which this mapping project is based include understanding the volcanic development, including identification of volcanic unit source areas, and subsequent modification by structural, aeolian, and possibly glacial processes.

Methods: To address our science questions we conducted morphology mapping at ~ 1:300,000

scale using the Context Camera (CTX) and High Resolution Stereo Camera (HRSC) image mosaic as our base data. This scale enables a distinction between sinuous rilles and leveed channels, which is fundamental for interpreting abundances among, and changes between, tube- and channel-forming eruptions. We have combined our map with Mougini-Mark's Planetary Geology & Geophysics-funded geologic map of the Olympus Mons Caldera that was produced at 1:200,000 scale and provides additional detail of the summit region. We are currently working to finalize the DOMU and COMU for submission to the USGS for external review.

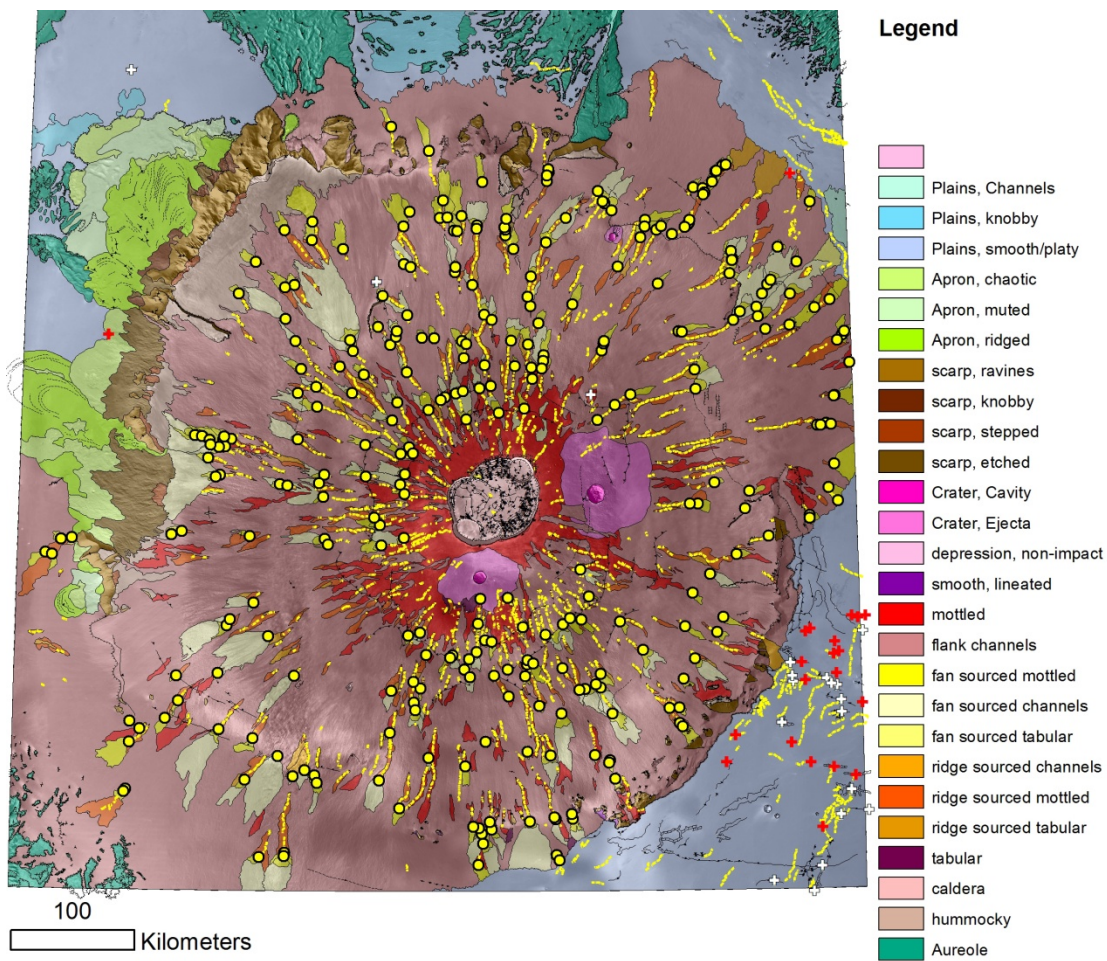


Figure 1. Line work and map units for the Olympus Mons Geologic Map. Yellow dashed lines are sinuous that mark the path of lava tubes on the main flank and rilles of questionable origin on the plains. Yellow circles are rootless vents associated with lava tube breakouts. Red crosses represent low shield volcanoes and fissures and white crosses represent source regions for plains channels.

THE NASA REGIONAL PLANETARY IMAGE FACILITY NETWORK: A FIVE YEAR PLAN.

J. J. Hagerty, U.S.G.S. Astrogeology Science Center, Flagstaff, AZ 86001 email: jhagerty@usgs.gov.

Introduction: NASA's Regional Planetary Image Facilities (RPIFs) are planetary data and information centers located throughout the United States, in Canada, and overseas. The U.S. locations are funded by both NASA and their host institutions [1]. A network of these facilities was established in 1977 to "maintain photographic and digital data as well as mission documentation. Each facility's general holdings contain images and maps of planets and their satellites taken by Solar System exploration spacecraft. These planetary data facilities, which are open to the public, are primarily reference centers for browsing, studying, and selecting planetary data including images, maps, supporting documentation, and outreach materials. Experienced staff at each of the facilities can assist scientists, educators, students, media, and the public in ordering materials for their own use" [2].

Since it was formally established, the network of RPIFs has expanded to nine U.S. facilities and eight facilities in other countries. The first RPIF to be established outside of the U.S. was in the United Kingdom in 1980 at University College London (UCL), and since then RPIFs have been set up in Canada, Finland, France, Germany, Israel, Italy, and Japan. Through its longevity and ability to adapt, the RPIF Network has leveraged its global reach to become a unique resource covering 60 years of international planetary science.

Historically the Network nodes have had an inward focus, providing resources to local clients, and communicating with other nodes only when the need arose. Using this methodology, the nodes of the RPIF Network, hereafter referred to as RPIFN, have combined to serve an average of ~65,000 people per year since 2000. However, with the advent of simpler and more wide-ranging forms of data transfer and sharing, it is clear that the nodes can operate together to provide the planetary science community and the public with greater access to: 1) archived mission products (e.g., maps, photographs, films, and documents); 2) mission-enabling documentation (e.g., data on previous mission design, development, implementation, and evaluation); 3) science and public research support, and 4) outreach experience and capabilities. Each node of the Network has unique capabilities that meet one or more of the above criteria; however, by linking the nodes through a centralized website and database, it is now possible to provide a wider array of materials to a wider array of customers.

Distribution of Planetary Geologic Maps: Each node of the RPIFN maintains a mixture of common and unique collections. The Regional Planetary Information Facility at the USGS Astrogeology Science Center is unique in that one of its primary functions is

to serve as a store house and distribution point for planetary geologic maps. At present, the USGS RPIF has an inventory of 60,000 USGS lunar and planetary maps and now has a full inventory of all maps in the collection.

The USGS RPIF is responsible for distributing (free of charge) newly published I-maps to the other nodes of the RPIFN as well as to interested members of the planetary science community. In recent years it became clear that the distribution process was outdated and inefficient. Given this motivation, the USGS RPIF has been working with leaders in the planetary mapping community to increase the efficiency of the distribution process and to raise awareness of the importance of planetary geologic maps. One of our major continuing efforts is to meet with members of the community at the Annual Planetary Geologic Mappers meeting to discuss the importance and distribution of planetary geologic maps. As a result of these efforts we have established a web-based distribution point (Fig. 1) that is accessible to users who are sent an invitation email with a link to the distribution page.

USGS
Research for a changing world
Astrogeology Science Center
Home About Labs/Facilities Maps/Products Members/Research Tools

Home / RPIF / Map Request Form

This is the USGS Astrogeology Regional Planetary Information Facility (RPIF) form for ordering folded paper USGS planetary maps. Maps are available at no cost to the requester. Please click the box next to the map or maps you require and fill in your complete Shipping Address below. If you require none of the maps listed below, no response is necessary.

By NASA mandate, paper USGS planetary maps are intended primarily for distribution to members of the planetary science community. Maps are available on a first-come, first-served basis. Specific maps might become unavailable if demand is great.

If you have any questions, please [contact the RPIF](#).

If you are requesting maps, the fields with an * are required.

Name *

Email *

Maps Requested *

<input type="checkbox"/>	SM-3116 Geologic Map of the Lakshmi Planum Quadrangle (V-7), Venus, 1:5 000 000 series, M. Ivanov, J. Head, 2010
<input type="checkbox"/>	SM-3121 Geologic Map of the Ganiki Quadrangle (V-14), Venus, 1:5 000 000 series, E. Grosfils, S. Long, E. Venechuk, D. Hurwitz, J. Richards, B. Klotz, D. Drury, J. Hardin, 2011
<input type="checkbox"/>	SM-3158 Geologic Map of the Metis Vicus Quadrangle (V-6), Venus, 1:5 000 000 series, J. Dohrn, K. Tanaka, J. Skinner, 2011
<input type="checkbox"/>	SM-3163 Geologic Map of the Heraclea Chasma Quadrangle (V-28), Venus, 1:5 000 000 series, E. Stefan, J. Guest, A. Brian, 2012
<input type="checkbox"/>	SM-3165 Geologic Map of the Themis Regio Quadrangle (V-53), Venus, 1:5 000 000 series, E. Stefan, A. Brian, 2012

Figure 1. New online order form for the USGS Planetary Map collection.

Five Year Plan: The role of the RPIF Network is evolving as key historical planetary data sets are converted to digital files and are made available online. Instead of trying to compete with vast array of materials housed in digital servers (i.e., the PDS, whose goal is to focus on serving more technically oriented NASA-funded users), *the RPIF Network will serve as a valuable resource for specialized knowledge and services that will make it possible to remove the barriers associated with locating, accessing, and using planetary science data, particularly derived data products. The goal of the Network is to provide support to a broad audience of planetary data users.*

The RPIF Network nodes will continue to serve as reference centers that are needed for preserving and accessing derived products from Solar System exploration missions, and will continue to do so for future missions as well. In an effort to meet our customer's needs, we aim to achieve the following primary goals:

1. Maintain and improve the foundation that has been established over the past four decades so as not to lose critical, historical information. This goal will be aided by a systematic effort to scan and digitize fragile materials as a means of increasing access and preservation of the materials.
2. Help users to locate, access, visualize, and use planetary science data. In an effort to make this possible, RPIF staff are being trained in the use of common planetary data sets and processing tools such that they can assist novice researchers with locating and using planetary data. One tool that will be used in this effort is the Magic Planet from Global Imagination (Fig. 2). Each US facility of the Network now has one of these globes which will make it easier for researchers to visualize and work with global data sets.
3. Improve the connection between the Network nodes while also leveraging the unique resources of each node. To achieve this goal, each facility will develop and share searchable databases of their entire collections.
4. Promote the Network in an effort to make potential users aware of resources and services provided by the Network.

By achieving these goals, we will introduce new users to data products from past, current, and new missions. The underlying premise of data needs for users of the RPIF Network (whether hard copy or digital) is that research and discovery does not end with each mission, but continues for generations to come. As such, the RPIF Network provides the bridge between generations as one phase of exploration ends and another begins.

In summary, over the next five years the RPIF Network will continue its traditional service as a

source of derived data products and expand its reach through new technologies, making obscure, but critical data sets available to a wider user community. New initiatives in digitizing hard copy data will make valuable resources widely available and provide a mechanism for long term preservation. It should be noted however, that digitization of all photographic imaging data at the same resolution as the original, cannot be fully achieved except at large cost; therefore, access to hard copy materials remains necessary. Consequently, the distributed reference collections held by the RPIF's remain an important and accessible resource. By leveraging the expertise and resources of the RPIF Network NASA will be able to make exciting new discoveries of planetary science more widely available, which will allow the Network to better serve NASA, the planetary science community, and the general public.

For more information, or to request materials, please contact any of the RPIFs listed below. Additional, detailed information can also be found at <http://www.lpi.usra.edu/library/RPIF>

Acknowledgements: The U.S. nodes of the RPIF Network are supported by NASA as well as by leveraging funds from host institutions.

References: [1] Shirley and Fairbridge, eds. (1997) *Encyclopedia of Planetary Sciences*, Chapman and Hall, London, 686; [2] Muller and Grindrod (2010) *European Planetary Science Congress 2010*, 883;



Figure 2. Magic Planet from Global Imagination. A new visualization tool for global planetary data.

PROGRESS ON 1:10M GEOLOGIC MAPPING OF THE APHRODITE MAP AREA, VENUS. V.L. Hansen¹, I. López², K.G. Thaisen¹, ¹University of Minnesota Duluth, Duluth, MN 55812 (vhansen@d.umn.edu), ²Área de Geología. Universidad Rey Juan Carlos. 28933. Mostoles. Madrid (ivan.lopez@urjc.es).

Introduction: We are conducting 1:10M geologic mapping of the Aphrodite 1:10M map sheet (0°-57°S/60°-180°E, I-2476) with the goal to establish the geologic history of this region, and discover implications for the geodynamic evolution of Venus. The Aphrodite Map Area (AMA) contains a rich assemblage of basement (crustal plateaus and lowland tessera inliers) and plains materials (shield terrain, volcano- and corona-related materials and expanses of apparently undivided plain materials), and, perhaps most notable, the map area's namesake, Artemis, which lies just east of the center of AMA. A combined progress report for the AMA and the Niobe Planitia 1:10M map sheet (NMA) were presented at last year's NASA's Mappers Meeting [1]. The AMA-NMA together include over 25% of Venus' surface.

We present results of complete structural mapping of the AMA, and describe broad spatial and temporal patterns that emerge. Delineation of structural suites, recognition of their characteristics, and their interaction with one another and with volcanic materials is fundamental for future delineation of material units and discovery of geologic histories at both local and regional scales [2].

Data and methods: Geologic mapping was carried out using: (1) NASA Magellan full-resolution SAR data (left- and right-look; normal and inverted modes) [3]; (2) NASA Magellan altimetry; and (3) synthetic stereo images constructed using NIH-Image macros developed by D.A. Young.

Data visualization and geologic mapping was conducted using Adobe Illustrator[™] with linked data layers, MAPublisher[™] to scale and georeferenced raster datasets, and ArcGIS[™] and ArcGlobe[™] for compilation, projection and analysis.

Geologic mapping began with delineation of secondary structures, with attention to structural character, orientation, patterns and temporal relations; material units are defined based on the patterns of secondary structures and the nature of radar characteristics. Map relations determined using full-resolution data were translated to the 1:10M map scale.

Overview of the Aphrodite Map Area (Fig. 1): The AMA is broadly divisible into four major geologic domains, which spatially overlap: (1) crustal plateaus (Ovda (& western Ovda) and Thetis regiones) and lowland inliers of ribbon tessera terrain; (2) Artemis, including Artemis chasma and the interior region, and a huge radial dyke swarm and concentric wrinkle ridge

suite, 12,000- and 13,000-km diameter, respectively [1, 4]; (3) chains of coronae marked by large coronae across a more narrowly defined region to the east (Diana-Dali chasma), that widens or splits into a broad fan of generally smaller coronae to the west; and (4) an extensive fracture zone that overlaps with the focused corona chain (Diana-Dali region) to the east, and splits into various regional splays to the west, cutting crustal plateaus in the highlands to the NW along a NW-trend and lowland regions along W, WSW and SW trends. Artemis chasma and interior generally spatially coincides with the east-to-west transition for both the corona-chain/fan and the fracture zone.

Domains 1 and 2 also occur in NMA, whereas domains 3 and 4 appear to occur only in AMA. Crustal plateaus, marked by highland regions of unique ribbon-tessera terrain fabric [5], share the boundary with NMA; ribbon-tessera inliers also occur as relatively small and spatially limited outcroppings to the south. The SE part of AMA lacks ribbon-tessera terrain [6], and is the only part of AMA that corresponds to the old-AMSAP (average model surface age province) [7,8; the rest of the AMA falls within the intermediate-AMSAP]. Artemis' footprint—radial dyke swarm and concentric wrinkle ridges—is discussed further below.

The coronae-chain/fan and fracture zone domains (3 & 4) broadly overlap spatially and temporally, with the main exception being that the fracture zone cuts the highland, whereas coronae do not. Within the highland the fracture zone is characterized by hybrid structures that variably change along strike forming fractures, pitchains, graben, leaky dykes, and even channels. Lava lakes also occur locally. It appears that the geodynamic driver at depth is similar to other parts of these domains, but that the surface expression changes as a result of the overlying crust-lithosphere [9]. Elsewhere fracture zone structures cut and are buried by corona-fed flows, indicating broad temporal overlap. Fracture formation locally outlasted emplacement of many corona-fed flows; yet locally corona-fed flows bury fracture-zone structures. The spaced nature/splays of these domains results in the preservation of intervening tracts of the surface that preserve a record of Artemis.

Artemis: The impressive regional extent of Artemis was noted previously [4]. More detailed geologic mapping across the NMA and the AMA (discussed herein) confirms earlier observations, but also contributes further to the history of Artemis, and by comparison geologic events not associated with the

Artemis superplume. Artemis-radial fractures (ARF) and Artemis-concentric wrinkle ridges (ACWR) occur across the AMA (and into much of the NMA). They are broadly divisible into four type-areas: (1) well-expressed ARF; (2) ACWR; (3) buried-ARF and ACWR; and (4) regions lacking both ARF and ACWR. The latter type-area is further divisible into regions defined by: (a) ribbon-tessera terrain, (b) local structural suites (radial or concentric patterns), (c) penetratively developed fractures, or (d) corona- or fracture-fed flows. Collectively these represent regions where ARF or ACWR did not/could not form (a), or where these structures formed, but were disrupted by younger structures/flows (b-d). Diana-Dali coronae-chasmata chain represents a regional-scale version of b-d.

Regional patterns and detailed relations preserved in type-areas 1-3 record a coherent picture of the effect on the surface by, and the evolution of, the Artemis superplume. Type area-1 represent regions of preexisting surfaces cut by ARF; they correspond to local basement terrain, and locally include shield terrain [10,11]. These regions were not resurfaced by Artemis-fed flows. Type area-2, regions of ACWR, were resurfaced by (generally) Artemis-fed flows (locally corona flows), and later cut by ACWR. Type area-3 preserves an intermediate record—cut by ARF, locally resurfaced by Artemis-fed flows and/or hosting a thin veneer of shield-sourced material, and deformed by ACWR; these regions mark areas of emplacement of relatively thinner-flows compared to area-type 2.

First-order timing emerges from mapping. Ribbon-tessera terrain and crustal plateaus mark an early era of crustal evolution. Later the Artemis superplume impacted the entire region, with ARF forming early and serving as feeders to local, but regionally extensive, flows, and ACWR marking superplume collapse. Artemis chasmata and the interior region formed late in superplume evolution. Late during the Artemis era the coronae-chain/fan and fracture zone formed. Cross-cutting relations indicate that some coronae began to form during the Artemis era given that some coronae-fed flows are cut by ACWR. Other corona-fed flows lack this suite of wrinkle ridges.

References: [1] Hansen V.L. & López I. (2013) *Abstracts of the NASA's Mappers Meeting*. [2] Hansen V.L. (2000) *EPSL* 527-542. [3] Ford J.P. et al. (1993) *JPL Publ.* 93-24. [4] Hansen V.L. & Olive A. (2010) *Geol.* 38, 467-470. [5] Hansen V.L. & Willis J.J. (1998) *Icarus* 132, 312-343. [6] Hansen V.L. & López I. (2014) *Geol.* 38, 311-314. [7] Phillips R.J. & Izenberg N.R. (1995) *GRL* 22, 1517-20. [8] Hansen V.L. & Young D.A. (2007) *GSA SP* 492, 367-82. [9] Bleamaster L.F. & Hansen V.L. (2004) *JGR* 109. [10] Aubele J. (1996) *LPSC* 27, 49-50; [11] Hansen V.L. (2005) *GSAB* 117, 808-820.

Fig. 1. Aphrodite structure map: Artemis interior and chasmata (orange/yellow); ribbon-tessera terrain (pink), fracture zone (blue); ACWR, red; ARF, dark green; buried fractures, light green; local radial structures, purple; local concentric structures, orange; channels, black; fz fractures, light blue; pitchains/hybrid lineaments, dark blue.



PROGRESS ON THE 1:10M GEOLOGIC MAPPING OF THE NIOBE MAP AREA, VENUS: RESULTS FROM THE STRUCTURAL MAPPING OF THE VOLCANIC PLAINS. I. López¹ and V. L. Hansen², ¹Área de Geología. Universidad Rey Juan Carlos. 28933. Mostoles. Madrid (ivan.lopez@urjc.es), ²University of Minnesota Duluth, Duluth, MN 55812 (vhansen@d.umn.edu).

Introduction: We are conducting 1:10M geologic mapping of Niobe Planitia (0°-57°N/60°-180°E, I-2467) with the aim of establish the geologic history of this region, and discover implications for the geodynamic evolution of Venus. The Niobe Map Area (NMA) contains a rich assemblage of basement (crustal plateaus and lowland tessera inliers) and plains materials (shield plains, volcano- and corona-related materials and large expanses of apparently undivided plain materials). Initial observations on the characteristics and distribution of the basement units were presented in last year's NASA's Mappers Meeting [1].

We present the result of the complete structural mapping of the NMA volcanic plains and describe the regional-scale patterns, local modifications of these regional patterns, and the effect of large tectonomagmatic structures on these regional fractures suites. Delineation of the structural suites, recognition of their characteristics, and their interaction with one another and with volcanic materials is fundamental for the future delineation of plain units and the establishment of a geologic history at regional scale [2].

Data and methods: Geologic mapping was carried out using: (1) NASA Magellan full-resolution SAR data (left- and right-look; normal and inverted modes) [3]; (2) NASA Magellan altimetry; and (3) synthetic stereo images constructed using NIH-Image macros developed by D.A. Young.

Data visualization and geologic mapping was conducted using Adobe Illustrator[™] with linked data layers, MAPublisher[™] to scale and georeferenced raster datasets, and ArcGIS[™] and ArcGlobe[™] for compilation, projection and analysis.

Geologic mapping began with delineation of secondary structures, with attention to structural character, orientation, patterns and temporal relations; material units are defined based on the patterns of secondary structures and the nature of radar characteristics. Map relations determined using full-resolution data were translated to the 1:10M map scale.

Structures on the volcanic plains of the Niobe Map Area: Structures in the volcanic plains of the Niobe map area are divided into two groups: (a) *regional structures* that extend across huge regions, and which are not obviously related to local features; and (b) *local structures* relate to large, but localized,

tectonomagmatic centers. The former are interpreted as recording regional stress fields, and the latter as recording stress fields associated with individual tectonogeomorphic features.

Regional contractional structure suites.

Folds. Broad folds deform some basal units of the volcanic plains. These folds are found in areas of concentrated deformation in two areas: (a) NNE-trending folds that deform basal plain materials of eastern NMA (Llorona, Vellamo and Atalanta planitiae); and (b) NNW-trending folds located in Lemkechen and Unelanuhi Dorsa that deform basal plain materials in Akhtamar Planitia, western NMA.

Wrinkle ridges. We recognize different suites of wrinkle ridges: (a) regional suites; (b) local inversion structures; (c) local suites concentric to individual coronae; and (d) local reorientation of wrinkle ridge trends around tectonomagmatic features and deformation belts. The circum-Artemis trend [4], the most regionally extensive suite in the NMA, is composed of a huge suite of wrinkle ridges that extends beyond the map area to the south. The suite defines a region >13,000 km in diameter around Artemis in the Aphrodite Terra Map Area [4, 5]. Some wrinkle ridges of this regional trend are locally reoriented around large tectonomagmatic centers and deformation belts; locally wrinkle ridges are reoriented parallel to deformation belt folds (e.g., deformation belts in Atalanta Planitia and Vellamo Planitia), which trend nearly orthogonal to the main circum-Artemis regional trend. This observation indicates that the deformation belts influenced the local stress field during wrinkle ridge formation, and thus the deformation belts almost certainly predated the formation of the Artemis-centered suite of wrinkle ridges. In western NMA deformation belts trends broadly parallel that of the local trends of the Artemis-centered wrinkle ridge suite; locally where deformation belts trend at a higher angle, wrinkle ridges locally parallel belt trends. These relations indicate that deformation belts likely pre-date Artemis-center wrinkle ridge formation.

In the central NMA local N-trending wrinkle ridges show clear evidence of inversion structures [e.g., 6]; these wrinkle ridges occur along strike with open fractures and buried fractures. The N-trending fractures in these locations correspond to portions of the Artemis-radial fracture suite [4, 5]. Well exposed Artemis radial

fractures occur to the south, whereas the band of inverted wrinkle ridges occurs radially outward from these fractures. As discussed in [5] the Artemis radial fractures fed surface deposits, which locally filled these fractures, and these same structures were later inverted, similar to the history documented in Rusalka Planitia [6].

In Leda Planitia wrinkle ridges define a reticulate pattern similar to that present in the basement materials and in the volcanic materials that postdate these basement materials but the existence of reactivation has not yet clearly established (i.e. no direct observation of fractures covered with lava flows inverted as wrinkle ridges).

Regional extensional structure suites.

Regional fractures. We identify three regional fracture suites based on trend, spacing, pattern, and temporal relations with materials units.

Suite 1. NNW-trending fractures mark the oldest fracture suite. This suite, which occurs across NMA, dominantly cuts lower plain materials, but it also locally cuts younger flows where later reactivation is evident. The trend parallels the orientation of local ribbon structures that comprise extensional structures in ribbon-tessera terrain [7, 8]. In some locations it seems clear that this fracture suite marks reactivation of basement structures covered by thin flows/discontinuous materials from small shield clustering (shield plains or shield terrain [9, 10]) in which the underlying fractures are apparent in high resolution SAR images. Fracture trend and spacing is constant across a great expanse of terrain, consistent with a strong control of basement structures on the local expression of regional stress fields at the time of formation/reactivation.

Suite 2. A suite of NNE-trending fracture cuts central NMA band of similar trend. This suite, which postdates suite 1, may include multiple fracture suites. There is no clear evidence for reactivation of underlying basement structures, except perhaps SW of Ananke Tesserae, where a consistent fracture spacing may belie the presence of a buried rheological discontinuity; additionally, the fractures parallel Ananke Tessera tectonic-fabric trends. Fractures east of Tellus Regio, which are currently included in suite 3 (see below), could also be part of suite 2.

Suite 3, or the 'Artemis-radial suite' consists of generally N-trending fractures across NMA with NE-trends to the east and NW-trends to the west. This suite is part of the previously identified, regionally extensive, Artemis-radial fracture/dyke/graben suite [4]. Locally coronae line up with this suite and may represent reactivated parts of the fracture suite. This fracture

suite predates the formation of both Kunhild and Ereshkigal coronae (W-central NMA), which each display radial fractures and flows, and locally corona-concentric wrinkle ridge suites. These coronae have been interpreted as an extinct hot-spot [11].

Local secondary structure suites.

Radial fracture suites are spatially associated with large tectonomagmatic centers; locally extending great distances from centers (e.g. Holde Corona, Atalanta Planitia; Kurukulla Mons, Till-Hanun Planitia).

In the western NMA (Akhtamar Planitia) radial fracture suites connect individual large tectonomagmatic centers (Hatshepsut Patera-H'uraru Corona, Uli-Ata Mons, Kaltash Corona-Kunhild Corona, Ereshkigal Corona) forming an interconnected suite that is difficult to differentiate from regional fracture trends.

Concentric fracture suites mark the annuli of coronae in central NMA; these coronae mark circular depressions, or circular lows, and may comprise a unique class of coronae [12, 13]; typically these coronae lack radial fractures and obvious associated flows. Kaltash and Rosmerta coronae, located in Aphrodite Terra, display annuli of concentric fractures, radial fracture suites, and extensive flows that embay and postdate adjacent crustal plateaus and ribbon-tessera terrain.

Concentric ridges form the annuli of some coronae (e.g. Ituana and Bil coronae, eastern NMA), which source large radial flows. Similar concentric ridges in Irnini Mons are interpreted as result of tectonic inversion or warping of regional stress around a hole in a plate (empty magmatic reservoir) [14]. Testing of this hypothesis will require further detailed mapping.

Further work: Work in progress includes: (a) delineation of map units from published 1:5M maps; (b) delineation of material units; (c) establishing local geologic histories where structural markers (e.g. dykes or regional structures) constrain relative ages between material units; (d) implications for models on the geodynamic evolution of Venus at map scale.

References: [1] Hansen V.L. & López I. (2013) *Abstracts of the NASA's Mappers Meeting*. [2] Hansen V.L. (2000) *EPSL* 527-542. [3] Ford J.P. et al. (1993) *JPL Publ.* 93-24. [4] Hansen V.L. & Olive A. (2010) *Geol.* 38, 467-470. [5] Hansen V.L. et al. (2014) *This volume*. [6] Deshon et al. (2000) *JGR* 105, 6983-95. [7] Hansen V.L. & Willis J.J. (1998) *Icarus* 132, 312-343. [8] Hansen V.L. & López, I. (2010) *Geol.* 38, 311-314. [9] Aubele J. (1996) *LPSC* 27, 49-50; [10] Hansen V.L. (2005) *GSAB* 117, 808-820. [11] Herrick R.R. & McGovern P.J. (2000) *GRL* 27, 839-842. [12] Shankar B. & Hansen V.L. *LPSC* 29, 1813.pdf. [13] Shankar B. (2008) MS thesis, UMD. [14] Buczkowski D.L. (2002) *J. Struc. Geol.* 28, 2156-2168.